

# A Graph Theoretical Approach to the Analysis, Comparison, and Enumeration of Crystal Structures

Dissertation  
zur Erlangung des Doktorgrades der Naturwissenschaften  
im Fachbereich Geowissenschaft  
der Johann Wolfgang Goethe Universität  
in Frankfurt am Main

vorgelegt von  
Georg Thimm  
aus Trossingen

2008  
(Erscheinungsjahr)

2008  
(Einreichungsjahr)

---

1. Gutachter: Prof. Dr. Björn Winkler  
2. Gutachter: Prof. Dr. Wulf Depmeier  
Datum der Disputation: 25 Juni 2008



## Acknowledgments

My most sincere gratitude goes to my mentor W. E. Klee, without whom this fascinating topic would have been inaccessible to me.

Björn Winkler deserves a great deal of thanks for his encouragement and support during the edition of this dissertation and papers, my sister Marlene and Elke Messal for correcting my German, and Detlef Schmicker for suggestions to improve this work and numerous discussions on physics, life, and the rest.

And above all, I am glad that my wife Marie-Claude, Théo and Anna showed some interest in this work and keeping reminding me that there is much more to life than work, paper, and computers.



# Zusammenfassung

Üblicherweise werden Kristalle unter Zuhilfenahme von Gittern, Einheitszellen, Raumgruppen und auf diesen aufbauenden Modellen beschrieben. Diese Modelle beruhen auf dimensionalen Grössen: Gitter und Einheitszellen werden durch Längen und Winkel beschrieben; Raumgruppen beruhen darauf, dass sich Atome an bestimmten Koordinaten in diesen Einheitszellen befinden. In der hier vorgestellten Arbeit wird ein grundlegend anderer Weg verfolgt: Kristalle werden durch Quotientengraphen beschrieben. Vereinfacht ausgedrückt, werden Atome und Bindungen einer Einheitszelle durch Knoten und Kanten beschrieben.

Die Überführung von Kristallstrukturen in Quotientengraphen und die zugehörige Umkehrung, die Einbettung von Netzen in den Euklidischen Raum, wird erläutert. Verbindungen zwischen Netzen oder den sie beschreibenden Quotientengraphen und der spezifischen Dichte von Kristallstrukturen werden hergestellt: Die topologische Dichte wird definiert und dazu benutzt für eine Untergrenze der spezifischen Dichte zu finden. Weiter werden die maximalen Längen der Kanten von Einheitszellen, und somit das Volumen einer Einheitszelle, nach oben abgeschätzt.

Zwei neue Klassen von geschlossenen Pfaden werden eingeführt und daraufhin untersucht, wie spezifisch sie für Netze sind. Darüber hinaus werden Kriterien aufgestellt, die es erlauben Netze ohne eine Einbettung (das heißt die Quotientengraphen) daraufhin zu untersuchen, ob sie aus nicht zusammenhängenden Teilnetzen bestehen. Diese Kriterien erlauben es, Netze zu unterscheiden, bei denen diese Teilnetze die Form von Inseln, Ketten oder Schichten haben, oder die aus sich gegenseitig durchdringenden parallelen Netzen (wie zum Beispiel in Cuprit) bestehen. Die Kriterien werden an den Quotientengraphen von Graphit, Talk, Cristobalit und Cuprit vorgeführt.

Ein Algorithmus zur Aufzählung von Quotientengraphen, mit dem Ziel Kristallstrukturen *ab initio* zu erzeugen, wird vorgestellt. Um diese Aufzählung so effizient wie möglich zu gestalten, werden Regeln aufgestellt, die es erlauben viele redundante oder für Kristallstrukturen unzulässige Quotientengraphen von einer Aufzählung auszuschließen. Eine vollständige Aufzählung aller vierfach koordinierten Netze, deren Einbettungen vier Knoten in einer Einheitszelle besitzen, ergab mehr als 67'000 Netze. Unter diesen befanden sich das Diamant-Netz (mit doppelter Einheitszelle), das Lonsdaelit-Netz und drei weitere Netze, die möglicherweise bisher unbekanntes  $sp^2$ -Kohlenstoffmodifikationen entsprechen könnten.

Eine neu eingeführte Definition von Netzen und Quotientengraphen beruht nicht auf Translationen und Atompositionen und hat somit den Vorteil von Kristallstrukturen unabhängig zu sein. Beweise über die Isomorphie von

Quotientengraphen für diese Definition werden durchgeführt. Der vermutlich wichtigste Beitrag dieser Arbeit ist ein Vergleich der Automorphismen der Quotientengraphen mit Raumgruppen. Es wird gezeigt, dass die Annahme einer Einbettung maximaler Symmetrie effektiv die Raumgruppe (die Punktgruppe und die den einzelnen Rotationen oder Spiegelungen zugehörigen inhärenten Vektoren) einer solchen Einbettung bestimmt. Der Ansatz wird dazu benutzt zu zeigen, dass die Struktur von Markasit durch eine Verzerrung aus der Pyrit-Struktur hervorgeht. Der Vergleich der Strukturen von Markasit und Rutil lässt vermuten (ohne Zuhilfenahme von Quantenphysik oder ähnlicher Hilfsmittel), dass in Markasit S-S Bindungen existieren. Eine Analyse von Hoch- und Tiefquarzen zeigt, dass ein bindungserhaltender Phasenübergang nur zwischen gewissen Paaren der enantiomorphen Strukturen möglich ist und ein displaziver Phasenübergang der Hochquarze zu höhersymmetrischen Strukturen ausgeschlossen ist. Drei Graphitmodifikationen werden diskutiert.

Gewisse Quotientengraphen besitzen Automorphismen, die Translationen einer Einbettung eines Netzes entsprechen, die mit dem Gitter der ursprünglichen benutzten Einbettung unvereinbar sind. Ein Algorithmus, der direkt die den höhersymmetrischen Gittern entsprechenden Quotientengraphen bestimmt, wird vorgestellt. Dies entspricht, grob ausgedrückt, einer Verkleinerung einer Superzelle zu einer anderen Super- oder Einheitszelle, möglicherweise in Verbindung mit einer Drehung der Koordinatensystems.

Für das Halit-Netz wird gezeigt, dass unter der Voraussetzung, dass die beiden Atomsorten nicht unterschieden werden, die Zahl der Knoten im reduzierten Quotientengraph halbiert werden kann. Für Quotientengraphen, die aus zentrierten Zellen der Magnesit- und Kalkspat-Strukturen hervorgehen, wird gezeigt, dass sie auf Quotientengraphen die primitiven Zelle entsprechen reduziert werden können, und dass ihre Topologien sich von der eines Barytokalzits unterscheiden. Am Beispiel der Struktur eines Strontium-Feldspats wird gezeigt, wie der reduzierte Graph benutzt werden kann um abzuschätzen ob eine (Un-)Ordnung einer Struktur einen translations(un-)gleichen Phasenübergang nach sich zieht.

Zusammenfassend zeigt die hier vorgestellte Arbeit, dass Quotientengraphen und Netze Vorteile in Bezug auf den zur Bestimmung gewisser Eigenschaften nötigen Rechenaufwands mitbringen.

# Erweiterte Zusammenfassung

Üblicherweise werden Kristalle unter Zuhilfenahme von Gittern, Einheitszellen, Raumgruppen und auf diesen aufbauenden Modellen beschrieben. Diese Modelle beruhen auf dimensional Grössen: Gitter und Einheitszellen werden durch Längen und Winkel beschrieben; Raumgruppen beruhen darauf, dass sich Atome an bestimmten Koordinaten in diesen Einheitszellen befinden.

In der hier vorgestellten Arbeit wird ein grundlegend anderer Weg verfolgt: Kristalle werden durch Graphen beschrieben. Vereinfacht ausgedrückt, werden Atome und Bindungen durch Knoten und Kanten beschrieben. Kristalle werden damit in unendliche Graphen überführt, die Netze genannt werden. Diese Art Strukturen zu beschreiben ist der Kristallographie geläufig und in der Chemie und Biologie weit verbreitet. Die Unendlichkeit der Netze stellte jedoch ein großes Hindernis bei einer Bearbeitung durch Rechner dar. Dieses änderte sich, als Chung et al. [1984] vorschlugen, diese Netze mit sogenannten Quotientengraphen zu beschreiben. Diese Quotientengraphen sind für alle (periodische) Kristalle endlich und damit auf Rechnern bearbeitbar.

Im 2. Kapitel wird diese Überführung einer Kristallstruktur in einen Quotientengraphen und die zugehörige Umkehrung, die Einbettung von Netzen in den Euklidischen Raum, erläutert. Dies wird durch eine Übersicht für spätere Kapitel wichtiger Eigenschaften von Quotientengraphen und Netzen vervollständigt. Dies schließt eine hinreichende Bedingung für Isomorphie von Netzen basierend auf Automorphismen von Quotientengraphen ein. Darüberhinaus werden Invarianten von Netzen und Koordinationsfolgen<sup>1</sup> eingeführt.

Verbindungen zwischen Netzen oder den sie beschreibenden Quotientengraphen und physikalischen Eigenschaften der entsprechenden Kristallstrukturen werden im 3. Kapitel hergestellt. So wird zuerst die der spezifischen Dichte entsprechende topologische spezifische Dichte definiert. Die Definition der topologischen Dichte basiert auf Koordinationsfolgen und kann dazu benutzt werden, für eine hypothetische Struktur (das heißt die Einbettung eines Netzes in den Euklidischen Raum) eine Untergrenze der spezifischen Dichte zu finden. Diese Untergrenze wird für einige Strukturen mit der spezifischen Dichte verglichen. Weiter werden die maximalen Längen der Kanten der Einheitszellen aller möglichen Einbettungen eines Netzes nach oben abgeschätzt. Diese Abschätzung erfolgt ausschließlich durch eine Betrachtung von geschlossenen Pfaden im Quotientengraphen und ist somit sehr einfach durchzuführen. Sie erlaubt es, das Volumen einer Einheitszelle nach oben und

---

<sup>1</sup>Coordination sequences

somit die spezifische Dichte nach unten abzuschätzen.

Diese beiden Abschätzungen werden hier dazu benutzt, in einer Aufzählung solche Quotientengraphen auszuschließen, die offensichtlich nicht in der Natur vorkommenden Kristallstrukturen entsprechen können. Mit Hilfe der in Kapitel 4 aufgezählten Netze wird gezeigt, dass Netze existieren, die ausschließlich anhand einer der beiden Kriterien ausgeschlossen werden können. Die Berechnung beider Abschätzungen stellen im Vergleich zu einer Einbettung eines Netzes und der dazu nötigen Optimierung der Zellparameter, einen wesentlich geringeren Rechenaufwand dar. Ihre Berechnung führt deswegen indirekt zu einer bedeutenden Reduzierung des allgemeinen Aufwands bei Aufzählung von kristallographischen Netzen.

Weiterhin werden zwei neue Klassen von geschlossenen Pfaden<sup>2</sup> eingeführt: gestreckte und vollständig gestreckte geschlossene Pfade<sup>3</sup>. Diese werden daraufhin untersucht, wie spezifisch sie für Netze sind. Drei Beobachtungen sind bemerkenswert:

- Beide Klassen von Pfaden erlauben es Folgen zu definieren, die für über 67'000 nicht-isomorphe Netze unterschiedlich sind. Die Menge dieser Netze beinhaltet alle Netze die durch Quotientengraphen mit vier Knoten vom Grade vier beschrieben werden können,
- Genauer, für die in Kapitel 4 aufgezählten Netzen stellt sich heraus, dass die vollständig gestreckten und geschlossenen Pfade die höchste Spezifität haben (einschließlich geschlossener Pfade und Koordinationsfolgen).
- Diese Pfade erfordern im Vergleich mit den anderen geschlossenen Pfaden den kleinsten rechnerischen Aufwand.

Darüber hinaus werden Kriterien aufgestellt, die es erlauben Netze ohne eine Einbettung (das heißt die Quotientengraphen) daraufhin zu untersuchen, ob sie aus nicht zusammenhängenden Teilnetzen bestehen. Diese Kriterien erlauben es, Netze zu unterscheiden, bei denen diese Teilnetze die Form von Inseln, Ketten oder Schichten (wie zum Beispiel in Talk oder Graphit) haben, oder die aus sich gegenseitig durchdringenden parallelen Netzen (wie zum Beispiel in Cuprit) bestehen. Die Kriterien werden an den Quotientengraphen von Graphit, Talk, Cristobalit und Cuprit vorgeführt.

Ein Algorithmus zur Aufzählung von Quotientengraphen wird im 4. Kapitel vorgestellt. Der Algorithmus wurde mit dem Ziel entwickelt, Kristallstrukturen *ab initio* zu erzeugen. Um diese Aufzählung so effizient wie möglich zu

---

<sup>2</sup>Cycle

<sup>3</sup>Stretched and fully stretched cycle sequences.



gestalten, werden Regeln aufgestellt, die es erlauben viele redundante oder für Kristallstrukturen unzulässige Quotientengraphen von einer Aufzählung auszuschließen:

- Es wird gezeigt, dass gewisse Kombinationen von Vektoren an (anti-) parallelen Kanten ‘Doppelbindungen’ oder sich kreuzenden Bindungen in einer Einbettung entsprechen.
- Eine Betrachtung der Automorphien von Quotientengraphen wird dazu benutzt, um eine Großzahl von Netzen auszuschließen, deren Einbettungen durch Spiegelungen oder durch gewisse Rotationen ineinander übergehen würden.

Eine vollständige Aufzählung aller vierfach koordinierten Netze, deren Einbettungen vier Knoten in einer Einheitszelle besitzen, schließt das Kapitel ab. Diese Aufzählung ergab mehr als 67’000 Netze, unter denen sich das Diamant-Netz (mit doppelter Einheitszelle), das Lonsdaelit-Netz und drei weitere Netze, die möglicherweise bisher unbekanntes  $sp^2$ -Kohlenstoffmodifikationen entsprechen könnten, befanden.

In Kapitel 5 werden Netze und Quotientengraphen neu definiert. Die Definitionen von Netzen und Quotientengraphen folgt der Definition von *voltage graphs*. Die Definitionen haben den Vorteil, dass sie nicht auf Translationen und Atompositionen beruhen und somit von Kristallstrukturen unabhängig sind. Da die Beweise über die Isomorphie von Quotientengraphen gemäß der herkömmlichen Definition nicht mehr anzuwenden sind, werden sie neu durchgeführt. Der wohl wichtigste Beitrag dieser Arbeit ist vermutlich die darauf folgende Betrachtung der Automorphien der Quotientengraphen. Zuerst wird an einem einfachen Beispiel gezeigt, dass unter Zuhilfenahme der Automorphien eines Netzes die Punktgruppe einer Einbettung mit (maximaler) Symmetrie bestimmt werden kann. Weiterhin ergibt sich aus der Annahme einer Einbettung maximaler Symmetrie ein Gleichungssystem, das effektiv die Raumgruppe einer solchen Einbettung bestimmt. Da die Lösung eines solchen Gleichungssystems sehr kompliziert werden kann, wird ein alternativer, direkter und systematischer Ansatz vorgestellt. Dieser Ansatz bestimmt die Punktgruppe und die den einzelnen Rotationen oder Spiegelungen zugehörigen inhärenten Vektoren<sup>4</sup> ausschließlich unter Betrachtung des Quotientengraphen. Der Ansatz wird dazu benutzt zu zeigen, dass die Struktur von Markasit durch eine Verzerrung aus der Pyrit-Struktur hervorgeht. Der Vergleich der Strukturen von Markasit und Rutil lässt vermuten (ohne Zuhilfenahme von Quantenphysik oder ähnlicher Hilfsmittel), dass in Markasit

---

<sup>4</sup>Intrinsic vectors

S-S Bindungen existieren. Dies beruht auf der Beobachtung, dass die An- oder Abwesenheit der entsprechenden Kanten im Quotientengraphen zu unterschiedlichen Automorphismen führen: in Anwesenheit dieser Kanten entspricht der Automorphismus der Raumgruppe in der Markasit kristallisiert, in Abwesenheit der Rutil-Struktur. Eine Analyse von Hoch- und Tiefquarzen zeigt, dass ein bindungserhaltender Phasenübergang nur zwischen gewissen Paaren der enatiomorphen Strukturen möglich ist und ein displaziver Phasenübergang der Hochquarze zu höhersymmetrischen Strukturen ausgeschlossen ist. Eine Diskussion von drei Graphitmodifikationen schließt das Kapitel ab.

Gewisse Quotientengraphen besitzen Automorphien, die Translationen einer Einbettung eines Netzes entsprechen, die nicht mit dem Gitter der ursprünglichen benutzten Einbettung vereinbar sind. Eine Untersuchung dieser Translationen im 6. Kapitel führt zu dem Ergebnis, dass sie Gitter definieren, die kleiner als das Gitter sind, das ursprünglich zur Erzeugung des Quotientengraphen benutzt worden ist. Eine ausführliche Diskussion 2-dimensionaler Beispiele führt zu der Definition des reduzierenden Vektors<sup>5</sup>, der die relative Größe der neuen Gitterkonstanten beschreibt. Dieser Vektor wird ausschließlich unter Zuhilfenahme des Quotientengraphen und eines auszuwählenden Automorphismus bestimmt. Dieser Vektor wird dazu benutzt um den Quotientengraphen zu reduzieren. In anderen Worten, der, dem verkleinerten Gitter entsprechende, Quotientengraph wird bestimmt. Dies entspricht, grob ausgedrückt, einer Verkleinerung einer Superzelle zu einer anderen Super- oder Einheitszelle, möglicherweise in Verbindung mit einer Drehung der Koordinatensystems. Zwei Beispiele mit zwei-dimensionalen Netzen erläutern das Vorgehen. Eines der 2-dimensionalen Beispiele und der einer zentrierten Zelle des Strontium-Feldspats entsprechenden Quotientengraphen zeigen, dass eine direkte Reduktion auf einen Graphen minimaler Größe, zumindest mit der hier vorgestellten Theorie, nicht immer möglich ist.

Für das Halit-Netz wird gezeigt, dass unter der Voraussetzung, dass die beiden Atomsorten nicht unterschieden werden, die Zahl der Knoten im reduzierten Quotientengraph halbiert werden kann. Für den Quotientengraphen, der aus einer rhomboedrisch zentrierten Zelle der Magnesit- oder Kalkspat-Strukturen hervorgeht, wird gezeigt, dass er auf dem einer primitiven Zelle entsprechenden Quotientengraphen reduziert werden kann (jedoch nicht weiter). Ähnlich wird für einen in Raumgruppe  $I2/c$  kristallisierenden Strontium-Feldspat gezeigt, dass eine Reduktion des Quotientengraphen zu einem, einer primitiven Zelle entsprechenden, Graphen führt. Wird angenommen, dass die in dieser Struktur teilweise ungeordneten Al- und Si-Positionen

---

<sup>5</sup>Reduction vector

durch eine Atomsorte ersetzt werden können, besitzt der reduzierte Graph noch einen weiteren reduzierenden Vektor (der einer zentrierten Zelle entsprechende Graph insgesamt drei). Ein Vergleich der unter dem entsprechenden Automorphismus auf einander abgebildeten Positionen und der dort dominierenden Atomsorten führt jedoch zu einem Widerspruch: Al-dominante Positionen werden unter diesem Automorphismus auf Si-dominante Positionen abgebildet. In anderen Worten, sollte eine geordnete Struktur existieren, würde diese eine Einheitszelle der gleichen Größe besitzen.

Zusammenfassend zeigt die hier vorgestellte Arbeit, dass Quotientengraphen und Netze Vorteile in Bezug auf den zur Bestimmung gewisser Eigenschaften nötigen Rechenaufwands mitbringen.

## Abstract

As an alternative approach to lattices and space groups, this work explores graph theory as a means to model crystal structures. The approach uses quotient graphs and nets - the graph theoretical equivalent of cells and lattices - to represent crystal structures.

After a short review of related work, new classes of cycles in nets are introduced and their ability to distinguish between non-isomorphic nets and their computational complexity are evaluated. Then, two methods to estimate a structure's density from the corresponding net are proposed. The first uses coordination sequences to estimate the number of nodes in a sphere, whereas the second method determines the maximal volume of a unit cell. Based on the quotient graph only, methods are proposed to determine whether nets consist of islands, chains, planes, or penetrating, disconnected sub-nets.

An algorithm for the enumeration of crystal structures is revised and extended to a search for structures possessing certain properties. Particular attention is given to the exclusion of redundant nets and those, which, by the nature of their connectivity, cannot correspond to a crystal structure. Nets with four four-coordinated nodes, corresponding to  $sp^3$  hybridised carbon polymorphs with four atoms per unit cell, are completely enumerated in order to demonstrate the approach.

In order to render quotient graphs and nets independent from crystal structures, they are reintroduced in a purely graph-theoretical way. Based on this, the issue of iso- and automorphism of nets is reexamined. It is shown that the topology of a net (that is the bonds in a crystal) constrains severely the symmetry of the embedding (that is the crystal), and in the case of connected nets the space group except for the setting. Several examples are studied and conclusions on phases are drawn (pseudo-cubic  $\text{FeS}_2$  *versus* pyrite;  $\alpha$ - *versus*  $\beta$ - quartz; marcasite- *versus* rutile-like phases).

As the automorphisms of certain quotient graphs stipulate a translational symmetry higher than an arbitrary embedding of the corresponding net would show, they are examined in more detail and a method to reduce the size of such quotient graphs is proposed. Besides two instructional examples with 2-dimensional graphs, the halite, calcite, magnesite, barytocalcite, and a strontium feldspar structures are discussed. For some of the structures it is shown that the quotient graph which is equivalent to a centred cell is reduced to a quotient graph equivalent to the primitive cell. For the partially disordered strontium feldspar, it is shown that even if it could be annealed to an ordered structure, the unit cell would likely remain unchanged. For the calcite and barytocalcite structures it is shown that the equivalent nets are not isomorphic.

# Contents

<b>1</b>	<b>Introduction</b>	<b>1</b>
1.1	Overview . . . . .	2
1.2	Objectives . . . . .	3
1.3	Contributions . . . . .	3
<b>2</b>	<b>Foundations</b>	<b>5</b>
2.1	From crystals to quotient graphs . . . . .	5
2.2	From quotient graphs to crystal structures . . . . .	7
2.3	Isomorphism of nets and quotient graphs . . . . .	7
2.4	Invariants . . . . .	10
2.5	Coordination sequences . . . . .	11
<b>3</b>	<b>Properties of Nets and Crystals</b>	<b>13</b>
3.1	Nets with non-penetrating, disconnected sub-nets . . . . .	13
3.2	Penetrating, disconnected nets . . . . .	14
3.3	Cycle sequences . . . . .	20
3.4	Stretched and fully stretched cycles . . . . .	21
3.5	Density and coordination sequences . . . . .	24
3.6	Density <i>versus</i> unit cell volume . . . . .	27
<b>4</b>	<b>Nets and Their Enumeration</b>	<b>31</b>
4.1	The enumeration of crystal structures . . . . .	32
4.1.1	The basic enumeration procedure . . . . .	33
4.1.2	Parallel edges in quotient graphs . . . . .	34
4.1.3	Penetrating and non-penetrating sub-nets . . . . .	35
4.1.4	Elimination of redundant nets . . . . .	35
4.1.5	Desired properties of crystals . . . . .	36
4.2	The nets with 4 nodes of degree 4 . . . . .	36
<b>5</b>	<b>Nets and Space Groups</b>	<b>39</b>
5.1	Crystals, graphs, and voltage graphs . . . . .	39

5.2	Isomorphism of quotient graphs and nets . . . . .	41
5.3	The space group of possible embeddings. . . . .	47
5.4	Automorphism of QGs and crystal structures . . . . .	52
5.5	Pyrite . . . . .	54
5.6	Marcasite and rutile . . . . .	54
5.7	Quartz . . . . .	60
5.8	Graphite . . . . .	62
<b>6</b>	<b>Reduction of Quotient Graphs</b>	<b>65</b>
6.1	Automorphism and translational symmetry . . . . .	66
6.1.1	Reduction for vectors of type $\mathbf{t} = (\frac{1}{k}, \frac{1}{\ell}, \frac{1}{m}, \dots)$ . . . . .	71
6.1.2	Reduction for vectors of type $\mathbf{t} = (\frac{1}{\mathcal{O}}, \frac{1}{\mathcal{O}}, \dots)$ . . . . .	72
6.1.3	Reduction of disconnected QGs . . . . .	73
6.2	The reduction of the square net . . . . .	74
6.3	The reduction of the triangle net . . . . .	74
6.4	Halite . . . . .	76
6.5	Calcite and magnesite . . . . .	77
6.6	Barytocalcite . . . . .	81
6.7	Celsian and strontium feldspar . . . . .	82
6.8	Remarks . . . . .	85
<b>7</b>	<b>Conclusion</b>	<b>87</b>
7.1	Future work . . . . .	89
<b>A</b>	<b>Crystal Structures</b>	<b>91</b>
<b>B</b>	<b>Quotient Graphs</b>	<b>99</b>

# Chapter 1

## Introduction

The most common models of crystals are based on the observation that an (ideal) crystal possesses a periodic arrangement of atoms in a lattice with a translational symmetry. This lattice is used to define unit cells and a coordinate system. Most importantly, within these unit cells, atoms are attributed with coordinates, called positions and their ensemble show symmetries, which are usually classified by point or space groups. These coordinates and symmetries are then, in combination with quantum and other theories, used to determine physical properties of a crystal structure; or *vice versa*, physical properties are used to determine these coordinates [Wenk and Bulakh, 2004, Putnis, 1992].

The approach presented here follows a different strategy: crystals are interpreted as graphs<sup>1</sup>, in which atoms are interpreted as nodes and bonds as edges. Or, in a generalised interpretation, groups of bond atoms (molecules) can be mapped onto a single node, and sequences of bonds, 2-coordinated atoms (e.g. -O- bridges) as edges. This type of model is commonplace in chemistry or biology: it often gives a good insight to a substance's properties. This approach is not foreign to crystallography; early in the last century, Laves [1926a,b] used graphs (though he did not explicitly use the term *graph*) to describe and analyse crystal structures. However, graphs were exclusively used in figures to visually represent crystals, only informal links to their physical properties were established. Probably the main reason for this was the inability to mathematically manipulate the infinite graphs which crystals effectively represent.

About a half a century after F. Laves introduced the use of graphs into crystallography, Wells [1977, 1979] used graph theory to predict crystal structures. Though his contribution is certainly ground breaking, no link is yet

---

<sup>1</sup>See Wilson and Watkins [1990], Harary [1969] for an introduction to graph theory.

made between graphs and physical properties, and the difficulty with the infinity of graphs persists. The latter is overcome by Chung et al. [1984]: they proposed to describe the infinite crystal graphs or *nets* by finite *quotient graphs* (QG). This opened the avenue for the use of graph theory in approaches that characterise, analyse, or predict crystal structures in new ways [Goetzke and Klein, 1991, Beukeman and Klee, 1994, Klein, 1996, Meier et al., 1996, Thimm and Klee, 1997, Peresypkina and Blatov, 2000, Blatov, 2000, Baerlocher and McCusker, 2007]. Yet, the theory of properties particular to these nets, which describe atoms and bonds in a crystal, is little developed and their relation to physical properties of crystal structures has not been studied to any significant extent.

## 1.1 Overview

The following chapter presents work related to the later chapters. In particular, it presents the conventional way of defining quotient graphs, outlines the transformation of QGs into crystal structures and back, and discusses past work on the isomorphism of nets and their invariants.

In chapter 3, coordination sequences are set into a relation with the specific density and the maximal size of unit cells in crystals. Then, conventional, stretched, and fully stretched cycle sequences are examined with respect to their specificity in distinguishing different topologies. This is followed by a discussion of two types of disconnected sub-nets, penetrating and non-penetrating nets, and means to determine to which of these sets a net belongs.

The enumeration of QGs is addressed in chapter 4. This chapter proposes a basic enumeration procedure and means to improve its efficiency. The chapter concludes with results from a complete enumeration of nets equivalent to all crystal structures with four four-coordinated atoms per unit cell. These nets were then examined for whether they could represent  $sp^3$  carbon structures. This resulted in known structures, as for example diamond and lonsdaleite, and in three nets for which an analysis based on quantum mechanical principles stipulates that equivalent non-metallic carbon modifications are stable.

On a first impression, graphs have little in common with space groups: graphs retain no obvious trace of atom positions, whereas space groups ignore inter-atomic bonds. That this first impression is wrong is shown in chapter 5, where first quotient graphs and nets - the graph theoretical equivalent of cells and crystal structures - are reintroduced independent from crystal structures. Based on this, iso- and automorphisms of nets, the graph theoretical equiv-



alent of symmetry operations, are closer examined. As result, it is shown that the topology of a net (that is the bonds in a crystal) constrains severely the symmetry of all possible embeddings (that is the crystal structures with this topology). This observation allows to determine the space group of a maximal-symmetry embedding in the case of a connected net except for the setting.

Chapter 6 discusses the reduction of quotient graphs. This reduction is comparable to changing the cell used to represent a structure to a smaller cell (*e.g.* use a primitive cell instead of a super- or centred cell). The procedure is demonstrated using artificial 2-dimensional examples and several known crystal structures.

## 1.2 Objectives

This work has as objective

- to establish links between the net topology (as defined by a QG) and physical properties of crystal structures, and
- to enumerate net topologies which may represent crystal structures.

## 1.3 Contributions

- A definition of nets and QGs based on voltage graphs that does not rely on a crystal structure.
- A proof that the topology of a net (that is the automorphisms of the quotient graph) determines to a wide extend the maximal symmetry of a structure that possesses this topology. Examples illustrating the determination of the space group with a maximal symmetry and implications of this theorem are given.
- An algorithm that allows a reduction of a QG in the presence of QG automorphisms. This reduction corresponds to finding a smaller unit cell of a net embedded with a translational higher symmetry than that of the QG determined from the original embedding.
- A general algorithm that allows in principle a complete enumeration of all periodic crystal structures. The computational complexity is prohibitive for structures represented by quotient graphs in which the number of edges significantly exceeds the number of nodes. Hence,

several criteria are proposed that allow a more directed search and therefore the expansion of the searchable domain of quotient graphs if the topology of the structure is significantly reduced.

- A link from coordination sequences to a minimal specific density and maximal volume of a unit cell in an arbitrary embedding of a net.
- Definitions of stretched and fully stretched cycle sequences, which share some of the properties of cycle sequences, yet have a significantly lower computational complexity.

# Chapter 2

## Foundations

This section presents the transformation of a crystal structure into a quotient graph (QG) as originally introduced by Chung et al. [1984]. In most of this dissertation, their definition is applicable. However, in chapter 5 QGs and nets are redefined independent of crystal structures. This is mainly done with the intention to allow a discussion that is independent of cell parameters and atom positions. As Chung's definition is somewhat more intuitive, the newer definition is used only where a more rigorous discussion is of order.

Furthermore, some properties of nets, which play a role in later chapters, are discussed.

### 2.1 From crystals to quotient graphs

The most natural way to achieve a transformation of a crystal structure into a QG is the association of atoms with nodes and covalent bonds with edges in a graph. However, other, herein not further discussed possibilities exist. For example, groups of atoms can be mapped onto one node, or an oxygen bridge could be identified with a single edge. In any case, the transformation results into an infinite, periodic graph called *net*. The net is referred to as being or being not embedded; where an embedded net differs from the later by having precise locations assigned to each node (a crystal is therefore an embedded net) [see Goetzke, 1992, Goetzke and Klein, 1991, Schumacher, 1994, Chung et al., 1984].

The transformation of a crystal structure into a quotient graph depends on conventional structural properties. Let vectors  $\mathbf{a}$ ,  $\mathbf{b}$ , and  $\mathbf{c}$  define a coordinate system that is compatible with the examined structure. Then, in this coordinate system, coordinates of atoms are described by  $(k \cdot \mathbf{a} + x, l \cdot \mathbf{b} + y, m \cdot \mathbf{c} + z)$  where  $0 \leq x, y, z < 1$  are conventional (fractional) atom coordinates

and the integers  $k, l$ , and  $m$  enumerate the unit cells. The components  $k, l$  and  $m$  are grouped together in a vector  $\mathbf{x} \in \mathbb{I}^3$  and attributed to each node in the net.  $n_1, n_2, n_3, \dots$  are sets of translationally equivalent nodes (atoms). Then each node (atom) is uniquely identified as  $n_i(\mathbf{x})$ ; that is by its set and a vector (nodes in a unit cell are labelled with the same vector).

A quotient graph is then defined as a graph with nodes  $n_1, n_2, n_3, \dots$ , which are associated with the sets of nodes in the net of the same name. Furthermore, for each set of translationally equivalent atom bonds, which connect atoms  $n_i(\mathbf{x})$  and  $n_j(\mathbf{x}')$ , the quotient graph has an edge  $n_i \xrightarrow{\mathbf{x}' - \mathbf{x}} n_j$ , with the orientation from  $n_i$  to  $n_j$  and the label (vector)  $\mathbf{v} = \mathbf{x} - \mathbf{x}'$  attached to it.

Similar definitions can be made for crystal-like structures in any dimension and most results can be extrapolated. For the reason that 3-dimensional graphs are difficult to visualise, 2-dimensional examples will often be used. An example for transformations of a 2-dimensional hexagonal net into a quotient graph is illustrated in figure 2.1.

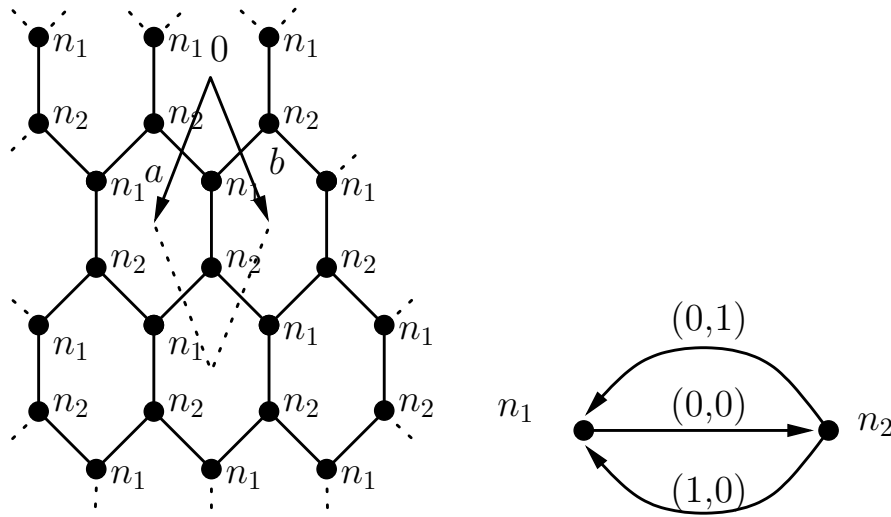


Figure 2.1: The 2-dimensional, hexagonal net and a possible representation as quotient graph.

A quotient graph for a crystal (embedded net) is not unique. For example, the labels attached to the edges depend on the choice of the coordinate system. Also, the shape of the quotient graph may vary (as shown in Bader et al. [1997]), depending on the way the net is embedded in Euclidean space.

## 2.2 From quotient graphs to crystal structures

The creation of an embedded net from a quotient graph is in principle very simple: it is sufficient to assign to each node in the quotient graph a vector  $(x, y, z)$ , select a coordinate system (*i.e.* the lengths of the unit vectors and angles between the axes) and unfold the QG. However, the choice of the coordinate system and positions of nodes in a unit cell is difficult, as nature imposes constraints such as minimal and maximal distances between bond and unbound atoms. Due to the high number of constraints and free variables, no direct solution to the problem is known. The only feasible way is to formulate the problem as an optimisation problem. A *crystallographic embedding*, that is an embedding in Euclidean space which agrees well with the laws of physics, can for example be attempted using quantum mechanical calculations [Winkler et al., 1999].

A serious shortcoming of this approach is that a majority of the enumerated quotient graphs are equivalent to nets for which no crystal structure can exist. Several ways to eliminate some of them beforehand are discussed later. Unfortunately, current knowledge does not permit an elimination of all pathological quotient graphs without an attempt to embed the corresponding nets. As embedding a net is essentially an optimisation, it is computationally costly and may result in an erroneous rejection of a net.

## 2.3 Isomorphism of nets and quotient graphs

In the same spirit in which structures are classified into structure types, it is desirable to have the means to compare nets and quotient graphs for similarity. This is achieved by applying the conventional definition of graph isomorphism to nets [Gould, 1988]. Two net are isomorphic, if a bijective function exists, which maps all nodes in the first graph such on the nodes in the second graph so that if, and only if, two nodes in the first graph are linked by an edge, then there is also an edge between the images of these nodes. More formally:

**Definition 2.3.1.** *Let  $\mathbf{G}$  and  $\mathbf{G}'$  be two nets with nodes  $\mathbf{G}_N$  and  $\mathbf{G}'_N$  and edges  $\mathbf{G}_E$  and  $\mathbf{G}'_E$ . Then  $\mathbf{G}$  and  $\mathbf{G}'$  are isomorphic if, and only if, a bijective function  $\phi : \mathbf{G}_N \rightarrow \mathbf{G}'_N$  exists such that for all edges  $n \leftrightarrow m \in \mathbf{G}_E$  the edge  $\phi(n) \leftrightarrow \phi(m)$  exists in  $\mathbf{G}'_E$ .*

Unfortunately, this definition cannot be consistently applied to QGs, as QG with rather different appearance can be derived from the same net or

structure; yet the nets are the entities one is interested in. Consequently:

**Definition 2.3.2.** *Quotient graphs are isomorphic if, and only if, they can be derived from the same or an isomorphic net (or, alternatively, define isomorphic nets).*

Net isomorphism is defined in the same way as for finite graphs. However, unlike finite graphs, nets cannot easily be examined with a computer. On the other hand, the quotient graph's shape and labels depend much on the embedding of the net and the choice of the cell used for its creation. Therefore, other means of comparing nets based on QGs are necessary.

This definition of (graph) isomorphism does often match the crystallographic understanding of isomorphism, in which the morphology of crystals is compared [*e.g.* Wenk and Bulakh, 2004]. Consider, for example, the rhombohedral carbonates magnesite, smithsonite, siderite, rhodochrosite, and calcite, which are isostructural (structure data from Downs and Hall-Wallace [2003]). Their respective QGs differ only in the labels of the nodes equivalent to the cations<sup>1</sup> and are isomorphic in both interpretations. On the other hand, the rhombohedral carbonates are not isomorphic to their orthorhombic counterparts in either sense: the coordination of the cations is 9 instead of 6 [see Pannhorst and Lohn, 1970], implying that the nets cannot be isomorphic.

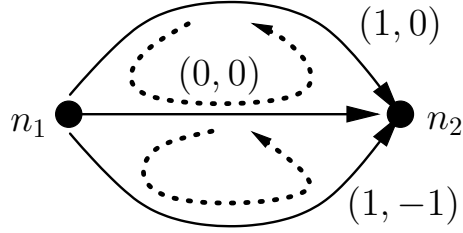
However, in some cases the two definitions may conflict. For example the graphs describing pyrite and marcasite are isomorphic, yet the appearance of their crystals is rather distinct (compare sections 5.5 and 5.6).

In cases where the base graphs, that is the QGs stripped of all labels, of QGs are isomorphic, a possible isomorphism of the net can be shown. Goetzke proposed to use QGs to conclude on a possible isomorphism of the equivalent nets (see the remainder of this section and sections 5.2). This requires the knowledge of so-called *cycle sums*, which are calculated from the quotient graph. In an embedded net equivalent to a QG, a cycle sum  $\oplus$  describes the relative position of two translationally equivalent atoms in terms of unit cells. The relative positions together with the topology of the quotient graph provide enough information to determine a net's topology. A cycle sum  $\oplus$  can be calculated by orienting all edges in the sense of the cycle and then adding all labels of edges. The reorientation of an edge  $n_i \xrightarrow{\mathbf{v}} n_j$  is achieved by replacing the edge with  $n_j \xrightarrow{-\mathbf{v}} n_i$  (i.e. by negating the label and inverting the orientation to the edge). See figure 2.2 for an example.

In the following, a *basic set of cycles* is always used, where *basic* means that the explicitly given cycle sums are sufficient to determine the cycle sums of all other cycles in the QG (the cycle sums form a vector space with a finite

---

<sup>1</sup>This only minor difference is also due to the similar settings in the structure data.



Upper cycle without reorientation:  $\mathcal{C}_1 = n_1 \xrightarrow{(0,0)} n_2, n_1 \xrightarrow{(1,0)} n_2$   
 Cycle sum:  $\mathcal{C}_1 = (-1, 0)$

Upper cycle after reorientation:  $\mathcal{C}_1 = n_1 \xrightarrow{(0,0)} n_2, n_2 \xrightarrow{(-1,0)} n_1$   
 Cycle sum:  $\mathcal{C}_1 = (-1, 0)$

Lower cycle after reorientation:  $\mathcal{C}_2 = n_2 \xrightarrow{(0,0)} n_1, n_1 \xrightarrow{(1,-1)} n_2$   
 Cycle sum:  $\mathcal{C}_2 = (1, -1)$

Figure 2.2: An example for cycle sums.

base). If a quotient graph comprises  $n$  nodes and  $m$  edges, a basic set of cycle sums consists of  $m - n + 1$  cycles. A convenient way to obtain a basic set is to chose an arbitrary spanning tree of the QG. Then, the basic set consists of all cycles, which possess exactly one edge that is not part of this tree and zero or more edges that are (the spanning tree may have non-zero labels).

Goetzke defines two QGs to be isomorphic if and only if an isomorphism of the two quotient graphs  $\mathbf{Q}$  and  $\mathbf{Q}'$  as plain graphs exist such that the cycle sums  $\mathcal{C}_k$  and  $\mathcal{C}'_k$  over all cycles  $\mathcal{C}_k$  of  $\mathbf{Q}$  and the equivalent  $\mathcal{C}'_k$  of  $\mathbf{Q}'$  can be transformed into each other via an orthogonal matrix  $\mathbf{W}$  (adapted from Goetzke [1992]):

$$\text{for all } k: \mathcal{C}_k * \mathbf{W} = \mathcal{C}'_k. \tag{2.1}$$

It can be easily seen, that if two QGs are isomorphic according to Goetzke, the equivalent nets are isomorphic. However, the inverse statement is false. Two possible known reasons for this are:

1. The embedding of one net is the result of a non-affine distortion of the other embedding.
2. The selected cells for the transformation of the net to the QG are different in shape (*e.g.* include a different number of atoms).

Both cases lead to QGs that are non-isomorphic as plain graphs. However, it is an open question, whether nets can be isomorphic, possess QGs, which are isomorphic as plain graphs, but the representing QGs are not isomorphic according to Goetzke.

Klee [2004] examined automorphisms of quotient graphs closer and discovered that they allow to determine the point group and lattice type of a possible embedding.

## 2.4 Invariants

An invariant of a quotient graph or a net is typically a sequence of numbers which is identical for isomorphic nets or QGs. They are of some importance in the classification of crystal structures as a direct comparison is often difficult or impossible [Meier et al., 1996, Baerlocher and McCusker, 2007, Peresypkina and Blatov, 2000, Thimm and Klee, 1997]. These properties also have some importance for the enumeration of nets, as they permit to recognise pathological nets, help to target the search for new structures and to reduce significantly the complexity of eliminating redundant QGs (chapter 4).

A few among many invariants are:

- The spectrum of the degrees of nodes.
- The sizes of rings<sup>2</sup> or the loop configuration showing the number of 3- or 4-member rings a node or atom is part of [O’Keeffe and Brese, 1992, Baerlocher and McCusker, 2007, Meier et al., 1996, Yuan and Cormack, 2002].
- Coordination sequences (see section 2.5).
- Cycle sequences (see section 3.3).

In contrast to what may be expected is the observation that most properties of the QGs are not invariants. For example:

- The size (the number of nodes) of a QG is not an invariant as larger QGs describing the same net can be systematically constructed [Schumacher, 1994].
- QGs with the same size but a different connectivity of the base graph can describe the same net [Schumacher, 1994].

Rings and certain variations of them have a (weak) link to crystal properties; further references can be found in [Yuan and Cormack, 2002].

---

<sup>2</sup>A ring is a closed path, in which for all pairs of nodes at least one of the shortest paths between these nodes is part of the path.



## 2.5 Coordination sequences

Coordination sequences are a property common to a set of isomorphic nodes and are used in various ways [Beukeman and Klee, 1994, Blatov, 2000, Brunner, 1979, Grosse-Kunstleve et al., 1996]. Let  $n_i(\mathbf{0})$  be the starting node<sup>3</sup> of an infinite sequence  $(s_1^{n_i}, s_2^{n_i}, s_3^{n_i}, \dots)$  that describes the number of nodes that are reachable by following paths<sup>4</sup> of lengths 1, 2, 3 and so on, where each node is counted only once in the coefficient with the lowest index. In these sequences,  $s_1^{n_i}$  is equal to the degree of node  $n_i(\mathbf{0})$ . The superscript in the sequence contains the set (and not the node) as, due to the translational symmetry of the net-defining crystal structure, sequences starting at nodes in the same set  $n_i$  are identical. A set of initial sequences, or more convenient for comparison, the average sequence  $(\overline{s}_1, \overline{s}_2, \dots)$  over of all coordination sequences, are invariant of a set of isomorphic nets. Unfortunately, some non-isomorphic nets bear identical sequences, and the average sequences are in general not integer.

Coordination sequences were used by Grosse-Kunstleve et al. [1996] to define the *topological density* of a crystal in an algebraic definition (based on polynomials describing the coordination sequences). This density (or more precisely, an estimate of it) is catalogued in a database of zeolite structures [Meier et al., 1996, Baerlocher and McCusker, 2007], but no relation to, for example, specific densities was drawn. TOPOLAN - a program for the calculation of coordination sequences - can be obtained from Thimm [2007].

---

<sup>3</sup> $\mathbf{x} = \mathbf{0}$  can be chosen as the sequences are identical for isomorphic nodes, including all  $\mathbf{x} \in \mathbb{I}^3$ .

<sup>4</sup>A path is sequence of nodes connected by edges, where no node appears more than once.



# Chapter 3

## Properties of Nets and Crystals

This chapter tries to establish relationships between certain graph theoretical properties and physical properties of crystal structures.

### 3.1 Nets with non-penetrating, disconnected sub-nets

Numerous nets obtained from crystals are disconnected and, if embedded, sub-nets can be placed at any arbitrary distance to each other without changing the distance between connected nodes. This is, for example, the case for graphite as shown in figure 3.1 or talc ( $\text{Mg}_3\text{Si}_4\text{O}_{12}\text{H}_2$  [Gruner, 1934, Putnis, 1992]). The QG of talc is shown in table 3.1 (see also figure 3.2 and table A.16).

Depending on the chosen orientation of the coordinate system and chosen origin used during the construction of the QG, this may or may not be obvious from the QG. For example: all  $z$ -components of labels in the QG of graphite in figure 3.3 are zero. Consequently, the net is not connected in this orientation.

For some choices of the coordinate system, non-zero components may exist for each dimension. This is the case for the QG of talc. Although some edges have labels with non-zero elements for all coordinates (including the direction of the  $z$ -axis), the cycle sum matrix is of rank 2 and it can be correctly concluded that talc has a sheet-like structure.

**Definition 3.1.1.** *The dimensionality  $\hat{d}$  of a net defined by a connected QG with cycle sum matrix  $\mathbf{C}$  is defined as*

$$\hat{d} = \text{rank}(\mathbf{C}) \tag{3.1}$$

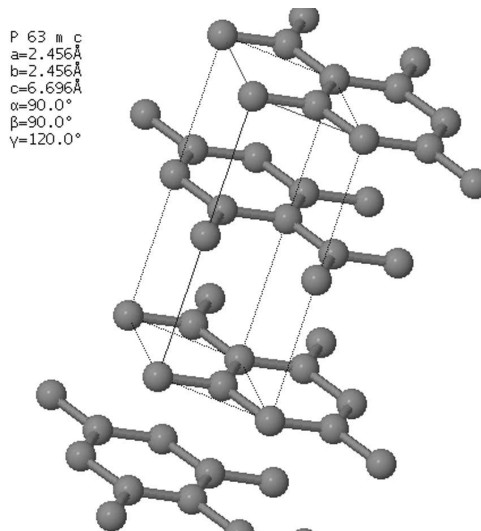


Figure 3.1: The structure of “un-buckled” graphite (figure created using data from Downs and Hall-Wallace [2003]). Carbons are located at  $(0, 0, 0)$  and  $(\frac{1}{3}, \frac{2}{3}, 0)$  and symmetrically equivalent positions.

If embedded, (sub-)nets have the form of islands, chains, or planes, as already observed by Laves [1926a]. The types of nets depend on whether  $\hat{d}$  has the value 0, 1, or 2, respectively.

## 3.2 Penetrating, disconnected nets

Simply connected QGs may define nets with disconnected, isomorphic sub-nets. However, unlike the nets considered in section 3.1, the shortest distance between nodes of disconnected sub-nets cannot be arbitrary large without changing the distances between connected nodes. For these nets, the dimensionality of (sub-)nets is equal to the dimensionality of the edge labels. The situation is illustrated in figure 3.4: the isomorphic sub-nets with black and white nodes are disconnected as no edge connects a white and a black node. However, all nodes in the net are mapped onto the same node in the QG. The resulting QG has therefore only one node and is connected.

Three-dimensional nets in this category are not pathological, and are observable in nature. For example, cuprite ( $\text{Cu}_2\text{O}$  [Downs and Hall-Wallace, 2003]) consists of two cristobalite-like structures [Laves, 1926b]. Some of these nets are equivalent to the isomorphic, dual nets as described in Delgado-Friedrichs et al. [2003].

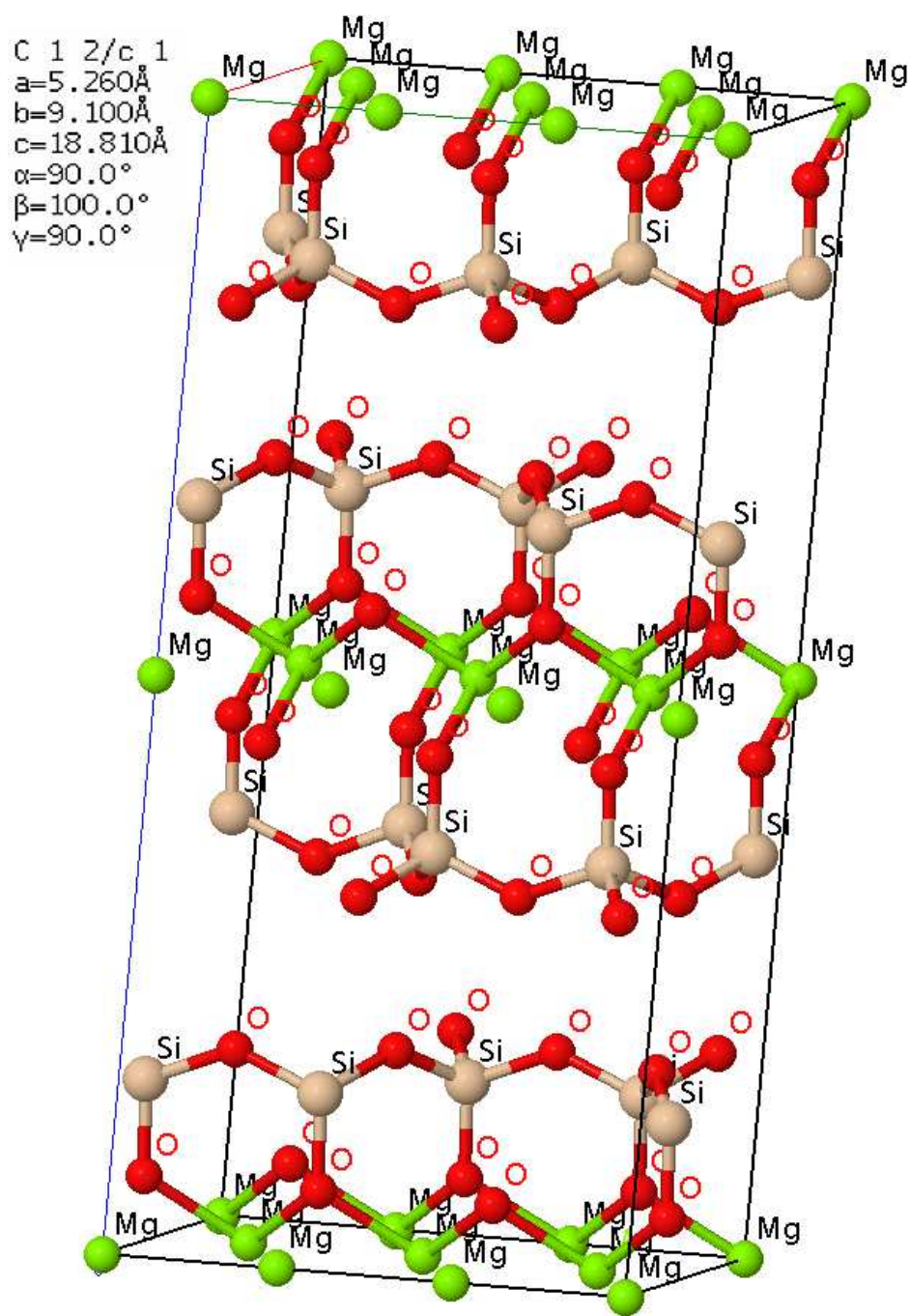


Figure 3.2: A unit cell of the talc structure: the sheets extend horizontally out of the page (see also table A.16, Gruner [1934]).

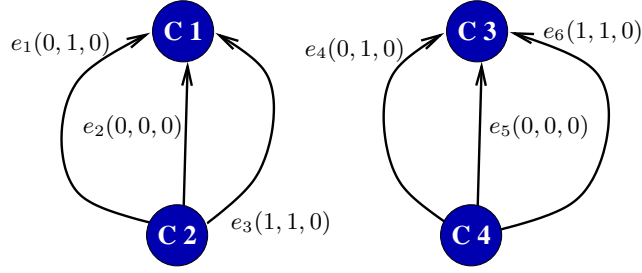


Figure 3.3: The graphite QG

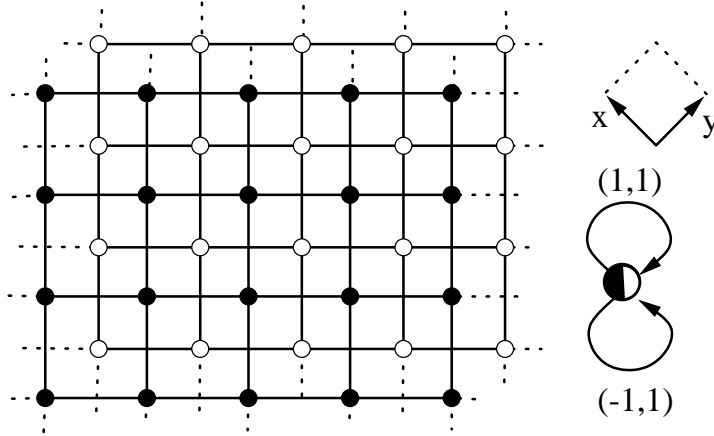


Figure 3.4: A net with disconnected sub-nets and its quotient graph.

Whether or not a quotient graph describes a disconnected three-dimensional net can be easily determined (without proof).

**Definition 3.2.1.** *Be  $\mathbf{Q}$  a connected QG and the matrix  $\mathbf{C}$  be comprised of rows of cycle sum vectors. Then, the multiplicity  $m$  of all nets described by  $\mathbf{Q}$  is defined as*

$$\hat{m} = \min_{\mathbf{C}'} |\det(\mathbf{C}')| \text{ with } \det(\mathbf{C}') \neq 0 \quad (3.2)$$

*where the matrices  $\mathbf{C}'$  are of the same rank as  $\mathbf{C}$ , square, and obtained by an arbitrary deletion of rows and columns from  $\mathbf{C}$ .*

From observation,  $\hat{m}$  equals the number of disconnected sub-nets in the net defined by the QG. For example, the net is composed of two isomorphic sub-nets if  $\hat{m} = 2$ , or using Delgado-Friedrichs' nomenclature, it consists of two isomorphic, dual nets.

For example, figure 3.5 shows the cuprite structure: atoms represented as large spheres form one the dual nets, small spheres the other (structures see

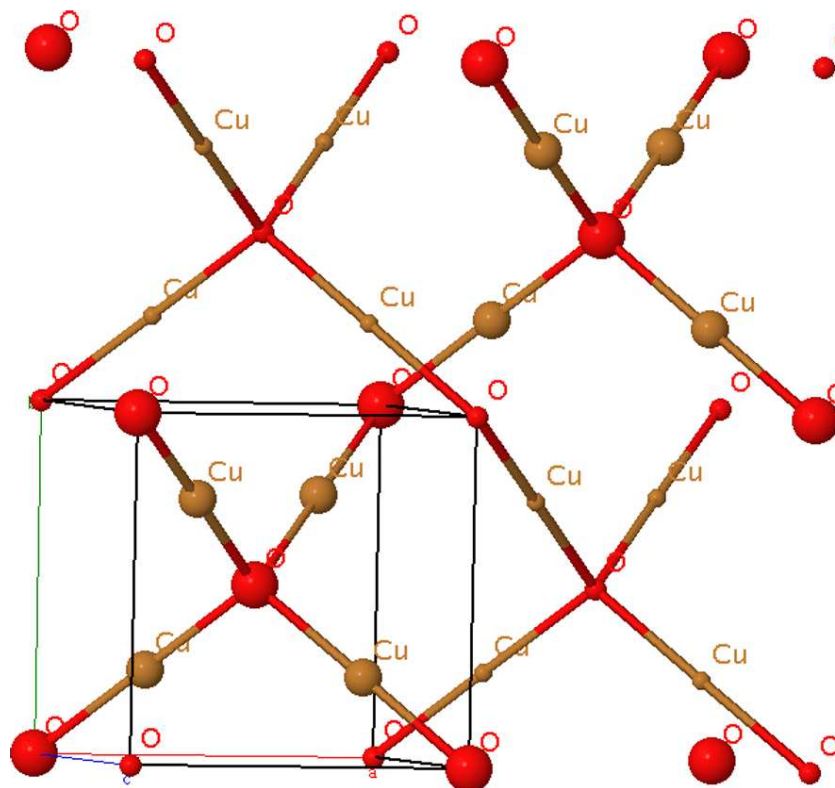


Figure 3.5: The cuprite structure ([Downs and Palmer, 1994, Downs and Hall-Wallace, 2003].

$\text{Mg}_1 \xrightarrow{(-1,-1,0)} \text{O}_1$	$\text{Mg}_1 \xrightarrow{(-1,-1,0)} \text{O}_2$	$\text{Mg}_1 \xrightarrow{(-1,-1,0)} \text{OH}_1$	$\text{Mg}_1 \xrightarrow{(0,0,0)} \text{O}_3$
$\text{Mg}_1 \xrightarrow{(0,0,0)} \text{O}_4$	$\text{Mg}_1 \xrightarrow{(0,0,0)} \text{OH}_2$	$\text{Mg}_2 \xrightarrow{(-1,0,0)} \text{O}_2$	$\text{Mg}_2 \xrightarrow{(0,0,0)} \text{O}_3$
$\text{Mg}_2 \xrightarrow{(0,0,0)} \text{O}_1$	$\text{Mg}_2 \xrightarrow{(0,0,0)} \text{O}_4$	$\text{Mg}_2 \xrightarrow{(0,0,0)} \text{OH}_1$	$\text{Mg}_2 \xrightarrow{(0,1,0)} \text{OH}_2$
$\text{Mg}_3 \xrightarrow{(-1,0,1)} \text{OH}_3$	$\text{Mg}_3 \xrightarrow{(0,-1,0)} \text{O}_5$	$\text{Mg}_3 \xrightarrow{(0,0,-1)} \text{O}_7$	$\text{Mg}_3 \xrightarrow{(0,0,-1)} \text{O}_8$
$\text{Mg}_3 \xrightarrow{(0,0,0)} \text{O}_6$	$\text{Mg}_3 \xrightarrow{(0,0,0)} \text{OH}_4$	$\text{Mg}_4 \xrightarrow{(-1,0,0)} \text{OH}_4$	$\text{Mg}_4 \xrightarrow{(0,0,-1)} \text{O}_7$
$\text{Mg}_4 \xrightarrow{(0,0,-1)} \text{OH}_3$	$\text{Mg}_4 \xrightarrow{(0,0,0)} \text{O}_5$	$\text{Mg}_4 \xrightarrow{(0,0,0)} \text{O}_6$	$\text{Mg}_4 \xrightarrow{(0,1,-1)} \text{O}_8$
$\text{Mg}_5 \xrightarrow{(-1,-1,-1)} \text{O}_7$	$\text{Mg}_5 \xrightarrow{(-1,-1,0)} \text{O}_5$	$\text{Mg}_5 \xrightarrow{(-1,-1,0)} \text{OH}_4$	$\text{Mg}_5 \xrightarrow{(0,0,-1)} \text{O}_8$
$\text{Mg}_5 \xrightarrow{(0,0,-1)} \text{OH}_3$	$\text{Mg}_5 \xrightarrow{(0,0,0)} \text{O}_6$	$\text{Mg}_6 \xrightarrow{(0,-1,0)} \text{OH}_1$	$\text{Mg}_6 \xrightarrow{(0,0,0)} \text{O}_1$
$\text{Mg}_6 \xrightarrow{(0,0,0)} \text{O}_2$	$\text{Mg}_6 \xrightarrow{(0,0,0)} \text{O}_3$	$\text{Mg}_6 \xrightarrow{(0,0,0)} \text{OH}_2$	$\text{Mg}_6 \xrightarrow{(1,0,0)} \text{O}_4$
$\text{O}_1 \xrightarrow{(0,0,0)} \text{Si}_3$	$\text{O}_2 \xrightarrow{(0,0,0)} \text{Si}_4$	$\text{O}_9 \xrightarrow{(-1,0,0)} \text{Si}_4$	$\text{O}_9 \xrightarrow{(0,1,0)} \text{Si}_1$
$\text{O}_{10} \xrightarrow{(0,-1,0)} \text{Si}_5$	$\text{O}_{10} \xrightarrow{(1,0,0)} \text{Si}_2$	$\text{O}_{11} \xrightarrow{(0,-1,0)} \text{Si}_3$	$\text{O}_{11} \xrightarrow{(1,0,0)} \text{Si}_6$
$\text{O}_3 \xrightarrow{(0,0,0)} \text{Si}_1$	$\text{O}_4 \xrightarrow{(0,0,0)} \text{Si}_6$	$\text{O}_5 \xrightarrow{(0,0,0)} \text{Si}_5$	$\text{O}_6 \xrightarrow{(0,0,0)} \text{Si}_2$
$\text{O}_7 \xrightarrow{(0,0,0)} \text{Si}_7$	$\text{O}_8 \xrightarrow{(0,0,0)} \text{Si}_8$	$\text{O}_{12} \xrightarrow{(-1,0,0)} \text{Si}_7$	$\text{O}_{12} \xrightarrow{(0,1,0)} \text{Si}_8$
$\text{O}_{13} \xrightarrow{(0,0,0)} \text{Si}_1$	$\text{O}_{13} \xrightarrow{(0,0,0)} \text{Si}_4$	$\text{O}_{14} \xrightarrow{(0,0,0)} \text{Si}_2$	$\text{O}_{14} \xrightarrow{(0,0,0)} \text{Si}_5$
$\text{O}_{15} \xrightarrow{(0,0,0)} \text{Si}_3$	$\text{O}_{15} \xrightarrow{(0,0,0)} \text{Si}_6$	$\text{O}_{16} \xrightarrow{(0,0,0)} \text{Si}_7$	$\text{O}_{16} \xrightarrow{(0,0,0)} \text{Si}_8$
$\text{O}_{17} \xrightarrow{(-1,0,0)} \text{Si}_4$	$\text{O}_{17} \xrightarrow{(0,0,0)} \text{Si}_1$	$\text{O}_{18} \xrightarrow{(0,-1,0)} \text{Si}_5$	$\text{O}_{18} \xrightarrow{(0,0,0)} \text{Si}_2$
$\text{O}_{19} \xrightarrow{(0,0,0)} \text{Si}_3$	$\text{O}_{19} \xrightarrow{(1,0,0)} \text{Si}_6$	$\text{O}_{20} \xrightarrow{(0,0,0)} \text{Si}_7$	$\text{O}_{20} \xrightarrow{(0,1,0)} \text{Si}_8$

Table 3.1: The QG of talc

tables A.5 and A.6). If, say, the sub-structure comprising the small spheres is removed, a structure similar to that of cristobalite is obtained.

Figure 3.6 shows two possible QGs for the cycle sum matrices and their determinants. The cycle sum matrices are calculated for spanning trees comprising the four edges on the left and the top right edge in each graph.

Assuming that the minimal absolute, non-zero determinant of the cycle sum matrix equals the multiplicity  $\hat{m}$  of the net described by the QG,

- the QG possesses a spanning tree with zero-labels (*i.e.* all atoms in a unit cell are linked by a chain of bonds contained in the cell) and
- only edge labels in  $\{-1, 0, 1\}$  are permitted (*i.e.* the distances between parallel faces of a unit cell is larger than an atom bond),

then the multiplicity of a  $D$ -dimensional nets is limited by the numbers given in table 3.2. In this table, the multiplicity is calculated as the maximal absolute determinant over all matrices in  $\{-1, 0, 1\}^{D \times D}$ .



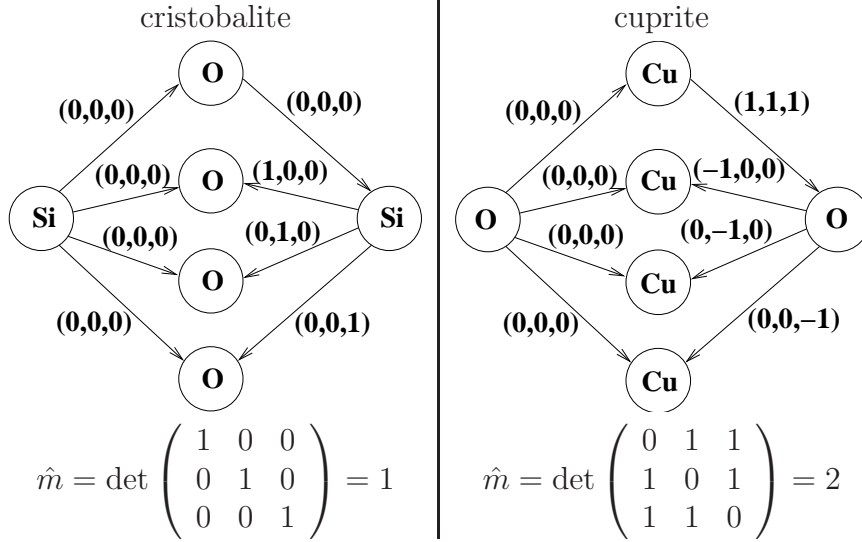


Figure 3.6: QGs for cristobalite and cuprite, as well as possible cycle sum matrices and their determinants.

Dimensions $D$	1	2	3	4	5
Multiplicity $\hat{m}$	1	2	4	16	48

Table 3.2: The multiplicity  $\hat{m}$  of nets as a function of their dimensions  $D$ .

Experiments with the enumeration procedure presented in section 4.1 confirm this deduction. Nets with an even higher multiplicity exist if

- the constraint on the labels to consist only of values in  $\{-1, 0, 1\}$  is relaxed (*e.g.* for  $D = 3$  and  $v_i \in \{-2, -1, 0, 1, 2\}$  up to 32 parallel nets exist),
- no spanning tree possesses non-zero labels, or
- the QG is composed of identical (sub-)QGs.

In definitions 3.1.1 and 3.2.1, the constrain that the QGs have to be connected is important. Otherwise - even so this seems to be a contradiction - nets can be at the same time penetrating and non-penetrating and the values of dimensionality  $\hat{d}$  and multiplicity  $\hat{m}$  (even so they can be calculated) do not match the underlying ideas of these definitions. For example, the QG in figure 3.7 defines a net that is made of infinitely repeated sub-nets similar to the one shown in figure 3.4. In an embedding, each connected sub-net lies in a plane. If a pair of sub-nets originates from the same sub-QG, these planes are parallel; otherwise the planes intersect each other. All edges are loops

and their labels therefore equivalent to cycle sums. Applying equations (3.1) and (3.2) results in a dimensionality of 3 and a multiplicity of 2. Both values are not matching the intentions for the two definitions (redefinitions of the two properties based on sub-graphs are possible, but not of much relevance in crystallography).

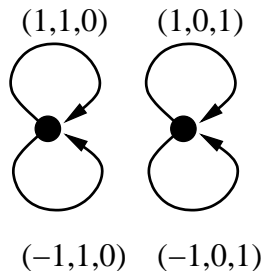


Figure 3.7: Example of a QG defining a penetrating and non-penetrating net.

Beside others, dual, non-isomorphic nets can be represented by disconnected quotient graphs.

### 3.3 Cycle sequences

Cycles  $\circlearrowleft$  are closed trails<sup>1</sup> in a graph. Similarly to the way coordination sequences are defined based on paths of given lengths, cycles can be used to define (infinite) cycle sequences  $(c_1^{n_i}, c_2^{n_i}, c_3^{n_i}, \dots)$ , which are identical for all isomorphic atoms [Beukeman and Klee, 1994]. Each  $c_i^{n_i}$  is defined as the number of cycles including a given atom  $n_i(\mathbf{0})$  with size of  $i$  ( $c_i^{n_i}$  is the size of the set  $\{\circlearrowleft \mid n_i(\mathbf{0}) \in \circlearrowleft \text{ and } |\circlearrowleft| = i\}$ ). For crystals,  $c_1^{n_i} = c_2^{n_i} = 0$  as self-bonds and double-bonds are meaningless.

From experiments with the nets described in section 4.2, it is evident that cycle sequences are more discriminative for non-isomorphic nets with a minimal node degree of two<sup>2</sup> than coordination sequences<sup>3</sup>. The author suspects that cycle sequences of a sufficient length are distinct for non-isomorphic nets in this set. However, even if this unproven proposition is valid, the problem arises that there is no indication on how long a finite sequence must be in order to prove isomorphism. In experiments, non-isomorphic nets were found, where the cycle sequences up to a length of 30 nodes are indistinguishable.

<sup>1</sup>A trail is a sequence of connected edges (a walk) where an edge occurs at most once.

<sup>2</sup>Nodes of degree zero and one are by definition not part of any cycle and are therefore not reflected in a cycle sequence.

<sup>3</sup>These and other sequences were calculated using TOPOLAN; see [Thimm, 2007]

This is a serious shortcoming for a practical application, as the calculation of cycle sequences is particularly expensive; the computation time appears to be proportional to the faculty of the length of the sequence. The calculation for a single node in a net with nodes of degree four requires several days on a modern workstation. Another disadvantage is that cycle sequences are not well understood (*i.e.* no algebraic expression describing them is known) and non-zero elements seem to grow at least with the faculty of the sequence length.

### 3.4 Stretched and fully stretched cycles

Stretched and fully stretched cycles are defined to counteract the excessive computational complexity of cycle sequences, though retaining their high specificity. Both sets are subsets of the cycles defined in section 3.3.

**Definition 3.4.1.** A cycle is stretched *with respect to a starting node*  $n_i(\mathbf{0})$ , if it consists of two paths of the same length, both commencing at node  $n_i(\mathbf{0})$  and each consisting of nodes in a non-decreasing distance<sup>4</sup> to node  $n_i(\mathbf{0})$  and

- either the end nodes of both paths are identical
- or the end nodes are connected by an edge.

**Definition 3.4.2.** A cycle is fully stretched, if it is a stretched cycle and the distances of the nodes to  $n_i(\mathbf{0})$  in both paths are strictly increasing (though the last nodes in both sequences may be at the same distance from  $n_i(\mathbf{0})$ ).

Examples of a general, not stretched cycle, a stretched but not fully stretched and a fully stretched cycle are depicted in figure 3.8. The starting node is marked with a circle; numbers give the distance to the starting nodes and the dotted lines mark the paths into which the cycle is split.

Obviously, a fully stretched cycle is a stretched cycle but not necessarily *vice versa*. However, for certain graphs, all stretched cycles are also fully stretched, as for example the square and the diamond net. For other nets a discrepancy exist: coesite ( $\text{SiO}_2$ ) possesses for a given node about 15 times more stretched cycles of size 25 than fully stretched cycles (structure see table A.4, [Levien and Prewitt, 1981]). Note that stretched and fully stretched cycles are not equivalent to circles or rings as defined in standard graph theory; shortcuts may well exist.

Nets can be classified by using the average stretched cycle sequences, which is the sum over all nodes' sequences divided by the number of nodes

---

<sup>4</sup>The distance of two nodes in a graph is the length of the shortest path between them.

in the QG. This sequence is in general rational but yet an invariant of the net.

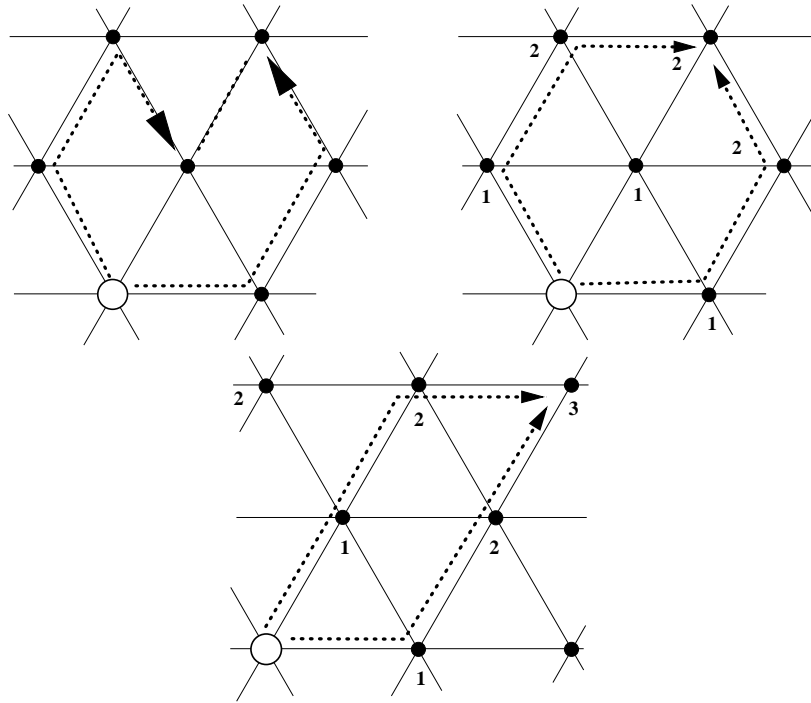


Figure 3.8: Cycles: a (plain) cycle, a stretched and a fully stretched cycle. Numbers indicate the distance to the starting node represented as a circle, arrows the ends of the two paths.

An advantage of the stretched and fully stretched cycles over normal cycles is the lower computational effort. For example, in the case of the nets with nodes of degree four, the stretched cycle sequences appear to grow exponentially with the cycle size. This represents a big computational advantage over cycle sequences, which grow in the order of faculty of the cycle size. In the case of the nets of degree 4, the non-zero elements of the average stretched cycle sequences were observed to approximate  $\exp(\alpha N)$  with  $0.5 < \alpha < 1.0$  and  $N > 10$ . For example the calculation of cycle sequences for diamond and cycles of sizes up to 20 requires about 50 times the time required for stretched cycle sequences of the same size (diamond QG see table B.4). For the over 67'000 nets described in section 4.2, averaged stretched and fully stretched cycle sequences of a maximal length of 32 are distinct for all non-isomorphic nets. For smaller cycle sizes, the fully stretched cycle sequences were observed to be slightly more discriminative than stretched cycle sequences. Both show higher discriminative capabilities than cycle se-

quences. Furthermore, the computational effort turned out to be prohibitive to calculate cycle sequences of length 32.

Figure 3.9 illustrates how specific the three types of cycle sequences classify the nets. Although the curves are very similar, a close examination reveals that fully stretched cycles are more specific than stretched cycles, which in turn are more specific than cycle sequences. Compared to these, much shorter average coordination sequences are necessary to distinguish between most network topologies. However, 285 nets fall into 136 sets, for which the coordination sequences seem to be equal, although the nets are not isomorphic. For distinguishable nets, sequences of length 22 are specific, but sequences of length 50 could not split the 136 classes further. The specificity is still rather high: 99.579%. This may be considered a small risk, taken into account that

- The calculation of the apparent 100% specific fully stretched cycle sequences is computationally more expensive.
- The nets used in the experiment are rather similar: their quotient graphs possess the same number of nodes of degree 4.

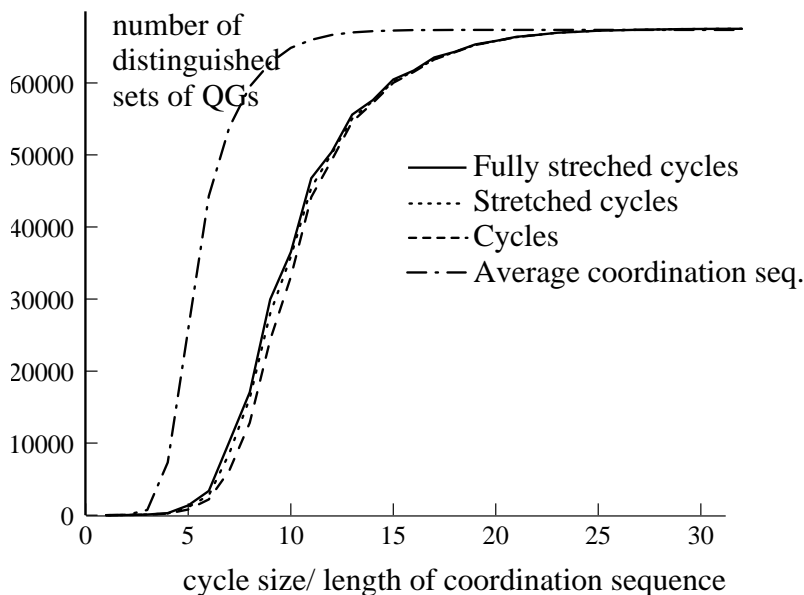


Figure 3.9: The number of sets of nets depending on the cycle sizes and average coordination sequences. Calculated for all nets with connected QGs consisting of four nodes of degree four.

### 3.5 Density and coordination sequences

It is quite evident that coordination sequences give an indication on how “dense” a possible crystal structure is. Generally, average coordination sequences for structures representing simply connected nets in a  $n$ -dimensional space can be approximated by a polynomial of the degree  $n-1$ . For the average coordination sequences of silicates and aluminium-silicates, a linear relationship between the specific density and the coefficient of the fastest growing sequence was shown by Thimm et al. [2000].

In general, all nodes reachable via a path of a maximal length  $\ell$  are necessarily contained in a sphere with a radius of  $\ell$  times the maximal diameter of an atom or bond length in the structure. Figure 3.10 illustrates the principle: the numbers indicate the distance to the centre node in terms of path length. If furthermore, an atom is assumed to occupy a minimal (average) volume

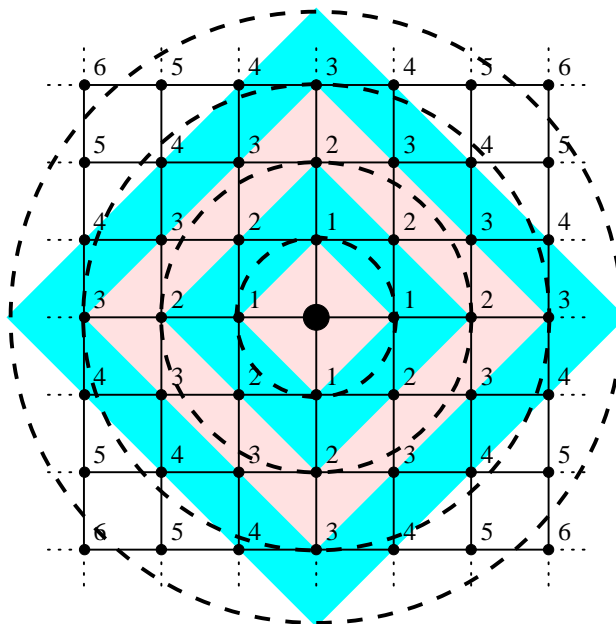


Figure 3.10: Density in a 2-dimensional net.

equivalent to a sphere with the diameter equal to a bond length, a necessary criteria for crystallographic nets can be deduced: the volume occupied by the nodes as calculated of the sum of coordination sequence must be smaller than the volume of the sphere in which they are contained. In figure 3.10, these spheres (circles to be precise) are drawn as dashed lines. Obviously, a circle with a radius of  $k$  “bonds” contains all nodes reachable by a path of at most  $k$  edges (the shaded areas). More generally:

- if  $s^{n_i}$  is the coordination sequence calculated for some arbitrary set of nodes  $n_i$ ,
- $\bar{V}$  is the average volume of atoms or building blocks which are mapped on a node,
- $f$  a factor compensating for dual nets (see also section 3.2;  $f = 1$  for simply connected nets and  $f = \hat{m}$  for penetrating nets, *i.e.*  $f = 2$  for cuprite).
- $\ell$  is the length of the sequence,
- and  $\odot(n_i)$  is the diameter of the atoms in set  $n_i$ ,

then a net must fulfil equation (3.3) in order to be crystallographic.

$$\bar{V} \cdot f \max_{n_i \in \text{net}} \sum_{k=1}^{\ell} s_k^{n_i} \leq \frac{4\pi}{3} \left( \ell \cdot \max_{n_i \in \text{net}} (\odot(n_i))^3 \right) \quad (3.3)$$

The length of the coordination sequence  $\ell$  should be chosen larger than a few times the number of nodes in a unit cell (the estimation of the density improves with  $\ell$ ). If  $\bar{V}$  is approximated by a sphere with diameter  $\bar{\odot}$ , the quotient graph of a crystallographic net must fulfil equation (3.4).

$$\bar{\odot}^3 f \max_{a \in \text{QG}} \sum_{i=1}^{\ell} s_i^a \leq 8\ell^3 \max_{a \in \text{QG}} (\odot(a))^3 \quad (3.4)$$

Or, equivalent by:

$$1 \geq \hat{\rho} \cdot \delta := \frac{f \max_{a \in \text{QG}} \sum_{i=1}^{\ell} s_i^a}{8\ell^3} \cdot \frac{\bar{\odot}^3}{\max_{a \in \text{QG}} (\odot(a))^3}, \quad (3.5)$$

where  $\hat{\rho}$  is called the *specific topological density* and depends on the topology of the structure and  $\delta$  is determined by the chemical composition of the structure ( $\hat{\rho}$  and  $\delta$  are dimensionless).

In the case of an embedding of a net consisting of disconnected sheets in the 3-dimensional space, two extreme situations exist:

- all connected nodes are in one plane (as in the graphite), or
- the nodes are arranged perpendicular to the sheet (as in talc; compare section 3.1 and [Gruner, 1934, Downs and Hall-Wallace, 2003]).

In the latter case, the thickness is limited by the product of the (maximal) sum of the bond lengths along the path(s) that define the diameter of the QG<sup>5</sup>. Similarly for structures consisting of disconnected “bars”, as in pyroxenes or amphiboles, the cross sectional area of these “bars” has to be estimated.

This definition differs from the definition by Grosse-Kunstleve et al. [1996]: it is related closer to the density determined by mass and volume. For large  $\ell$ , one density can be estimated from the other, as Grosse-Kunstleve’s definition measures the surface of a polygon inscribed in the sphere from which  $\hat{\rho}$  is calculated. For crystals,  $\hat{\rho}$  is smaller than 1.0 as:

- The nodes reached from a central node by paths of a length  $\ell$  are actually contained in polyhedra, of shapes determined by the connectivity of the net. As these polyhedra are enclosed by spheres of radius  $\ell$ , the volume available to the atoms is overestimated.
- Atom bonds are rarely at a 180° degree angle, which implies that the radius of the sphere well exceeds the maximal distance between its centre and the atom furthest away from the centre. In other words, the polyhedra formed by the growth sequences are always enclosed in this sphere but usually not inscribed.
- The value of  $\ell \max_{a \in \text{QG}} (\varnothing(a))$  is a conservative upper bound estimation for the radius of the enclosing sphere. The diameter of the enclosing spheres should be calculated as the maximum over the sums of the atom bond lengths of individual paths.

Table 3.3 shows some examples the topological density of existing structures (in number of atoms found in a given volume). As expected for real crystals, the values of  $\hat{\rho} \cdot \delta$  are smaller than one. Note that the specific topological density of cuprite is twice that of cristobalite due to the doubled net. Furthermore, “dense” structures as those of the alloy DyCu, diamond and perovskite (CaTiO<sub>3</sub>) show much higher values for  $\hat{\rho}$  than the framework silicates [Putnis, 1992]. This is not necessarily the case for nets that do not have a crystallographic correspondence. Among the nets enumerated in section 4.2, values for  $\hat{\rho}$  exceeding 2.7 were observed. It is possible to construct QGs with a  $\hat{\rho}$  that exceeds any given value.

As there is strong evidence that the specific densities of structures with a similar chemical compositions are almost linearly related to their topological

---

<sup>5</sup>The diameter of a connected graph is the maximal distance over all pairs of its nodes. Several paths of the same minimal length may exist between such pairs of nodes, of which several pairs may exist.



Structure	$\hat{\rho}$	$\delta$	$\hat{\rho}\delta$
CuDy (figures 6.1, 6.2)	0.270	0.712	0.192
Perovskite (table A.10)	0.516	0.160	0.083
Diamond (tables A.7, B.4)	0.113	1.000	0.113
Cristobalite (table A.5, 3.6)	0.043	0.316	0.014
Coesite (table A.4, figure B.1)	0.057	0.316	0.018
Cuprite (table A.6, figure B.1)	0.087	0.279	0.024

Table 3.3: Inverse specific topological densities and  $\hat{\rho}$  values for selected structures with  $\ell = 20$ . Based on  $\varnothing(\text{Dy}) = 3.18\text{\AA}$ ,  $\varnothing(\text{C}) = 1.54\text{\AA}$  (covalent radii from [PhysLink.com, 2007]);  $\varnothing(\text{Si}) = 2.3\text{\AA}$ ,  $\varnothing(\text{Ti}) = 2.9\text{\AA}$ ,  $\varnothing(\text{Ca}) = 3.795\text{\AA}$  [Laves, 1926b];  $\varnothing(\text{O}) = 1.2\text{\AA}$  (using the smallest metal-O distance as in [Cramer et al., 2003]);  $\varnothing(\text{Cu}) = 2.5\text{\AA}$  (calculated from the cuprite structure, see table A.6).

densities [Thimm et al., 2000], a more aggressive cut-off value for  $\hat{\rho} \cdot \delta$  can be used.

More generally, a known structure can be used to estimate sensible lower and/or upper bounds for  $\hat{\rho}$ . For example, it can be assumed that all possible  $sp^3$  carbon structures of dimensionality 3 (according to section 3.1) are not (much) denser than diamond. Allowing for some margin, a cut-off value corresponding to a topological density twice the density of diamond permits to reject more than 95% of all topologies enumerated by the basic enumeration procedure as non-crystallographic (as opposed to 16% for the criteria in equation (3.5)).

### 3.6 Density *versus* unit cell volume

For a crystallographic embedding of a net, a maximal bond length is usually known from conventional crystal chemical knowledge. Based on this length, the distance between any pair of nodes is limited by this maximal length times the number of edges in the shortest path between them. As this is also true for any pair of translationally equivalent nodes in neighbouring cells, upper limits for dimensions  $a$ ,  $b$ , and  $c$  of a cell exist. In other words, the topology of a net limits the dimensional cell parameters as a function of the bond lengths of the considered chemical composition. As the number of atoms in a cell is equal to the number of nodes in the QG, a minimal density of a possible structure can be estimated and some pathological nets recognised.

More precisely, the maximal volume of a cell can be estimated as follows.

Be  $\odot$  a cycle in a QG with maximal dimensionality for which some elements of the cycle sums are non-zero. Then, cell parameters  $a_{max}$ ,  $b_{max}$ , or  $c_{max}$ , respectively, are limited by the product of the sum of the diameters of the atoms (or bond lengths) in the cycle and the length of the cycle divided by the absolute value of the non-zero cycle sum element. Minimising the length of these cycles results in equations (3.6) to (3.8).

$$a_{max} = \min_{\odot \in \text{QG}} \frac{1}{|k|} \sum_{a \in \odot} \odot(a) \quad \text{with } \oplus = (k, l, m) \text{ and } k \neq 0 \quad (3.6)$$

$$b_{max} = \min_{\odot \in \text{QG}} \frac{1}{|l|} \sum_{a \in \odot} \odot(a) \quad \text{with } \oplus = (k, l, m) \text{ and } l \neq 0 \quad (3.7)$$

$$c_{max} = \min_{\odot \in \text{QG}} \frac{1}{|m|} \sum_{a \in \odot} \odot(a) \quad \text{with } \oplus = (k, l, m) \text{ and } m \neq 0 \quad (3.8)$$

The cell volume of an embedded net is consequently limited by  $V_{max} = a_{max}b_{max}c_{max}$ , presuming a cell with orthogonal axes. For other cells, the limit is still valid, though even more conservative.

On the other hand, the minimal volume  $V_{min}$  occupied by all atoms in a cell can be approximated as:

$$V_{min} = \sum_{a \in \text{QG}} \frac{\pi}{6} \odot(a)^3 \quad (3.9)$$

Obviously, for crystallographic topologies the space occupied by the atoms must be smaller than the maximal volume of the cell:  $V_{min} \leq V_{max}$ .

For example, the QG of the diamond lattice consists of 4 edges:  $C_1 \xrightarrow{0,0,0} C_2$ ,  $C_1 \xrightarrow{1,0,0} C_2$ ,  $C_1 \xrightarrow{0,1,0} C_2$  and  $C_1 \xrightarrow{0,0,1} C_2$ . A possible choice of a cycle to determine cell parameter  $a$  are the first two edges, resulting in  $k=1$  and  $\sum \odot(a) = 3.088\text{\AA}$ , assuming that a C-C bond is  $1.544\text{\AA}$  in length. This limits the maximal cell volume to  $29.45\text{\AA}^3$  (as compared to the observed value of  $11.35\text{\AA}^3$ ).

This condition is easily calculated for all quotient graphs, and turns out to be quite effective: for the nets described in section 4.2, only about 50% fulfil this condition.

The minimal density as calculated in section 3.5 and estimated density are to some extent independent: for certain nets, the minimal density is quite

low, whereas the estimated density is high and *vice versa*. For example,  $V_{max}$  and  $\hat{\rho}$  were calculated for the nets described in section 4.2 and the number of occurrences counted. The number of occurrences are depicted in figure 3.11 (top: gray values represent the number of occurrences; bottom: the length of the lines). Though most occurrences are for small  $V_{max}$  paired with small  $\hat{\rho}$ , the two values are not strictly correlated - implying that both criteria are complementing each other.

The absence of certain  $V_{max}$  has a combinatorial reason: cycles of sizes bigger than 4 in the considered QGs are always a combination of smaller cycles. This implies that  $1 \leq a_{max}, b_{max}, c_{max} \leq 4$  and consequently excludes values for  $V_{max}$  that are not a product of three integers in this range (values larger than 24 for  $V_{max}$  also seem to be impossible).

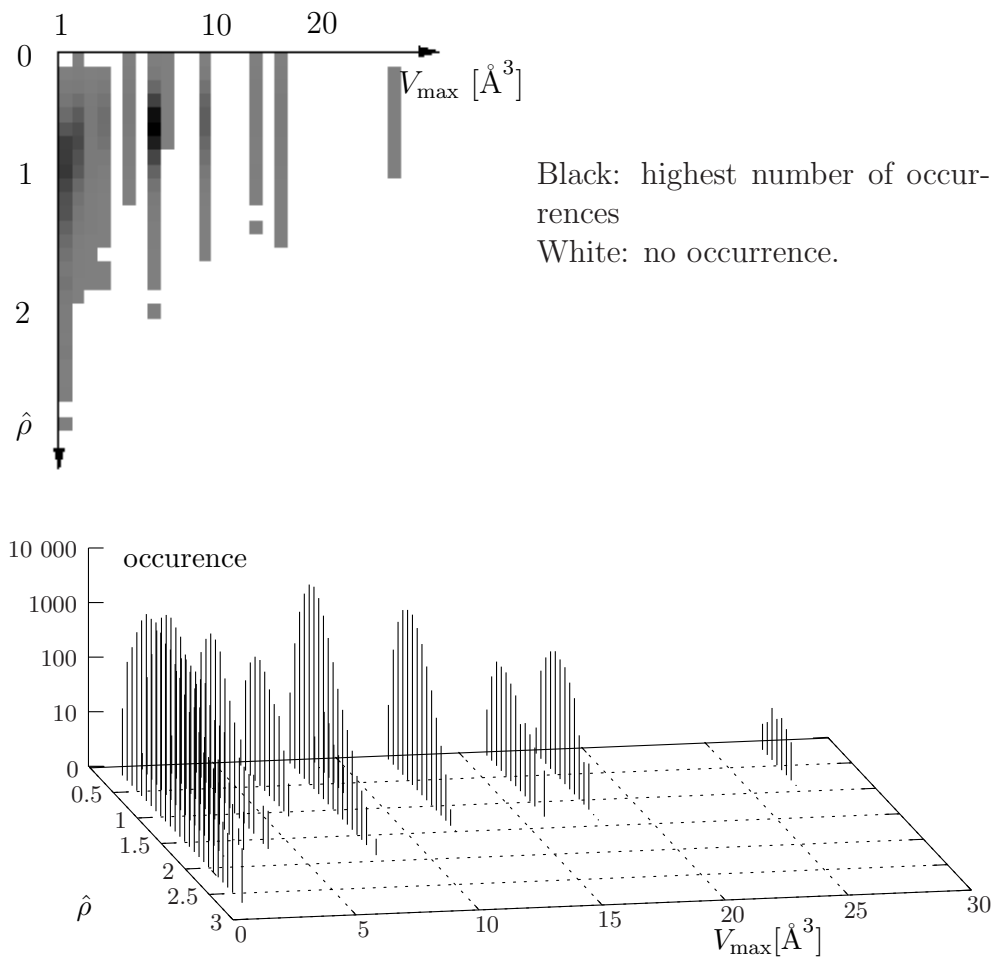


Figure 3.11: Occurrences of pairs of  $\hat{\rho}$  and  $V_{max}$ .



# Chapter 4

## Nets and Their Enumeration

The idea of creating crystal structures *ab initio* is not new and other approaches towards a systematic enumeration of possible crystal structures were proposed in literature:

- Delgado-Friedrichs et al. [1999] describe a systematic approach based on tiling theory. This is an alternative approach to the one described in this paper, with advantages (the generation of structures complying to crystallographic constraints is simpler) and disadvantages (1. the considerably more complicated theory, 2. the likely higher computational cost, and 3. the relationship between the complexities of structures and tilings being rather loose).
- Sphere packings were used by Koch and Fischer [1995]. Sphere packings have the disadvantage that structures with dominantly covalent bonds are difficult to model as these structures do not represent (dense) sphere packings.
- The work of Blatov [2000] is in some aspects very close to this publication. He and a collaborator also analysed crystal structures based on graph theory [Peresypkina and Blatov, 2000].
- Klein [1996] presented a method for enumerating crystal topologies with a given (minimal) symmetry by augmenting the quotient graph (called *dl-graph*) with symmetry labels. This has the advantage to reduce the size of the graph in the case that structures with a high symmetry are searched for as well as the search space for edge labels, and therefore being able to consider highly symmetric structures with larger unit cells. The drawback is that if (also) structures of minimal symmetry are considered, the same topology is generated in various

forms having low apparent and explicit high symmetries - and this worsens the computational complexity.

- Treacy et al. [2004] developed an approach which uses a mixture of tiling and graph theory, and takes advantage of space group information. Their group proposed approximately 2.5 million hypothetical zeolite structures (see [Foster and Treacy, accessed 2007]). However, their approach compares to the here presented approach in a similar way as the work by Klein [1996]. Notably, Treacy, Rivin, Balkovsky, Randall, and Foster decided not to enumerate structures in space group P1 (as the computational effort is quite excessive), which is effectively done here. Furthermore, their approach is very much tailored towards zeolites and other structures with tetragonal atoms.

The major focus of this chapter is a reduction of the number of nets (and, hence, quotient graphs) enumerated and considered for the proposition of possible crystal structures. Ideally, the tentative embedding succeeds only for so-called *crystallographic nets* (in contrast to *pathological nets*), which have an equivalent in nature and may feature desired properties.

## 4.1 The enumeration of crystal structures

The systematic examination of (potentially new) nets and crystal structures can be organised in four main steps:

1. The enumeration of quotient graphs.
2. The elimination of redundant and obviously pathological nets.
3. A tentative embedding under minimal crystallographic constraints.
4. A quantum mechanical based geometry optimisation and analysis; synthesis.

For the sake of readability, a rather inefficient enumeration procedure is described in section 4.1.1. Then, subsequent sections discuss how the efficiency is improved by excluding pathological and redundant QGs from the enumeration. Two vital assumptions with respect to the computational complexity of this approach are made. Firstly, for any crystal a unit cell can be chosen such that all inter-atomic bonds connect atoms located in neighbouring unit cells<sup>1</sup>. This has the benefit that the values of the elements

---

<sup>1</sup>This assumption reduces not only the number of vectors considered, but limits also the maximal number of parallel, disconnected sub-nets of the same dimensionality (see section 3.2)

of the QG's vector labels are limited to  $\{-1, 0, 1\}$ . Secondly, it is assumed, that a unit cell can be chosen such that between any pair of atoms in a unit cell that are connected via an arbitrary path there exists also a path following bonds not leaving the cell. This implies that only QGs having a spanning tree with zero labelled edges must be considered. This greatly reduces the number of edges in a QG for which non-zero edges need to be considered.

The theory presented in chapter 5 permits to determine the space group with a maximal symmetry compatible with a given QG. This simplifies a tentative embedding obeying symmetry constraints, possibly complemented with a geometric optimisation of cell parameters and atom positions in order to obtain a trial structure in which bond lengths and angles are within values observed in known crystal structures. The tentative embedding and the preliminary purely geometrical optimisation is important as the final step, the quantum mechanical analysis and optimisation of the proposed structures is a particularly time intensive and difficult procedure. Neither the tentative embedding nor the quantum mechanical based geometry optimisation are discussed further.

### 4.1.1 The basic enumeration procedure

The basic enumeration procedure starts with a given number of atoms in a unit cell of the considered crystal structures, as well as their degrees. The procedure consists of 5 steps, of which some are subjected to later refinement:

1. *Enumerate all non-isomorphic trees* with the required number of nodes, where all trees may be extensible to a graph with the specified properties [Gould, 1988, Harary, 1969, Wilson and Watkins, 1990]. The edges in the trees are labelled with zero-vectors.

2. *Extend the spanning trees* to all possible graphs which match the specification. This may include parallel edges and loops<sup>2</sup>.

3. *Completing the labelling of the graphs:* for each partially labelled quotient graph, all possible combinations of vectors with elements in  $\{-1, 0, 1\}$  are enumerated (exceptions are discussed later) and used to complete the labelling of the graphs. Furthermore, an arbitrary orientation (yet identical to all enumerated QGs) is assigned to all edges in a QG.

Not all combinatorially possible labels match constraints imposed by nature on crystal structures, some assignments are illicit. For example, loops may not have zero labels, as this would correspond to atoms bond to themselves. Furthermore, labels of parallel or anti-parallel edges are not allowed to be equal or that one is the negative of the other (see section 4.1.2). Fur-

---

<sup>2</sup>A loop is an edge connecting a node with itself.

ther restrictions on the quotient graphs, respectively the nets, are described in later sections.

4. *Elimination of quotient graphs describing isomorphic nets:* as the previous steps produce numerous quotient graphs describing isomorphic nets, it is important to eliminate such redundant graphs for efficiency reasons. This is done in several steps:

1. Classify quotient graphs using averaged coordination sequences with, for example, 10 elements.
2. For each set obtained, perform a comparison between pairs to detect isomorphism and remove redundant graphs.
3. If two non-isomorphic graphs have identical coordination sequences, test the isomorphism of their nets using longer coordination sequences or some variation of cycle sequences. However, no straightforward criteria known to the authors permit a decision. Help on how to decide the isomorphism by hand can be found in Schumacher [1994].

5. *Embed the nets tentatively* under minimal crystallographic constraints (*i.e.* the distance between bond and unbound nodes must be reasonable).

Note that if the approach proposed by Klein [1996] is preferred, steps 1 to 3 have to be modified accordingly. The elimination of isomorphic nets requires a prior translation of the symmetry labelled graphs into QGs.

## 4.1.2 Parallel edges in quotient graphs

(Anti-)parallel edges in quotient graphs with the same or negated labels are not permissible. Their presence would result in overlapping or intersecting edges in the embedded net. The following theorem puts this observation in precise terms.

**Theorem 4.1.1.** *Be net  $\mathbf{G}$  embedded in the  $D$ -dimensional space and  $\mathbf{Q}$  a QG of  $\mathbf{G}$ . Then, the line representing the edge  $e_1 = \left( n \xrightarrow{\mathbf{v}} n' \right)$  has more than the end points in common with lines equivalent to the embeddings of each of the edges  $e_2 = \left( n' \xrightarrow{\mathbf{v}} n \right)$ ,  $e_3 = \left( n \xrightarrow{-\mathbf{v}} n' \right)$ ,  $e_4 = \left( n' \xrightarrow{-\mathbf{v}} n \right)$ .*

*Proof.* Edges  $e_1$  and  $e_4$ , as well as  $e_2$  and  $e_3$  are identical according to the definition of QGs in section 2.1. It is therefore sufficient to show the theorem for  $e_1$  and  $e_2$ .

Let the positions  $\mathbf{x}$  and  $\mathbf{x}'$  be the positions of nodes  $n(\mathbf{0})$  and  $n'(\mathbf{0})$  in an arbitrary embedding with  $0 \leq x_i, x'_i < 1$ . Following the edge in the embedded



net equivalent to edge  $e_1$  in the QG from  $n(\mathbf{0})$  leads to the node  $n'(\mathbf{v})$  at the absolute position  $\mathbf{x}' + \mathbf{v}$  and correspondingly, from  $n'(\mathbf{0})$  the edge  $e_2$  leads to node  $n(\mathbf{v})$  at position  $\mathbf{x} + \mathbf{v}_1$ , respectively. Assuming straight lines between the nodes, the lines intersect *iff* some constants  $g$  and  $h$  with  $0 < h, g < 1$  exist such that

$$\begin{aligned} & \mathbf{x} + g \cdot (\mathbf{x}' + \mathbf{v}) - \mathbf{x} \\ = & \mathbf{x}' + h \cdot (\mathbf{x} + \mathbf{v}) - \mathbf{x}' \end{aligned}$$

Setting  $g = h = \frac{1}{2}$  shows that at least one more common point exists.  $\square$

### 4.1.3 Penetrating and non-penetrating sub-nets

Adding an edge to a QG can increase, decrease, or leave its multiplicity unchanged. Consequently, it is necessary to complete QGs during an enumeration before their multiplicity is evaluated (and used to discard or retain a particular QG).

Nets with a dimensionality smaller than the dimensionality of the space in which they are embedded are not pathological *per se* and numerous crystal structures fall into this category (*e.g.* graphite, talc). Yet, they are omitted here from an enumeration for two reasons:

- They may or may not be of interest due to their particular structure.
- The enumeration of these structures is done more efficiently achieved by enumerating nets of a lower dimensionality (*i.e.* the labels of the QG have only one or two elements), which are then “stacked” by adding to all labels additional elements equal to zero in order to form a net in the desired space.

### 4.1.4 Elimination of redundant nets

As indicated in section 5.2, multiple QGs may represent the same net. Some of them can be excluded without actually comparing nets, thus saving a considerable amount of computation time.

Assume that two quotient graphs  $\mathbf{Q}$  and  $\mathbf{Q}'$  are isomorphic and the edges are mapped such that the  $i$ th edge in  $\mathbf{Q}$  is mapped onto the  $i$ th edge in  $\mathbf{Q}'$  and this mapping respects the orientation of the edges. Suppose that further for all labels  $\ell_k$  and  $\ell'_k$  a common orthogonal matrix  $M$  exists such that

$$\text{for all } k: \ell_k * M = \ell'_k. \quad (4.1)$$

Clearly, this implies that equation (2.1) holds and the two QG are isomorphic.

Based on this observation, many redundant quotient graphs can be excluded from the enumeration beforehand. As the labels are attributed to the quotient graph in this particular manner, the labels not in the spanning tree are equivalent to the cycle sums. If these labels are gathered as rows in a matrix  $\mathbf{L}$ , only matrices where

- all the column vectors of  $\mathbf{L}$  have a positive or zero norm and
- Vector  $\mathbf{L}_i$  is lexicographically smaller<sup>3</sup> than  $\mathbf{L}_{i+1}$  for all  $1 \leq i < D$

are accepted as labels for a QG. This permits to reduce the number of redundant QGs by a factor of close to 48 for the QG enumerated in section 4.2.

### 4.1.5 Desired properties of crystals

Rings and cycles in a possible crystal structure are already defined by the net, respectively the quotient graphs. This permits, for example, to exclude structures that have or do not have cycles of a given size.

Furthermore, during a search for crystal structures with high degrees of symmetry, QGs with small automorphism groups can be dropped before a tentative embedding is attempted. This is possible, as the automorphism group of the QGs is homomorphic to all space groups of possible embedding of the equivalent net. This is computationally interesting as the calculation of the automorphism group is much less demanding than a full geometry optimisation of a crystal structure.

## 4.2 The nets with 4 nodes of degree 4

The author enumerated all simply connected nets with 4 translationally non-equivalent nodes of degree 4 in the intend to determine all  $sp^3$  carbon structures with 4 atoms per unit cell (a graph is simply connected if a path exists between all pairs of nodes). The total number of quotient graphs (describing pathological and crystallographic nets) is estimated to be larger than  $5 * 10^{10}$ , a certainly prohibitive number. Using the approaches described above (including QG with loops), the enumeration produced a manageable subset of roughly 40'000'000 quotient graphs from which 67510 potentially non-isomorphic nets emerged (for three nets between two to five, as plain graphs non-isomorphic, quotient graphs are still included). Using the presented constraints and the assumption that a  $sp^3$  carbon modification cannot

---

<sup>3</sup>E.g.: if the letter 'A' is associated with 1, 'B' with 0, and 'C' with -1, the "words" corresponding the  $\mathbf{L}_i$  are lexicographically ordered.

be much denser than diamond, a subset of 104 potentially crystallographic nets was obtained. These were then embedded and node positions and cell parameters optimised such that bond nodes are about  $1.60\text{\AA}$  apart and non-bond atoms at a minimal distance of at least  $2.26\text{\AA}$ . For 26 of the 104 nets an embedding could be found for which the error on the bonds is less than  $0.20\text{\AA}$ . Two of these nets describe the diamond topology (with a double cell), one lonsdaleite. Of the remaining 23 nets, an analysis based on quantum mechanical principles stipulates three non-metallic new or yet unidentified carbon modifications [Strong et al., 2004], other nets are still under investigation.



# Chapter 5

## Net Topologies, Space Groups, and Crystal Phases

The transformation of crystal structures into QG discussed in section 2.1 has the limitation that the spatial information on nodes in the crystal is of fundamental importance. This means that QGs and nets cannot be dissociated from cell parameters and atom positions. Here, an approach is introduced which does not rely on these and defines quotient graphs and nets independently of the arrangement of nodes in Euclidean space. Then, results on the isomorphism of nets by K. Goetzke are reformulated and complemented [Goetzke, 1992]. Findings are illustrated with 2-dimensional examples and known crystal structures.

### 5.1 Crystals, graphs, and voltage graphs

The approach presented here to express quotient graphs and nets was inspired by *voltage graphs* [Gross and Tucker, 2001]. In contrast to the conventional approach to QGs, QGs are first defined as a set of graphs labelled in a certain way, and only then are the nets defined as a cross product of a quotient graph and an integer vector space.

**Definition 5.1.1.** *A quotient graph  $\mathbf{Q}$  of dimension  $D$  is a finite graph consisting of  $N$  nodes  $\mathbf{Q}_N = \{n_i | 1 \leq i \leq N\}$  and directed, labelled edges  $\mathbf{Q}_E = \left\{ e = \left( n_i \xrightarrow{\mathbf{v}} n_j \right) \right\} \subset \mathbf{Q}_N \times \mathbb{Z}^D \times \mathbf{Q}_N$  with dimension  $D > 0$ . An edge  $n_i \xrightarrow{\mathbf{v}} n_j$  is identical to the edge  $n_j \xrightarrow{-\mathbf{v}} n_i$ .*

This definition uses the idea of *base graphs* and *voltages* proposed by Gross and Tucker [2001] with the restriction that the “voltages” are exclusively integer vectors. The definition of identical edges means that  $\mathbf{Q}_E$  is a

set of pairs of equivalent edges with respect to the given definition of the identity of edges. To avoid notational complexity, this rather trivial equivalence shall not be included in the notation but applied, whenever necessary. Furthermore, edges may be denoted as  $e_k = \left( n^{(k)} \xrightarrow{\mathbf{v}_k} n'^{(k)} \right)$ , where the superscript  $(k)$  indicates that the node is the start or end node of the  $k$ th edge. Identical edges having opposite edge orientations are being called *inverted* to each other. In the following, a *base graph* of a QG is defined as the QG stripped of labels and edge orientations (an edge and its inverted counterpart are indistinguishable).

**Definition 5.1.2.** A net  $\mathbf{G} = \langle \mathbf{Q}, \mathbb{Z}^D \rangle$  is the cross product of a quotient graph  $\mathbf{Q}$  of dimension  $D$  and an integer vector space of the same dimension. In this cross product,

$$\mathbf{G}_N = \{n_i(\mathbf{x}) | 1 \leq i \leq N, \mathbf{x} \in \mathbb{Z}^D\}$$

is the set of nodes in  $\mathbf{G}$  and

$$\mathbf{G}_E = \bigcup_{\substack{e \in \mathbf{Q}_E \\ \mathbf{x} \in \mathbb{Z}^D}} \left\{ n_i(\mathbf{x}) \leftrightarrow n_j(\mathbf{x} + \mathbf{v}) | e = \left( n_i \xrightarrow{\mathbf{v}} n_j \right) \right\}$$

the set of (undirected) edges.

Hereby, a net is defined without recurring to an embedding (or a crystal structure), cell parameters, or atom positions. Usually, only quotient graphs  $\mathbf{Q}$  of a finite degree<sup>1</sup> are considered, as a net  $\langle \mathbf{Q}, \mathbb{Z}^D \rangle$  is of the same degree and only those are meaningful in the context of this publication. In general, a net may or may not be connected. A minimal, yet insufficient, condition for a net being connected is that it's quotient graph is connected – which is assumed in the following (if not stated otherwise) for the sake of simplicity. Disconnected nets are discussed in sections 3.1 and 3.2.

**Definition 5.1.3.** Two quotient graphs  $\mathbf{Q}$  and  $\bar{\mathbf{Q}}$  are isomorphic if and only if the nets  $\langle \mathbf{Q}, \mathbb{Z}^D \rangle$  and  $\langle \bar{\mathbf{Q}}, \mathbb{Z}^D \rangle$  are isomorphic.

Obviously, if two QG are identical, except for the names of their nodes, they describe isomorphic nets. This can be expressed in a more rigorous way as follows: if a bijective mapping  $\phi$  – called *base graph isomorphism* – exists for the base graphs of  $\mathbf{Q}$  and  $\bar{\mathbf{Q}}$  with  $\phi(n_i) = \bar{n}_i$ ,  $\phi(e_k) = \bar{e}_k$ , and  $\mathbf{v}_k = \bar{\mathbf{v}}_k$  (that is the edges and nodes can be renumbered such that this is true), then the QGs (and their nets) are isomorphic.

---

<sup>1</sup>Only a finite number of edges are incident to a node.

## 5.2 Isomorphism of quotient graphs and nets

Isomorphisms of QGs and nets have only superficially been addressed by the closing statement in section 5.1, and Goetzke [1992] proposed several theorems on net and QG isomorphism, which are quite similar to some of the following theorems. However, as QGs and nets are redefined, the ideas proposed by Goetzke and others are revised accordingly. The isomorphism of nets and QGs is formulated here without consideration of atom types or similar concepts for the sake of simplicity and generality. In cases where this is not acceptable, the isomorphic mappings  $\phi$  can be restricted to those fulfilling such constraints.

The following theorem addresses cases of isomorphism that correspond to a modification of an embedding where sets of isomorphic nodes (with a fixed coordinate system and cell boundaries) are translated beyond cell boundaries (or the boundaries themselves are translated). This is reflected in the QG by the addition or subtraction of the same integer vector to the labels of the edges that link this node to the rest of the QG. Theorem 5.2.1 and theorem 5.2.2 are equivalent to K. Goetzke's definition of  $\mathcal{V}$ -variants.

**Theorem 5.2.1.** *Two QGs describe isomorphic nets if*

- a base graph isomorphism  $\phi : \mathbf{Q} \rightarrow \bar{\mathbf{Q}}$
- a set of nodes  $\mathbf{A} \subset \mathbf{Q}_N$ , as well as
- a vector  $\mathbf{t} \in \mathbb{Z}^D$

exist, such that for all edges  $n \xrightarrow{\mathbf{v}} n'$  in  $\mathbf{Q}$  there exists an edge  $\phi(n) \xrightarrow{\bar{\mathbf{v}}} \phi(n')$  in  $\bar{\mathbf{Q}}$  with

$$\left. \begin{array}{l} \bar{\mathbf{v}} = \mathbf{v} + \mathbf{t} \\ \bar{\mathbf{v}} = \mathbf{v} - \mathbf{t} \\ \bar{\mathbf{v}} = \mathbf{v} \end{array} \right\} \text{if} \left\{ \begin{array}{l} n \in \mathbf{A} \text{ and } n' \notin \mathbf{A} \\ n \notin \mathbf{A} \text{ and } n' \in \mathbf{A} \\ \text{otherwise} \end{array} \right. \quad (5.1)$$

*Proof.* It has to be shown that an isomorphism  $\phi$  between  $\mathbf{G} = \langle \mathbf{Q}, \mathbb{Z}^D \rangle$  and  $\bar{\mathbf{G}} = \langle \bar{\mathbf{Q}}, \mathbb{Z}^D \rangle$  exists. This is done by construction of isomorphism  $\phi : \mathbf{G} \rightarrow \bar{\mathbf{G}}$ .

Without loss of generality, assume that  $\bar{n}_i = \phi(n_i)$  for all  $n_i \in \mathbf{Q}_N$  and  $\phi(e_k) = \bar{e}_k$  for all  $e_k \in \mathbf{Q}_E$ . Then, define  $\phi(n_i(\mathbf{x})) = \bar{n}_i(\mathbf{x})$  for all  $\mathbf{x} \in \mathbb{Z}^D$  and  $n_i \in \mathbf{Q}_N$ , and in order to obtain an isomorphic mapping for the edges in the nets, define  $\phi$  for all  $\mathbf{x} \in \mathbb{Z}^D$  as

$$\phi(n(\mathbf{x}) \leftrightarrow n'(\mathbf{x} + \mathbf{v}))$$

$$= \left\{ \begin{array}{ll} \bar{n}(\mathbf{x}) \leftrightarrow \bar{n}'(\mathbf{x} + \mathbf{v} + \mathbf{t}) & \text{if } n \in \mathbf{A} \text{ and } n' \notin \mathbf{A} \\ \bar{n}(\mathbf{x}) \leftrightarrow \bar{n}'(\mathbf{x} + \mathbf{v} - \mathbf{t}) & \text{if } n \notin \mathbf{A} \text{ and } n' \in \mathbf{A} \\ \bar{n}(\mathbf{x}) \leftrightarrow \bar{n}'(\mathbf{x} + \mathbf{v}) & \text{otherwise.} \end{array} \right.$$

$\phi$  is the desired isomorphism, as it is bijective and consistent with the premises.  $\square$

Theorem 5.2.1 can be extended to include sequences of pairs of quotient graphs that fulfil the premises in this theorem, and the following theorem 5.2.2 is such an extension.

**Theorem 5.2.2.** *Two QGs describe isomorphic nets if*

- a base graph isomorphism  $\phi : \mathbf{Q} \rightarrow \bar{\mathbf{Q}}$ , and
- vectors  $\mathbf{t}_i \in \mathbb{R}^D$  ( $1 \leq i \leq |\mathbf{Q}_N|$ ,  $|\mathbf{Q}_N|$  the number of nodes in  $\mathbf{Q}$ )

exist, such that for all edges  $n_i \xrightarrow{\mathbf{v}} n_j$  in  $\mathbf{Q}$  exists an edge  $= \phi(n_i) \xrightarrow{\bar{\mathbf{v}}} \phi(n_j)$  in  $\bar{\mathbf{Q}}$  with

$$\bar{\mathbf{v}} = \mathbf{v} + \mathbf{t}_j - \mathbf{t}_i \quad (5.2)$$

*Proof.* Choose  $\phi$  and  $\mathbf{t}_i \in \mathbb{Z}^D$  such that the premises of theorem 5.2.2 hold.

Let  $\mathbf{Q} = \mathbf{Q}_1, \mathbf{Q}_2, \dots, \mathbf{Q}_N = \bar{\mathbf{Q}}$  be a sequence of QGs with  $q_i = \{n_i\}$  for  $2 \leq i \leq N$ . From the proof of theorem 5.2.1 it is clear that this sequence describes isomorphic nets (use  $\mathbf{t} = \mathbf{t}_i$  and  $\mathbf{q} = \mathbf{q}_i$  to show that  $\mathbf{Q}_{i-1}$  and  $\mathbf{Q}_i$  are isomorphic). A close examination of isomorphic edges in  $\mathbf{Q}_1$  and  $\mathbf{Q}_N$  shows that for all edges  $\left(n^{(k)} \xrightarrow{\mathbf{v}_k} n'^{(k)}\right) = \left(n_i \xrightarrow{\mathbf{v}_k} n_j\right)$

$$\phi \left( n_i \xrightarrow{\mathbf{v}_k} n_j \right) = \left( \phi(n_i) \xrightarrow{\mathbf{v}_k + \mathbf{t}_j - \mathbf{t}_i} \phi(n_j) \right).$$

Therefore, defining

$$\phi(n_i(\mathbf{x}) \leftrightarrow n_j(\mathbf{x} + \mathbf{v}_k)) = (\phi(n_i)(\mathbf{x}) \leftrightarrow \phi(n_j)(\mathbf{x} + \mathbf{v}_k + \mathbf{t}_j - \mathbf{t}_i))$$

for all  $\mathbf{x} \in \mathbb{Z}^D$  results into an isomorphic mapping of the nets.  $\square$

A closer examination of theorems 5.2.1 and 5.2.2 shows that QGs, which describe isomorphic nets in embeddings that are related by of a rotation, a reflection, or a non-linear transformation, will unlikely fulfil the respective premises. Theorem 5.2.3 address these cases.

**Theorem 5.2.3.** *Two QGs describe isomorphic nets if*

- a base graph isomorphism  $\phi : \mathbf{Q} \rightarrow \bar{\mathbf{Q}}$ , and
- vectors  $\mathbf{t}_i \in \mathbb{R}^D$  ( $1 \leq i \leq |\mathbf{Q}_N|$ ), and
- an orthogonal matrix  $\mathbf{W} \in \mathbb{Z}^D \times \mathbb{Z}^D$



exists, such that for all edges  $n_i \xrightarrow{\mathbf{v}} n_j$  in  $\mathbf{Q}$  exists an edge  $\phi(n_i) \xrightarrow{\bar{\mathbf{v}}} \phi(n_j)$  in  $\bar{\mathbf{Q}}$  with

$$\bar{\mathbf{v}} = \mathbf{W} \cdot (\mathbf{v} + \mathbf{t}_j - \mathbf{t}_i). \quad (5.3)$$

Two lemma and the respective proofs comprise the proof of theorem 5.2.3:

**Lemma 5.2.4.** *For a chosen spanning tree, a quotient graphs  $\mathbf{Q}$  is isomorphic to (at least one) QG  $\bar{\mathbf{Q}}$  that possesses only edges with zero-vector labels for this tree.*

*Proof.* By construction: chose a leaf as the root node of the spanning tree. Then, number the nodes such that the root node is  $n_1$  and for any path within the tree from  $n_1$  to any other node  $n_j$ ,  $j$  is the highest node index in this path. Then, successively for  $i = 2 \dots N$  select the edge  $n_h \xrightarrow{\mathbf{v}} n_i$  with  $h < i$  from the tree (only one exists), set  $\mathbf{t} = -\mathbf{v}$  and  $q = \{n_i\}$ , and modify the QG according to theorem 5.2.1. In the resulting sequence of QGs, each is isomorphic to the initial QG and the last QG possesses a spanning tree with only zero labels.  $\square$

Lemma 5.2.5 is equivalent to K. Goetzke's  $\mathcal{B}^M$ -variants, which roughly represent rotations and reflections of a net's embedding.

**Lemma 5.2.5.** *Two QGs describe isomorphic nets if*

- a base graph isomorphism  $\phi : \mathbf{Q} \rightarrow \bar{\mathbf{Q}}$ , and
- an orthogonal matrix  $\mathbf{W} \in \mathbb{Z}^D \times \mathbb{Z}^D$

exists, such that for all edges  $e_k = (n^{(k)} \xrightarrow{v_k} n'^{(k)})$  in  $\mathbf{Q}$  exists an edge  $\phi(n^{(k)}) \xrightarrow{\bar{v}_k} \phi(n'^{(k)})$  in  $\bar{\mathbf{Q}}$  with

$$\bar{\mathbf{v}}_k = \mathbf{W} \cdot \mathbf{v}_k. \quad (5.4)$$

*Proof of lemma 5.2.5.* By construction of  $\phi$ :

$$\phi(n^{(k)}(\mathbf{x}) \leftrightarrow n'^{(k)}(\mathbf{x} + \mathbf{v}_k)) = (\phi(n^{(k)})(\mathbf{W} \cdot \mathbf{x}) \leftrightarrow \phi(n'^{(k)})(\mathbf{W} \cdot (\mathbf{x} + \mathbf{v}_k)))$$

$\square$

Figure 5.1 illustrates a case where two obviously isomorphic nets are embedded in slightly different ways and for any choice of unit cell do not possess identical QGs (the labels in the nets indicate for each set of translationally equivalent edges the corresponding edge in the QG). However, the choice of  $\phi(n_i) = \bar{n}_i$  and  $\phi(e_i) = \bar{e}_i$  results in

$$\mathbf{W} = \begin{pmatrix} 0 & 1 \\ 1 & 0 \end{pmatrix}.$$

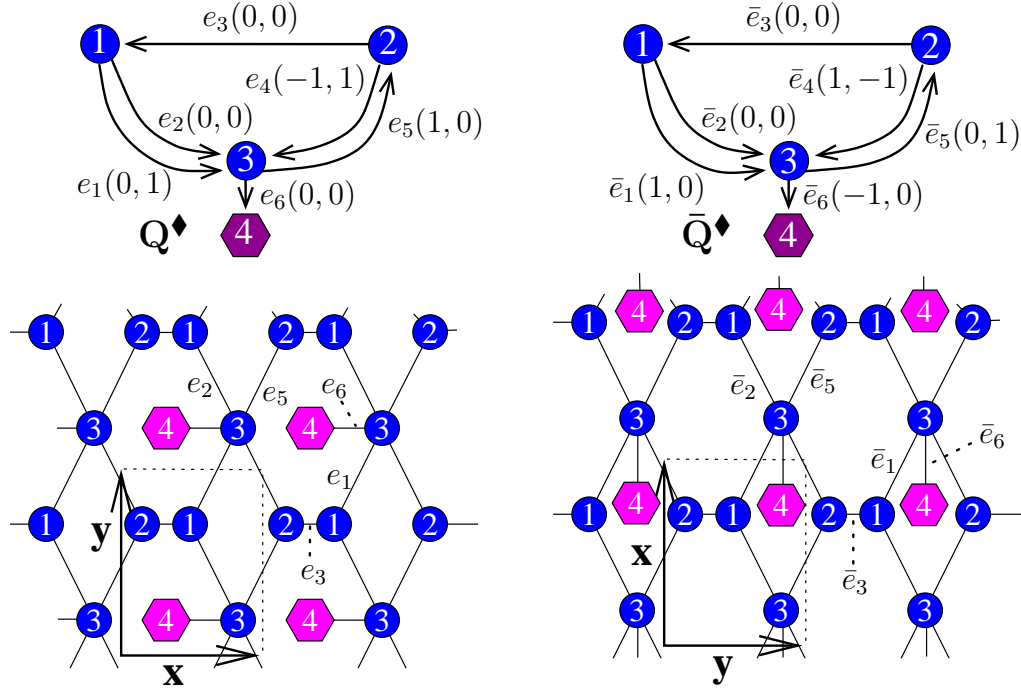


Figure 5.1: Two isomorphic QGs and possible corresponding embeddings of  $\langle \mathbf{Q}^\diamond, \mathbb{Z}^2 \rangle$  and  $\langle \bar{\mathbf{Q}}^\diamond, \mathbb{Z}^2 \rangle$ .

Then, the vectors  $t_1 = t_2 = t_3 = (0, 0)$  and  $t_4 = (0, -1)$  fulfil equation (5.3). Note that a solution for the vectors  $t_i$  is not unique. If a set of vectors  $t_i$  fulfils equation (5.3), then also the vectors  $t_i + u$  for any  $u \in \mathbb{Z}^D$ .

It can be shown that  $\mathbf{W}$  in equation (2.1) and  $\mathbf{W}$  in theorem 5.2.3 are identical, which allows a direct calculation of this matrix.

Theorem 5.2.3 does not allow a direct calculation of the  $\mathbf{t}_i$ 's for a given pair of quotient graphs. The following reformulation of the problem improves on this. Be

1.  $\mathbf{W}$  defined as in theorem 5.2.3,
2.  $\mathbf{V}, \bar{\mathbf{V}} \in \mathbb{Z}^{|\mathbf{Q}^E|} \times \mathbb{Z}^D$  matrices composed of rows of edge labels for an arbitrarily chosen but fixed orientation of the edges in  $\mathbf{Q}$  and  $\bar{\mathbf{Q}}$  (the rows  $\mathbf{V}_k$  and  $\bar{\mathbf{V}}_k$  belong to edges  $e_k$  and  $\phi(e_k)$ ),

3.  $\mathbf{P}$  a special permutation matrix with

$$\mathbf{P}_{k,i} = \begin{cases} 1 & \text{if } \phi(e_i) = \bar{e}_k \text{ and the} \\ & \text{orientation of the edges is maintained} \\ -1 & \text{if } \phi(e_i) = \bar{e}_k \text{ and the} \\ & \text{orientation of the edges is inverted} \\ 0 & \text{otherwise.} \end{cases}$$

4. Be  $\mathbf{R} \in \mathbb{Z}^{|\mathbf{Q}_E|} \times \mathbb{Z}^{|\mathbf{Q}_N|}$  with

$$\mathbf{R}_{k,i} = \begin{cases} 0 & \text{if } e_k \text{ neither originates nor terminates at } n_i \\ & \text{or if } e_k \text{ is a loop, } i.e. \text{ terminates} \\ & \text{at the same } n_i \text{ from which it originated} \\ 1 & \text{if } e_k \text{ terminates at } n_i \\ -1 & \text{if } e_k \text{ originates at } n_i, \end{cases}$$

with  $1 \leq i \leq |\mathbf{Q}_N|$  and  $1 \leq k \leq |\mathbf{Q}_E|$ .

5. Be  $\mathbf{T} \in \mathbb{Z}^{|\mathbf{Q}_N|} \times \mathbb{Z}^D$  (row  $\mathbf{T}_i$  in this matrix corresponds to the  $\mathbf{t}_i$ 's in theorem 5.2.3).

Then, the existence of  $\mathbf{W}$  and  $\mathbf{T}$  fulfilling

$$\bar{\mathbf{V}} = \mathbf{P}(\mathbf{V} + \mathbf{R} \cdot \mathbf{T}) \cdot \mathbf{W} \quad (5.5)$$

is equivalent to the condition in theorem 5.2.3. A reformulation results into  $\mathbf{R}\mathbf{T} = \mathbf{P}^{-1}\bar{\mathbf{V}}\mathbf{W}^{-1} - \mathbf{V}$ , which suggests to calculate  $\mathbf{T}$  by the means of a Moore-Penrose inverse. This approach has two difficulties, though: firstly,  $\mathbf{R}^T\mathbf{R}$  is singular. In the case of a connected<sup>2</sup> QG of dimensionality  $\hat{d} = D$  (compare section 3.1) matrix  $\mathbf{R}$  is of rank  $N - 1$ . This requires to remove, for instance, the first column of  $\mathbf{R}$  and the first row<sup>3</sup> of  $\mathbf{T}$  to obtain  $\hat{\mathbf{R}}$  and  $\hat{\mathbf{T}}$ , respectively. Furthermore  $\mathbf{t}_1$  is set to the zero vector. Then, the formula  $\hat{\mathbf{T}} = (\hat{\mathbf{R}}^T\hat{\mathbf{R}})^{-1}\hat{\mathbf{R}}^T(\mathbf{P}^{-1}\bar{\mathbf{V}}\mathbf{W}^{-1} - \mathbf{V})$  allows a direct calculation of  $\mathbf{T}$ . Secondly, the solution obtained by the Moore-Penrose inverse is not always in the integer domain. However, in all net automorphisms considered by the authors, this was not the case.

Consider, for example, the base graph automorphisms of  $\bar{\mathbf{Q}}^\diamond$  with  $\phi(\bar{n}_i) = \bar{n}_i$ ,  $\phi(\bar{e}_1) = \bar{e}_2$ ,  $\phi(\bar{e}_2) = \bar{e}_1$ ,  $\phi(\bar{e}_3) = \bar{e}_3$ ,  $\phi(\bar{e}_4) = \bar{e}_5$ ,  $\phi(\bar{e}_5) = \bar{e}_4$ , and  $\phi(\bar{e}_6) = \bar{e}_6$ .

---

<sup>2</sup>In the case of disconnected QG with  $k$  sub-graphs,  $k + 1$  suitable columns have to be removed such that  $\mathbf{R}$  is of full rank. More columns have to be removed the dimensionality  $\hat{d}$  of the QG is lower than  $D$ .

<sup>3</sup>The row(s) corresponding to the column(s) removed in  $\mathbf{R}$ .

This automorphisms corresponds to the special permutation matrix

$$\mathbf{P} = \begin{pmatrix} 0 & 1 & 0 & 0 & 0 & 0 \\ 1 & 0 & 0 & 0 & 0 & 0 \\ 0 & 0 & 1 & 0 & 0 & 0 \\ 0 & 0 & 0 & 0 & -1 & 0 \\ 0 & 0 & 0 & -1 & 0 & 0 \\ 0 & 0 & 0 & 0 & 0 & 1 \end{pmatrix}.$$

Among other choices, the following cycles span the vector space of cycle sums for  $\bar{\mathbf{Q}}^\diamond$ :

1. the cycle comprising  $\bar{e}_4$  plus the inverse of the edges  $\bar{e}_3$  and  $\bar{e}_2$  has the cycle sum  $(1, -1)$  and its image the cycle sum  $(-1, -1)$ ,
2. the cycle made of  $\bar{e}_1$  and the inverse of  $\bar{e}_2$  has the cycle sum  $(1, 0)$  and its image the cycle sum  $(-1, 0)$ , and
3. the cycle with edges  $\bar{e}_4$  and  $\bar{e}_5$  which has the same cycle sums as the previous cycle.

Matrix  $\mathbf{W}$  follows from equation (2.1):

$$\mathbf{W} = \begin{pmatrix} -1 & 0 \\ 0 & 1 \end{pmatrix}.$$

Furthermore, the matrices obtained from the edge labels and the connectivity of  $\bar{\mathbf{Q}}^\diamond$  are

$$\mathbf{R} = \begin{pmatrix} -1 & 0 & 1 & 0 \\ -1 & 0 & 1 & 0 \\ 1 & -1 & 0 & 0 \\ 0 & -1 & 1 & 0 \\ 0 & 1 & -1 & 0 \\ 0 & 0 & -1 & 1 \end{pmatrix} \text{ and } \mathbf{V} = \begin{pmatrix} 1 & 0 \\ 0 & 0 \\ 0 & 0 \\ 1 & -1 \\ 0 & 1 \\ -1 & 0 \end{pmatrix}.$$

Then, solving equation (5.5) for  $\mathbf{T}$  using the Moore-Penrose inverse results in the displacements

$$\mathbf{T} = \begin{pmatrix} 0 & 0 \\ 0 & 0 \\ -1 & 0 \\ 1 & 0 \end{pmatrix}$$

### 5.3 The space group of possible embeddings.

An automorphism of a QG is defined as an automorphism of the base graph of the QG which is compatible with some automorphism of the net it is equivalent with<sup>4</sup>. If an embedding of the net is respecting such an automorphism, the matrices  $\mathbf{M}$  and  $\mathbf{W}$  in equations (2.1) and (5.5), respectively, equal to the rotational component of a symmetry of the embedding. Consequently, the traces and determinants of these matrices allow to classify the symmetry operations of a suitable embedding [Grosse-Kunstleve, 1999]. It is therefore straightforward to identify the point group that is a super group to the point groups of all possible embeddings of the net. However, this information alone does not allow to gather more information on the space group or (relative) positions of the nodes in an embedding featuring such a symmetry.

Here, an *embedding of a net* is defined as

- an assignment of suitable vectors in  $\mathbb{R}^D$  to all nodes and
- a representation of the edges as line sections which have as endpoints the coordinates assigned to the corresponding nodes.

No constraint on the intersection or distance between edges, or edges and nodes sharing points other than endpoints is imposed.

More indications on these can be obtained from the orbits of edges in the QG. Consider, for example, the quotient graph  $\mathbf{Q}^\spadesuit$  with  $\mathbf{Q}_N^\spadesuit = \{n_1, n_2\}$  and the edges  $\mathbf{Q}_E^\spadesuit$  comprising:

$$\begin{aligned} e_1 &= n_1 \xrightarrow{(0,0)} n_2 \\ e_2 &= n_1 \xrightarrow{(0,-1)} n_2 \\ e_3 &= n_1 \xrightarrow{(1,0)} n_2 \end{aligned}$$

One of infinitely many possible embeddings of  $\langle \mathbf{Q}^\spadesuit, \mathbb{Z}^2 \rangle$  is shown in figure 5.2. The arbitrarily chosen coordinate system is depicted in the middle of the figure. The triangles and the circles are the nodes resulting from  $n_1$  and  $n_2$ , respectively. The parallelogram (unit cell) is formed by the coordinate system and the dotted lines contains the nodes  $n_1(0, 0)$  and  $n_2(0, 0)$ .

The quotient graph  $\mathbf{Q}^\spadesuit$  possesses 12 base graph automorphisms: either  $n_1$  is mapped onto itself or onto  $n_2$  and  $n_2$  accordingly onto  $n_2$  or  $n_1$ . For each of these two mappings of the nodes,  $3! = 6$  mappings of the edges exist. All 12 base graph automorphisms induce net automorphisms. From these

---

<sup>4</sup>It is not clear whether all automorphisms of a net are equivalent to an automorphism of the QG.

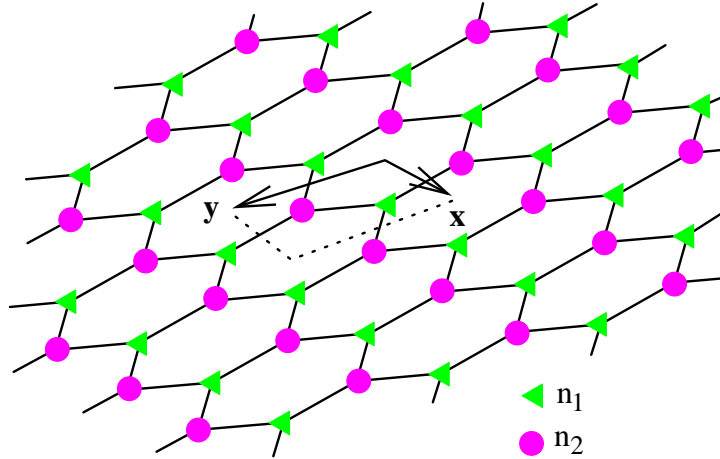


Figure 5.2: An embedding of  $\langle \mathbf{Q}^\spadesuit, \mathbb{Z}^2 \rangle$ .

automorphic mappings  $\phi_1$  and  $\phi_2$  were selected with the following generators and permutation matrices:

$$\mathbf{W}_1 = \begin{pmatrix} 0 & 1 \\ 1 & 0 \end{pmatrix}, \quad \mathbf{P}_1 = \begin{pmatrix} 1 & 0 & 0 \\ 0 & 0 & 1 \\ 0 & 1 & 0 \end{pmatrix},$$

$$\mathbf{W}_2 = \begin{pmatrix} 1 & -1 \\ 1 & 0 \end{pmatrix}, \quad \mathbf{P}_2 = \begin{pmatrix} 0 & -1 & 0 \\ 0 & 0 & -1 \\ -1 & 0 & 0 \end{pmatrix}.$$

These matrices indicate that an embedding with maximal symmetry possesses a reflection corresponding to  $\phi_1$  exchanging the  $x$ - and  $y$ -coordinates and a 6-fold rotation corresponding to  $\phi_2$ . To be precise, the set of these matrices allows to deduce the point group of a possible embedding with maximal symmetry (compare also [Klee, 2004]). In the example presented here, the two operations permute all three edges, though  $\phi_2$  additionally inverts their orientations. Consequently, an embedding realising this automorphism is in group is  $p6mm$ , as this is the only two-dimensional space group in the hexagonal crystal system. However, this does not allow conclusions on (relative) positions of the nodes in an embedding, nor the space group in the general case. More information comes from the orbits of the edges and nodes. All edges in  $\mathbf{Q}^\spadesuit$  are mutually exchanged by some automorphism, and consequently all equivalent edges in an embedding possess the same lengths. Thus,

if  $x_i$  and  $y_i$  are the cell coordinates of node  $n_i$  with cell parameters  $a = b = 1$ :

$$\begin{aligned} |e_1|^2 &= (x_2 - x_1)^2 + (y_2 - y_1)^2 \\ &\quad + 2(x_2 - x_1)(y_2 - y_1) \cos(\gamma) \\ |e_2|^2 &= (x_2 + 1 - x_1)^2 + (y_2 - y_1)^2 \\ &\quad + 2(x_2 + 1 - x_1)(y_2 - y_1) \cos(\gamma) \\ |e_3|^2 &= (x_2 - x_1)^2 + (y_2 - 1 - y_1)^2 \\ &\quad + 2(x_2 - x_1)(y_2 - 1 - y_1) \cos(\gamma) \end{aligned}$$

It follows from  $|e_1| = |e_2|$ ,  $|e_1| = |e_3|$ ,  $\delta_x = x_2 - x_1$ , and  $\delta_y = y_2 - y_1$  that

$$\delta_x = \frac{1}{2(\cos(\gamma) - 1)} \quad (5.6)$$

$$\delta_y = \frac{-1}{2(\cos(\gamma) - 1)} \quad (5.7)$$

As the space group of a maximal symmetry embedding is  $p6mm$ ,  $\gamma$  is either  $60^\circ$  or  $120^\circ$  ( $\gamma = 240^\circ$  and  $300^\circ$  give the same results as  $60^\circ$  and  $120^\circ$ , respectively). The latter results in  $\delta_y = \frac{1}{3}$  and  $\delta_x = -\frac{1}{3}$ , which determines the relative node positions. Setting  $\gamma = 60^\circ$  results in  $\delta_x = \delta_y = -1$  and a co-location of the two sets of nodes, and is therefore meaningless.

An additional source of information on the embedding is the link between the automorphisms of the net and the symmetry of node positions in the embedding. Supposed  $n_i(\mathbf{x})$  at the cell coordinates  $\mathbf{x}$  is mapped onto  $n_j(\mathbf{y})$  using  $(\mathbf{W}_k, \mathbf{w}_k)$ , then  $\mathbf{W}_k \cdot \mathbf{x} + \mathbf{w}_k \doteq \mathbf{y}$ . The notation  $x \doteq y$  signifies that  $x$  and  $y$  differ at most by an integer value. In other words, both sides of the equation are equal “modulus 1”. Equations can be added; a number added to both sides of an equation; but multiplications are forbidden.

In the case of the net  $\langle \mathbf{Q}^\blacklozenge, \mathbb{Z}^D \rangle$ , the matrix  $\mathbf{W}_1$ , and the corresponding automorphism of the QG  $\phi_1(n_i) = n_i$ , this results in

$$y_1 + a_1 \doteq x_1, \quad x_1 + b_1 \doteq y_1, \quad y_2 + a_1 \doteq x_2, \quad x_2 + b_1 \doteq y_2. \quad (5.8)$$

A solution to this redundant set of equations (5.8) is  $b_1 \doteq -a_1$  and  $x_1 \doteq y_1 + a_1$ . This solution is consistent with the facts that the position of (at least) one node relative to the coordinate system is arbitrary and the symmetry operation in question is a reflection. The constraints resulting from  $\phi_2(n_1) = n_2$  are:

$$x_1 - y_1 + a_2 \doteq x_2, \quad x_1 + b_2 \doteq y_2 \quad \text{and} \quad x_2 - y_2 + a_2 \doteq x_1. \quad (5.9)$$

This allows to conclude that  $a_2 \doteq y_1 + \frac{2}{3}$  and  $b_2 \doteq y_1 - x_1 + \frac{1}{3}$ . Setting further  $a_2 = b_2 = 0$  results in the node positions  $(x_1, y_1) = (\frac{2}{3}, \frac{1}{3})$  and  $(x_2, y_2) = (\frac{1}{3}, \frac{2}{3})$ , as well as  $a_1 = 0$ .

Even though this approach to determine details on atom positions and space groups appears to be straightforward, for more complex QGs, the equations can be rather complex. A more direct approach to the space group (that is the translational components  $\mathbf{w}$  of symmetry operations) is based on a dissociation of  $\mathbf{w}$  into

- the *intrinsic translation*  $\mathbf{w}^{(i)}$  of the symmetry operation (in other words, the translation of a glide or screw symmetry), and
- the *location translation*  $\mathbf{w}^{(\ell)}$  which depends on the relative location of the elements of a symmetry operation and the origin of the chosen unit cell (the setting).

so that  $\mathbf{w} = \mathbf{w}^{(i)} + \mathbf{w}^{(\ell)}$  [Hahn, 1992, Grosse-Kunstleve, 1999]. If the Seitz symbol  $(\mathbf{W}|\mathbf{w})$  describes a symmetry operation of order  $\mathcal{O}$ , then

$$(\mathbf{W}|\mathbf{w}^{(i)} + \mathbf{w}^{(\ell)})^{\mathcal{O}} = (\mathbf{I}, \mathbf{w}^{(i)})^{\mathcal{O}}.$$

Compared to this, a repetitive mapping of a node  $n_i$  using a QG automorphism  $\phi$  inducing  $(\mathbf{W}|\mathbf{w})$ , describes the orbit of  $n_i$  in the QG and  $\phi^{\mathcal{O}}(n_i) = n_i$ . The same is true for the embedding if a symmetry operation corresponding to  $\phi$  has zero-valued intrinsic translation. In general,  $\phi^{\mathcal{O}}(n_i(\mathbf{x})) = n_i(\mathbf{y})$  and  $\frac{1}{\mathcal{O}}(\mathbf{y} - \mathbf{x})$  is equal to the intrinsic translation of the symmetry operation. On the other hand, the difference  $\mathbf{y} - \mathbf{x}$  is determined by the QG if a path  $p = \left( n_i \xrightarrow{\mathbf{v}} n_j, n_j \xrightarrow{\mathbf{v}'} n_k \dots, n_o \xrightarrow{\mathbf{v}''} \phi(n_i) \right)$  exists. Be  $P$  the embedding of this path  $p$  with all edges oriented from  $n_i$  to  $\phi(n_i)$ , Then the path  $n_i(\mathbf{x}), n_j(\mathbf{x}'), \dots, n_i(\mathbf{y})$  is the concatenation of paths  $P, \phi(P), \dots, \phi^{\mathcal{O}-1}(P)$ , which in turn are the embeddings of the paths  $p, \phi(p), \dots, \phi^{\mathcal{O}-1}(p)$ . Consequently:

$$\mathbf{w}^{(i)} = \frac{1}{\mathcal{O}} \sum_{i=0}^{\mathcal{O}-1} \left( \sum_{e \in \phi^i(p)} \mathbf{v} \right). \quad (5.10)$$

In other words, if for an automorphism  $\phi$  of a QG a node  $n$  and its image  $\phi(n)$  are connected by a path  $p$ , the intrinsic translation of the symmetry operation is determined by equation (5.10). However, as path  $p$  from  $n_i$  to  $\phi(n_i)$  is not necessarily unique, the  $\mathbf{w}^{(i)}$  in equation (5.10) depends on  $p$ . A QG automorphism therefore may correspond to several distinct intrinsic translations and symmetry elements. This correlates nicely to the fact that certain symmetry operations have multiple symmetry elements with possibly distinct glide or screw components.

A maximal symmetry embedding of the net  $\langle \mathbf{Q}^\spadesuit, \mathbb{Z}^D \rangle$  (the perfect hexagon net similar to a layer of graphite) is used as example. This embedding has



the symmetry of space group of  $p6mm$  with 12 symmetry operations (see the International Tables A [Hahn, 1992]), with two mirror planes perpendicular to the  $x$ -axis:

- one without glide component and
- one with a glide vector parallel to the  $y$ -axis.

Compared to this, the QG automorphism with the rotational component  $\begin{pmatrix} -1 & -1 \\ 0 & 1 \end{pmatrix}$  has exactly two intrinsic vectors:  $(0, 0)$  and  $(0, \frac{1}{2})$ . Similarly for all other mirror planes, a corresponding QG automorphism with two intrinsic vectors exists. Compared to this, all rotations in the two-dimensional space have obviously no screw component. This is reflected by the QG as their automorphisms having only zero intrinsic vectors.

The same observation is true for the location parts, yet they depend much on the intrinsic translations: assumed that  $\phi(n_i(\mathbf{x})) = n_j(\mathbf{y})$  for some arbitrary nodes and cell coordinates  $\mathbf{x}$  and  $\mathbf{y}$  exist two intrinsic translations  $\mathbf{w}_1^{(i)}$  and  $\mathbf{w}_2^{(i)}$ . For symmetry reasons,  $\mathbf{W} \cdot \mathbf{x} + \mathbf{w}_1^{(i)} + \mathbf{w}_1^{(\ell)} \doteq \mathbf{y}$  and  $\mathbf{W} \cdot \mathbf{x} + \mathbf{w}_2^{(i)} + \mathbf{w}_2^{(\ell)} \doteq \mathbf{y}$ , which implies that  $\mathbf{w}_1^{(i)} + \mathbf{w}_1^{(\ell)} \doteq \mathbf{w}_2^{(i)} + \mathbf{w}_2^{(\ell)} \doteq \mathbf{y} = \mathbf{w}$ . Therefore, the locational and intrinsic translations for a symmetry element are inter-depend.

**Corollary 5.3.1.** *Let  $\phi$  be an automorphism of some QG with at least one path from some arbitrary node  $n$  to  $\phi(n)$ . Then, the QG defines the intrinsic translations of the symmetry operation equivalent to  $\phi$  of the embedding with respect to a right handed coordinate system. Furthermore, a connected QG fully determines the space group with maximal symmetry of an embedding, except for the setting of this embedding.*

A few notes concerning corollary 5.3.1 are due:

- The embedding with respect to a coordinate system of a certain handedness is required to be able to distinguish between space groups that differ only by the orientation of a screw (that is a  $3_1$  and  $3_2$ ,  $4_1$  and  $4_3$ ,  $6_1$  and  $6_5$  screw).
- No “reasonable” embedding having the maximal symmetry may exist. For example, an embedding with maximal symmetry may require that some nodes are at the same position. The QG with the edges  $\{n_1 \xrightarrow{0,1} n_1, n_1 \xrightarrow{1,0} n_1, n_1 \xrightarrow{0,0} n_2\}$  represents such a case.

- It is possible to define nets, for which some automorphisms are not represented by a base graph automorphism of all QG representing these nets. However, these nets are rare and are unlikely to represent crystal structures. A more detailed discussion of these nets would exceed the scope of this work.
- In the case that the QG is obtained from a crystal structure based on a supercell, or a cell that becomes a supercell in an embedding with a maximal symmetry, several QG automorphisms correspond to the same rotational matrix. Section 5.8 discusses such a case and chapter 6 uses this to reduce QGs in size.
- The space group (symbol) can be determined by the approaches proposed in Grosse-Kunstleve [1999] or Grosse-Kunstleve and Adams [2002].

For the quotient graph  $\mathbf{Q}^\spadesuit$  and the symmetry operation  $\mathbf{W}_1$ , three paths consisting of a single edge have to be considered as  $\phi(n_1) = n_2$ . As further  $\phi_1(e_2) = e_2$  the intrinsic translation for the corresponding reflection is  $\mathbf{w}_1^{(i)} = \frac{1}{2}(\mathbf{v}_1 - \mathbf{v}_1) = \mathbf{0}$ . Setting the path  $p$  to  $e_2$  and  $e_3$  results into the (effectively identical) intrinsic translations  $(-\frac{1}{2}, -\frac{1}{2})$  and  $(\frac{1}{2}, \frac{1}{2})$ , respectively ( $\phi_1$  exchanges the two edges). The two vectors correspond to the 8 reflection and 12 glide planes that are parallel or perpendicular to the vector  $(1, 1)$  of the space group  $p6mm$ . Accordingly for  $\phi_2$  and  $p = (e_1)$ :  $\mathbf{w}_2 = \frac{1}{6}(\mathbf{v}_1 - \mathbf{v}_2 + \mathbf{v}_3 - \mathbf{v}_1 + \mathbf{v}_2 - \mathbf{v}_3) = \mathbf{0}$ . All other choices for  $p$  result in the same intrinsic translations, which matches the fact that only one 6-fold rotation axis exists for the hexagon net. Placing  $n_1$  at the same cell coordinates used earlier allows the calculation of the locational parts:  $\mathbf{w}_1^{(i)} = (\frac{1}{3}, \frac{2}{3})^T - \mathbf{W}_1 \cdot (\frac{2}{3}, \frac{1}{3})^T - \mathbf{w}_1^{(i)} = \mathbf{0}$  and  $\mathbf{w}_2^{(i)} = \mathbf{0}$ .

## 5.4 Automorphism of QGs and crystal structures

As shown in section 5.3, a considerable amount of information on the space group of an embedding of a net with maximal symmetry can be gathered from the QG automorphisms. This can be used different ways:

- In an *ab initio* generation of crystal structures (compare [Strong et al., 2004, Winkler et al., 2001]), a structure optimisation could be primed with suitable cell parameters and atom positions.

- During a search using the approaches described in [Bader et al., 1997, Klein, 1996, Thimm, 2004] for nets with a given space group, QGs with incompatible automorphisms can be discarded early.
- For the prediction of pseudo-symmetries (compare [Abrahams, 1989, Fadda and Zanzotto, 2004, Igartua et al., 1999, 1996]). For this purpose, the QG, as obtained from the observed crystal structure, is analysed for automorphisms and an embedding of maximal symmetry. Then, the result is compared to the observed structure. Examples for this approach are discussed in sections 5.5 to 5.8.

It has to be noted that, even if the idea is similar, the concept of pseudo-symmetries in this paper is different from that used in [Igartua et al., 1999, Abrahams, 1989] and the papers referenced there. In the approach described in these papers, phase transitions to a structure with higher symmetry are only detected if the atom displacements are of the order of 0.1 to 2.0Å. As the minimal displacement considered to be a ‘transition’ and maximal permitted displacement is somewhat arbitrary (different limits are used), and no measure is taken to ensure the persistence of inter-atomic bonds, the procedure is somewhat arbitrary.

Opposed to this, the approach presented here does not impose any arbitrary constraint such as a maximal displacement and ensures that no bonds are broken. Also, our method has a much lower computational complexity and does not require that subgroup – super group relations have to be considered. Obvious draw backs are that the proposed structures may not be stable elastically and only constraints on positions (not exact values) may stand at the end of calculations. However, combining this approach with quantum mechanical calculations is possible, and that would then ensure that the structure is stable with respect to small distortions and that internal degrees of freedom would be optimised, so that the structure is force-free.

After the conclusion of this work, the author found that Delgado-Friedrichs and O’Keeffe [2003] realised that the QG contains sufficient information to determine the space group of an embedding. However, their less rigorous approach relies much on an actual embedding of a net and they do not distinguish between the intrinsic and location vector. This leads to a dependency of the resulting description of the symmetry operation on the arbitrary setting of the embedding and an identification of the space group is therefore somewhat tedious.

In order to show the potential of QGs to gain information on a crystal structure and demonstrate the application of the discussed theories, quartz, marcasite, pyrite, pseudo-cubic FeS<sub>2</sub> and graphite are closer examined in sections 5.5 to 5.8.

## 5.5 Pyrite

Pyrite ( $\text{FeS}_2$ ) crystallises in the cubic space group  $Pa\bar{3}$  [Bragg, 1913] (see also figure 5.3 and table A.11). However, some pyrites and a significant number

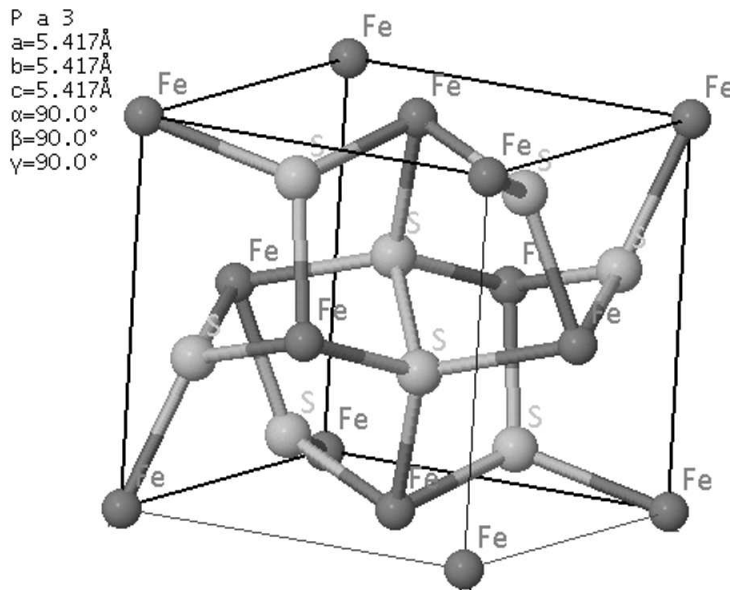


Figure 5.3: The structure of cubic pyrite (see table A.11, [Bayliss, 1977]).

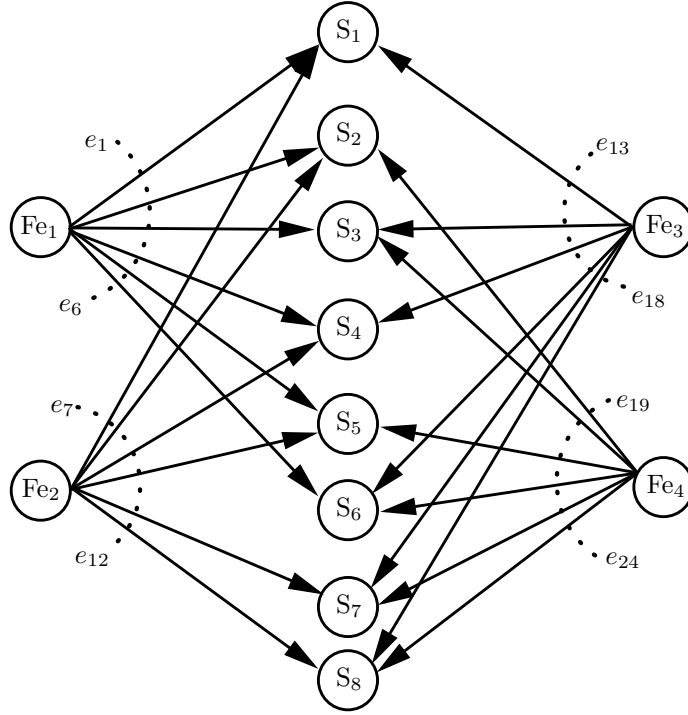
of related compounds crystallise in slightly distorted structures with lower symmetries (*e.g.* Bayliss [1977], Marcos et al. [1996]). The low symmetry structures can be derived from the cubic structure type by small atomic displacements, and have the same bonding system and topology, described by the edges in figure 5.4.

An examination of the QGs of these structures shows that each has 24 automorphisms (the order of  $Pa\bar{3}$ ). It can be concluded that the pyrite structure-type has a maximal symmetry for this topology.

## 5.6 Marcasite and rutile

Marcasite is an orthorhombic ( $\text{FeS}_2$ , space group  $Pnmm$ ) polymorph, whose structural relationship to pyrite has been discussed previously (see Dodony et al. [1996] and references therein). The marcasite structure is illustrated in figure 5.5 (dark coloured spheres represent Fe-atoms, light coloured S).

The structural differences between marcasite and pyrite manifest themselves in the respective coordination and cycle sequences (see Beukeman and



$$\begin{array}{lll}
 e_1 = \text{Fe}_1 \xrightarrow{0,0,-1} \text{S}_1 & e_2 = \text{Fe}_1 \xrightarrow{0,-1,0} \text{S}_2 & e_3 = \text{Fe}_1 \xrightarrow{-1,0,0} \text{S}_3 \\
 e_4 = \text{Fe}_1 \xrightarrow{-1,-1,0} \text{S}_4 & e_5 = \text{Fe}_1 \xrightarrow{-1,0,-1} \text{S}_5 & e_6 = \text{Fe}_1 \xrightarrow{0,-1,-1} \text{S}_6 \\
 e_7 = \text{Fe}_2 \xrightarrow{0,0,0} \text{S}_1 & e_8 = \text{Fe}_2 \xrightarrow{0,-1,0} \text{S}_2 & e_9 = \text{Fe}_2 \xrightarrow{0,-1,0} \text{S}_4 \\
 e_{10} = \text{Fe}_2 \xrightarrow{0,0,0} \text{S}_5 & e_{11} = \text{Fe}_2 \xrightarrow{0,-1,0} \text{S}_7 & e_{12} = \text{Fe}_2 \xrightarrow{0,0,0} \text{S}_8 \\
 e_{13} = \text{Fe}_3 \xrightarrow{0,0,-1} \text{S}_1 & e_{14} = \text{Fe}_3 \xrightarrow{0,0,0} \text{S}_3 & e_{15} = \text{Fe}_3 \xrightarrow{0,0,0} \text{S}_4 \\
 e_{16} = \text{Fe}_3 \xrightarrow{0,0,-1} \text{S}_6 & e_{17} = \text{Fe}_3 \xrightarrow{0,0,-1} \text{S}_7 & e_{18} = \text{Fe}_3 \xrightarrow{0,0,0} \text{S}_8 \\
 e_{19} = \text{Fe}_4 \xrightarrow{1,0,0} \text{S}_2 & e_{20} = \text{Fe}_4 \xrightarrow{0,0,0} \text{S}_3 & e_{21} = \text{Fe}_4 \xrightarrow{0,0,0} \text{S}_5 \\
 e_{22} = \text{Fe}_4 \xrightarrow{1,0,0} \text{S}_6 & e_{23} = \text{Fe}_4 \xrightarrow{0,0,0} \text{S}_7 & e_{24} = \text{Fe}_4 \xrightarrow{1,0,0} \text{S}_8
 \end{array}$$

Figure 5.4: The QG of pyrite (see table A.11).

Klee [1994], Conway and Sloane [1997]). The positions of the sulphur atoms are such that sulphur atoms are bound to four Fe- and possibly to one other S-atom. As the distance between the sulphur atoms of  $2.212\text{\AA}$  is noticeably larger than the bond lengths observed in sulphur allotrophs (about  $2.06\text{\AA}$  for  $S_6$  [Akahama et al., 1993] and  $2.032\text{\AA}$  to  $2.060\text{\AA}$  for  $\gamma$ -sulphur<sup>5</sup> at ambient conditions [Watanabe, 1974]), it is not obvious if they are bound together or not. We will show here that this question can be investigated by studying

<sup>5</sup> $2.047\text{\AA}$  to  $2.073\text{\AA}$  if corrected librational motion [Watanabe, 1974].

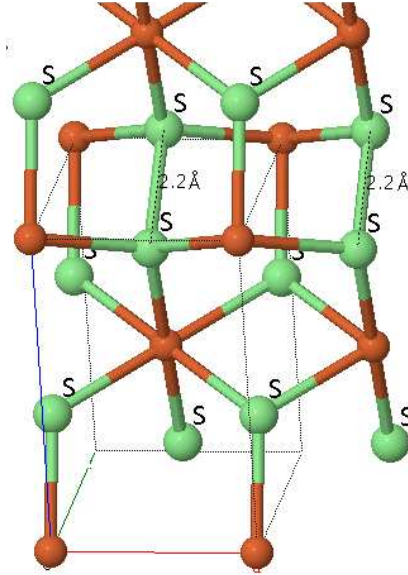


Figure 5.5: The marcasite structure (see table A.9, [CCMS, 2007])

the QG.

The QG  $\mathbf{Q}^{\text{marc}}$  of marcasite shown in figure 5.7 was created from the structural data in table A.9. The dashed edges  $e_{13}$  and  $e_{14}$  stand for these S-S contacts, equivalent bonds are shown near the centre of figure 5.5. If these edges are neglected, then marcasite QG possesses 16 automorphisms and is isomorphic to the QG of rutile, a  $\text{TiO}_2$  polymorph, and rutile-like structures without anion-anion bonds. Rutile crystallises in the tetragonal space group  $P\frac{4_2}{m}nm$  (see figure 5.6 and table A.14)

In the following, we first assume that there are no S-S bonds, and therefore the horizontally drawn, dashed edges ( $e_{13}$  and  $e_{14}$ ) in figure 5.7, are ignored in the analysis. The net  $\langle \mathbf{Q}^{\text{marc}} \setminus \{e_{13}, e_{14}\}, \mathbb{Z}^3 \rangle$  would therefore be the same as for rutile-like structures. We now proceed to embed it with a maximal symmetry, which will allow us to determine the highest space group and node positions. Then we consider the existence of S-S bonds and discuss the consequences.

In order to simplify the notation, the shorthand  $\phi[n_1, n_2, \dots, n_n][e_1, e_2, \dots][p_1, p_2, \dots]$  is used to indicate that  $\phi$  permutes the nodes  $n_i$ , edges  $e_k$ , or paths  $p_\ell$ . More precisely,  $\phi(n_1) = n_2$ ,  $\phi(n_2) = n_3$ , and so on until  $\phi(e_n) = e_1$  and similar for the  $e_k$  and  $p_\ell$ . Not all permutations are necessarily given.

An embedding with a maximal symmetry of marcasite has point group  $4/mmm$ . The corresponding structure therefore has a tetragonal space group in the range of space groups 123 to 142 in the International Tables A [Hahn,

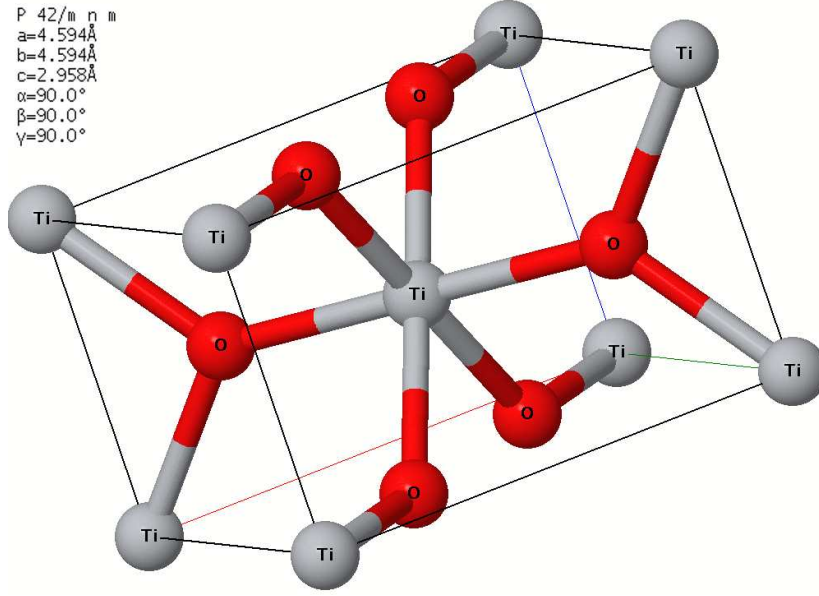


Figure 5.6: The rutile structure  $\text{TiO}_2$  (see table A.14).

1992]. The automorphism  $\phi_1$  corresponds to the matrix

$$\mathbf{W}_1 = \begin{pmatrix} 0 & 1 & 0 \\ 1 & 0 & 0 \\ 0 & 0 & 1 \end{pmatrix}$$

and exceeds the set of automorphisms expected for a structure in space group  $Pn\bar{m}$ . As the automorphism  $\phi_1[n_3][n_4][n_5][n_6][n_1, n_2]$  maps some nodes on themselves, the path  $p$  can be chosen to be a single node and therefore  $\mathbf{w}^{(i)} = \mathbf{0}$ . In order to reduce the number of variables (and to obtain the usual setting for the embedding),  $n_5$  is set to have the cell coordinates  $(0, 0, 0)$ . It then follows from  $\phi_1[n_5]$  that  $\mathbf{W}_1 \cdot \mathbf{0} + \mathbf{w}_1^{(\ell)} \doteq \mathbf{0}$  and therefore  $\mathbf{w}_1^{(\ell)} = \mathbf{0}$ . The symmetry operation is  $(\mathbf{W}_1 | \mathbf{0})$ . Furthermore,  $x_i$  is equal to  $y_i$  for all  $3 \leq i \leq 6$  as well as  $x_1 = y_2$ ,  $x_2 = y_1$ , and  $z_1 = z_2$ . Note that, although other choices for  $p$  lead to different intrinsic and location vectors, their sum is always zero.

$\phi_2[n_5, n_6][n_1, n_4, n_2, n_3]$  corresponds to the symmetry matrix

$$\mathbf{W}_2 = \begin{pmatrix} 0 & 1 & 0 \\ -1 & 0 & 0 \\ 0 & 0 & 1 \end{pmatrix}.$$

Choosing  $p = (e_1, e_7)$  with  $\phi_2[(e_1, e_7), (e_{12}, e_6), (e_3, e_8), (e_{10}, e_5)]$  results in  $\mathbf{w}_2^{(i)} = (0, 0, \frac{1}{2})$ . Setting  $\mathbf{w}_2^{(\ell)} = (u, v, w)$  and using  $\phi_2(\phi_2(n_5)) = n_5$  im-

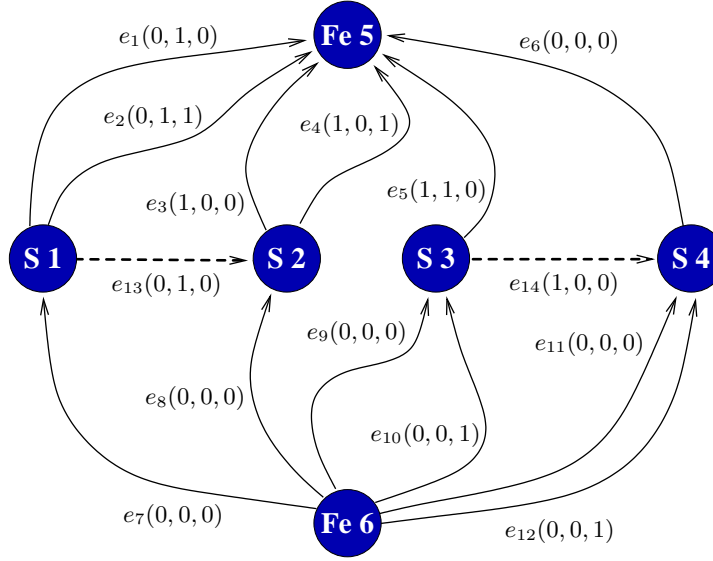


Figure 5.7: The quotient graph of marcasite  $\mathbf{Q}^{\text{marc}}$  (nodes are labelled with the element type and a node number). The dashed edges are the questionable sulphur-sulphur bonds.

plies that  $(u + v, v - u, 2w + 1) \doteq \mathbf{0}$ . This equation has two solutions for  $u, v, w \in [0, 1)$  with  $u = v = \frac{1}{2}$  and  $w \in \{0, \frac{1}{2}\}$ , resulting in  $\mathbf{w}_2 = (\frac{1}{2}, \frac{1}{2}, w + \frac{1}{2})$ . Furthermore,  $n_6$  has the coordinates  $(\frac{1}{2}, \frac{1}{2}, w + \frac{1}{2})$

$\phi_3[n_5, n_6][n_1, n_4, n_2, n_3][(e_1, e_7), (e_{11}, e_6), (e_3, e_8), (e_6, e_5)]$  with matrix

$$\mathbf{W}_3 = \begin{pmatrix} 0 & 1 & 0 \\ -1 & 0 & 0 \\ 0 & 0 & -1 \end{pmatrix},$$

results in  $\mathbf{w}_3^{(i)} = (0, 0, 0)$  and for symmetry reasons  $\mathbf{w}_3^{(\ell)} = (x_6, y_6, z_6) = (\frac{1}{2}, \frac{1}{2}, w + \frac{1}{2})$ , that is  $\mathbf{w}_3 = \mathbf{w}_2$ . The mapping  $\phi_2(n_1) = n_4 = \phi_3(n_1)$  implies that  $z_1 + w + \frac{1}{2} \doteq z_4 \doteq -z_1 + w + \frac{1}{2}$  which is equivalent to  $z_1 \in \{0, \frac{1}{2}\}$ . If furthermore  $n_1$  has the coordinates  $(x_1, y_1, z_1)$ , then  $n_4$  is located at  $(y_1 + \frac{1}{2}, -x_1 + \frac{1}{2}, -z_1 + w + \frac{1}{2})$ ,  $n_2$  at  $(-x_1, -y_1, z_1)$ , and  $n_3$  at  $(-y_1 + \frac{1}{2}, x_1 + \frac{1}{2}, -z_1 + w + \frac{1}{2})$ .

Combining this with the constraints on the node position obtained from  $\phi_1$  gives

- $n_1 : (x_1, -x_1, z_1)$ ,
- $n_2 : (-x_1, x_1, z_1)$ ,
- $n_3 : (x_1 + \frac{1}{2}, x_1 + \frac{1}{2}, -z_1 + w + \frac{1}{2})$ , and



- $n_4 : (-x_1 + \frac{1}{2}, -x_1 + \frac{1}{2}, -z_1 + w + \frac{1}{2})$ .

The automorphism

$\phi_4[n_5, n_6][n_1, n_4][n_2, n_3][(e_1, e_7)(e_{12}, e_6)]$  is paired with matrix

$$\mathbf{W}_4 = \begin{pmatrix} -1 & 0 & 0 \\ 0 & 1 & 0 \\ 0 & 0 & 1 \end{pmatrix}.$$

Choosing  $p = (e_1, e_7)$  results in  $\mathbf{w}_4^{(i)} = (0, \frac{1}{2}, \frac{1}{2})$  and for symmetry reasons  $\mathbf{w}_4^{(\ell)} = (x_6, y_6 - \frac{1}{2}, z_6 - \frac{1}{2}) = (\frac{1}{2}, 0, w)$ , implying that  $\mathbf{w}_4 = \mathbf{w}_2$ .

The generators of the space groups of the full symmetry embedding of marcasite without S-S bonds are therefore:

$$\begin{array}{ccc} y, & x, & z \\ y + \frac{1}{2}, & -x + \frac{1}{2}, & z + w + \frac{1}{2} \\ y + \frac{1}{2}, & -x + \frac{1}{2}, & -z + w + \frac{1}{2} \\ -x + \frac{1}{2}, & y + \frac{1}{2}, & z + w + \frac{1}{2}, \end{array}$$

which, for  $w = 0$ , are the generators of space group  $P\frac{4_2}{m}nm$  as listed in the International Tables A [Hahn, 1992]. A comparison with rutile, which has the symmetry  $P\frac{4_2}{m}nm$  and a QG isomorphic to the QG of marcasite, shows that for  $x_1 = 0.1947$  and  $z_1 = \frac{1}{2}$ , the lattice coordinates for the embedding of the marcasite quotient graph and the rutile structure are identical. An alternative setting for the same structure is obtained for  $x_1 = 0.1947$  and  $z_1 = 0$ . Even though the parameter  $x_1$  is not constrained further by the topology of the net and its automorphisms, it may appear reasonable that all bonds are of the same length. Setting, for example,  $|e_1| = |e_5|$  has the solution  $x_1 = \frac{2a^2 - c^2}{8a^2}$ . For the experimentally determined lattice parameters of rutile ( $a = 4.593 \text{ \AA}$ ,  $c = 2.956 \text{ \AA}$ ), yields  $x_1 = 0.198$ , which is close to the observed value for  $x_1$  (the bonds differ 2% in length). For marcasite ( $a = 4.443 \text{ \AA}$ ,  $b = 5.424 \text{ \AA}$ ,  $c = 3.386 \text{ \AA}$ )  $x_1$  becomes 0.1911 (if, in the latter case,  $a$  is set to the average of the experimentally determined  $a$  and  $b$  cell parameters). If  $w$  is chosen as  $\frac{1}{2}$ , this does obviously not change the intrinsic translations, and therefore only the setting of the embedding.

If, however, there are S-S bonds, the QG of marcasite has only the eight automorphisms equivalent to the symmetry operations in space group  $Pn\bar{1}m$  observed for the physical structure. This implies that if there are S-S bonds, any phase transitions between the two  $\text{FeS}_2$  polymorphs must be reconstructive, i.e. it would require that bonds are broken. It should be stressed that

a group theoretical analysis would not give this result.  $Pn\bar{m}$  is a maximal space group of  $P\frac{4}{m}nm$  [Stokes and Hatch, 1988], where a transition would be proper ferroelastic, and hence from this perspective, a displacive phase transition would be allowed. In practical terms, it is generally the case that reconstructive phase transitions require some activation energy and can be quenched, and hence metastable polymorphs can be obtained, while displacive phase transitions happen on the time scale of phonon frequencies and do not require any activation energy. As no prior crystal chemical knowledge has been used in this deduction, the finding of the importance of a bond between the anion applies to all structures with a marcasite-like structure. It would therefore now be of interest to systematically investigate these with respect to those where the anion-anion bond is very weak, as such border-line cases are probably most likely to allow to obtain new phases. That rutile is very far away from this border-line is clear from a consideration of the O-O distance: O-O bonds are expected to exist between oxygen atoms about 1.4Å apart, whereas the shortest observed distance between two oxygen atoms in the rutile structure is 2.53Å. With respect to their topologies, rutile and marcasite (presuming the presence of the S-S bonds) are of maximal symmetry.

## 5.7 Quartz

$\alpha$ - and  $\beta$ -quartz ( $\text{SiO}_2$ ) are known to possess the same topology [Heany, 1994]. Figure 5.8 shows the structures of two types of quartz structures (see also tables A.12 and A.13).

As to their QG, the enantiomorphic  $\alpha$ -quartz crystals with symmetries  $P3_121$  and  $P3_221$ , as well as the enantiomorphic crystals of  $\beta$ -quartz in  $P6_222$  and  $P6_422$  [Wenk and Bulakh, 2004, Levien et al., 1980, CCMS, 2007]) can be described by QGs similar to those in figures 5.9 or 5.10 (an edge is interpreted as a Si-O-Si bond). As that both quartz modifications have the same topology, it is no surprise that theorem 5.2.3 shows they are isomorphic. However, out of the 48 isomorphisms between the base graphs, only 12 correspond to a (net) isomorphism. One of these isomorphism matches nodes with the same names as well as  $\phi(e_i) = \bar{e}_i$  for all  $i$ . A possible choice of four cycles for the calculation of  $\mathbf{W}$  are the three pairs of (anti-)parallel edges and any cycle with three edges. This results in

$$\mathbf{W} = \begin{pmatrix} 1 & 0 & 0 \\ 0 & 1 & 0 \\ 0 & 0 & -1 \end{pmatrix}.$$

As none of the four space groups has a mirror plane perpendicular to the

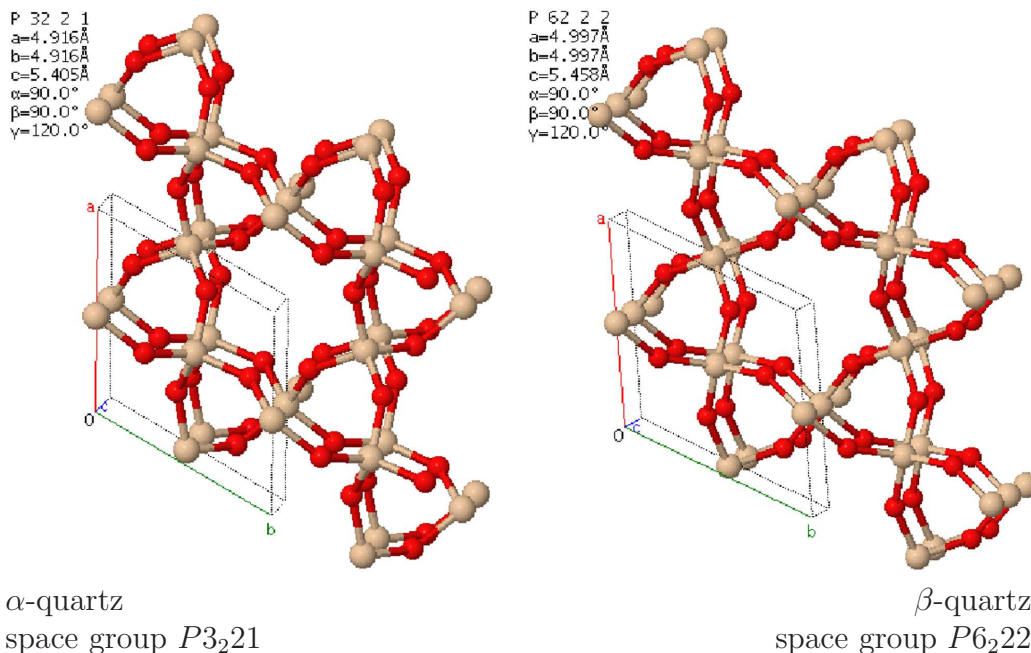


Figure 5.8: The structures of  $\alpha$ - and  $\beta$ -quartz  $\text{SiO}_2$  [Levien et al., 1980, CCMS, 2007].

$z$ -axis, or, equivalently, none of the net automorphisms features this matrix  $\mathbf{W}$ , it can be deduced that the two structures are enantiomorphic.

Furthermore, it can be shown that both QGs possess 12 automorphisms, which allows to conclude that  $\beta$ -quartz has the highest possible symmetry for its topology. Alternatively - even if  $\beta$ -quartz would be unknown - it could be concluded that a bond-preserving (displacive) phase transition of  $\alpha$ -quartz to a higher symmetry can result only in a structure having space group  $P6_222$  (for the lower symmetry phase in  $P3_221$ ) or  $P6_422$  (for the lower symmetry phase in  $P3_121$ ). Reasons for this are:

- For  $P3_121$ , space groups  $P6_122$  and  $P6_422$  are the only super groups of cardinality 12 with a 6-fold axis (see Hahn [1992]).
- An examination of the orbit of an edge under QG automorphisms of order 6 reveals that the equivalent symmetry operations in an embedding must have an intrinsic vector  $(0, 0, \pm\frac{1}{3})$ . This excludes  $P6_122$ .
- For  $P3_221$  space groups  $P6_222$  and  $P6_522$  are the only permissible super groups.
- For the same reason as in the earlier case,  $P6_522$  is excluded.

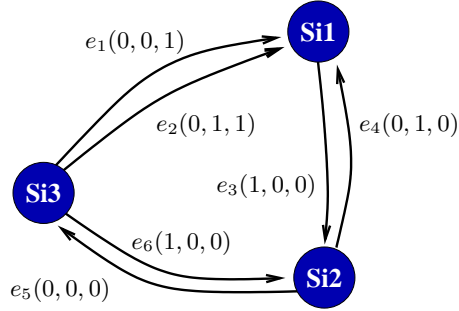


Figure 5.9: A QG derived from  $\alpha$ -quartz with a  $P3_121$  structure.

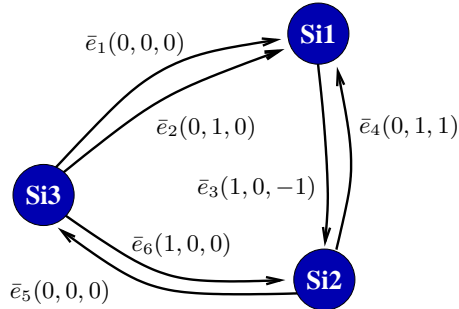


Figure 5.10: A QG derived from  $\beta$ -quartz with a  $P6_222$  structure.

This observation is consistent with the fact that phase transitions from  $\alpha$ - to  $\beta$ - or back are either between the structures in space groups  $P3_121$  and  $P6_422$  or  $P3_221$  and  $P6_222$  [Heany, 1994]: other transitions would be reconstructive and therefore require a higher activation energy.

Note that the approach is only valid for ‘strongly’ periodic structures and incommensurate structures cannot be represented or predicted. On the other hand, this test can be applied to all structures for possible higher symmetric phases with the same topology in a very straightforward manner.

## 5.8 Graphite

Graphite crystallises, among others, “un-buckled” in the hexagonal space groups  $P6_3mc$  or “buckled” in  $P6_3/mc$  if only polymorphs with two layers per unit cell are considered CCMS [2007]. The QGs of these modifications are somewhat special, as they consist of two disconnected sub-graphs as shown in figure 5.11. Each set of layers, each set containing layers that are translationally equivalent with respect to integer multiples of vector  $(0, 0, c)$ , is represented by a connected sub-graph (see also figure 3.1.).

Graphite crystallises also in a rhombohedral phase (space group  $R\bar{3}m$ ), in which the layers are stacked such that a primitive cell contains only two atoms CCMS [2007]. This implies that a QG representing this structure comprises only two nodes with three edges between them. However, doubling the size of the unit cell in the direction perpendicular to the layers results in a QG of the same appearance as shown in figure 5.11.

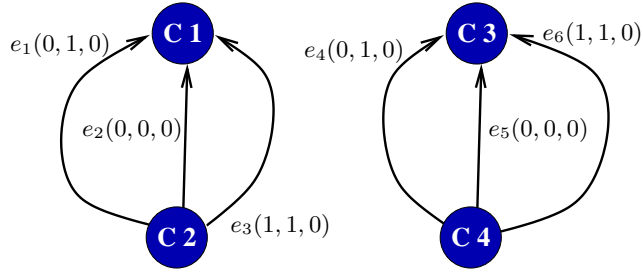


Figure 5.11: The QG of graphite.

Table 5.1 shows three matrices and the corresponding automorphisms with their intrinsic translations as far as they are defined by the QG. The automorphisms, for which no intrinsic translations are defined, correspond to symmetry operations in the graphite modifications which exchange atoms across layers. Therefore, for these automorphisms the translational part of the symmetry operation, that is the relative positions of the layers, can be arbitrarily chosen (if energy considerations are left aside). This ambiguity of the relative positions of the layers is consistent with the coexistence of the three considered graphite modifications.

$\mathbf{W}_1 = \begin{pmatrix} 0 & 1 & 0 \\ 1 & 0 & 0 \\ 0 & 0 & 1 \end{pmatrix}$ $\mathcal{O} = 2$	$\mathbf{W}_2 = \begin{pmatrix} 1 & 1 & 0 \\ -1 & 0 & 0 \\ 0 & 0 & 1 \end{pmatrix}$ $\mathcal{O} = 6$	$\mathbf{W}_3 = \begin{pmatrix} 1 & 0 & 0 \\ 0 & 1 & 0 \\ 0 & 0 & -1 \end{pmatrix}$ $\mathcal{O} = 2$
$\phi_1[n_1, n_2][n_3, n_4]$ $[e_2, e_3][e_1][e_5, e_6][e_4]$ $\mathbf{w}_{1a}^{(i)} = (0, 0, 0)$ $\mathbf{w}_{1b}^{(i)} = (\frac{1}{2}, \frac{1}{2}, 0)$	$\phi_2[n_1, n_2][n_3, n_4]$ $[e_1, e_2, e_3][e_4, e_5, e_6]$ $\mathbf{w}_2^{(i)} = (0, 0, 0)$	$\phi_3[n_1][n_2][n_3][n_4]$ $[e_1][e_2][e_3][e_4][e_5][e_6]$ $\mathbf{w}_3^{(i)} = (0, 0, 0)$
$\phi'_1[n_1, n_4][n_2, n_3]$ $[e_2, e_6][e_1, e_4][e_3, e_5]$	$\phi'_2[n_1, n_4][n_2, n_3]$ $[e_1, e_5, e_3][e_4, e_2, e_6]$	$\phi'_3[n_1, n_3][n_2, n_4]$ $[e_1, e_4][e_2, e_5][e_3, e_6]$
No path from $n$ to $\phi'_i(n)$ exists: $\mathbf{w}_i^{(i)}$ is undefined.		

Table 5.1: Details on the automorphism of the graphite QG

# Chapter 6

## Reduction of Quotient Graphs

This chapter presents an approach to reduce the size of quotient graphs in a way comparable to a reduction of a centred or supercell to a smaller (centred, super-, or primitive) cell. As quotient graphs and nets are independent of an embedding (that is the exact positions of atoms within a crystal structure), this can reveal structures with reduced translational symmetries. This may occur when

1. a structure is distorted in a non-affine manner,
2. a structure is the mixture of two end members (in which different atom types occupy otherwise comparable positions).

Reduced symmetries of the first case are, for example, observable in certain graphite polymorphs (compare section 5.8).

Examples for the second case are solid solutions that are isomorphic to one or more end members. For the sake of simplicity, the structure of copper-lanthanide alloys such as CuEr, CuEu, CuGd, CuHo, and CuDy are used as an example [Villars and Calvert, 1989]. These alloys crystallise in space group  $Pm\bar{3}m$ . In a standard setting, the copper atoms are located at the corners of the cubic unit cell and the lanthanide atom in the centre (fractional coordinates  $(0, 0, 0)$  and  $(\frac{1}{2}, \frac{1}{2}, \frac{1}{2})$ , respectively). The primitive cell contains therefore two atoms (see figure 6.1).

If in these structures the lanthanide atoms are replaced by copper atoms, additional symmetries, among which is  $(\mathbf{I}, (\frac{1}{2}, \frac{1}{2}, \frac{1}{2}))$ , are created. Even so this “replacement” incurs an expansion of the unit cell to that of pure copper with  $a = 3.615\text{\AA}$ , the fractional coordinates of the atoms and the unit cell are unchanged. However, the structure of Cu is in space group  $Fm\bar{3}m$  with one atom per primitive cell. This implies that the quotient graph of pure copper for a primitive cell contains half as many nodes and edges as compared to

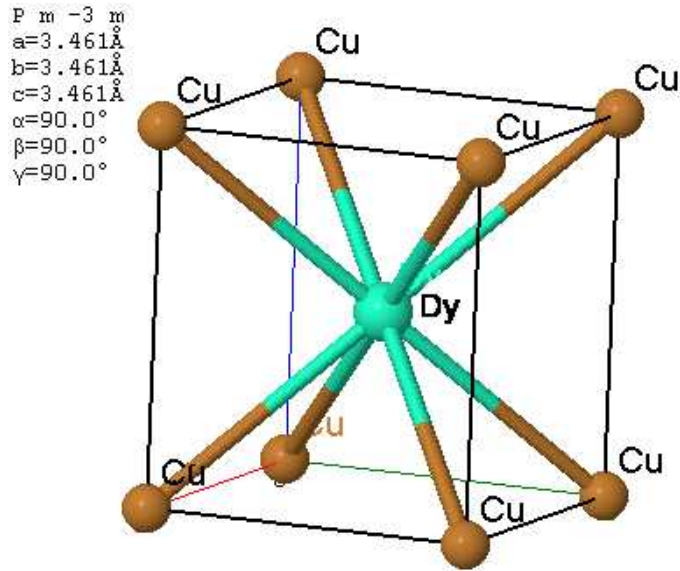


Figure 6.1: The CuDy structure.

the copper-lanthanide alloys discussed above. The two QGs are shown in figure 6.2.

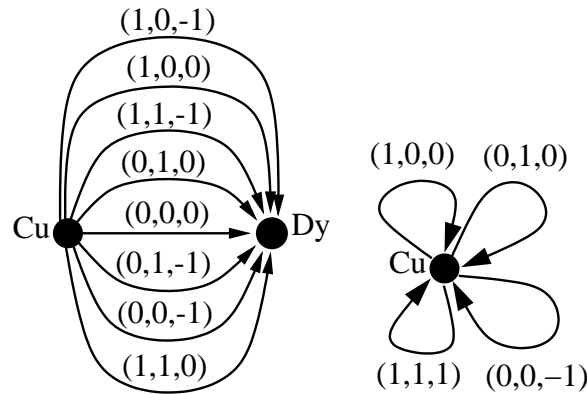


Figure 6.2: The CuDy and the Cu QGs for primitive cells.

## 6.1 Automorphism and translational symmetry

In chapter 5 it was shown that in a maximal symmetry embedding (if atom types disregarded) all symmetries are equivalent to a QG automorphism.



This obviously includes purely translational symmetries, some of which may not be observed in the original structure (as for example the symmetries stated above for the copper-lanthanide alloys).

Automorphisms  $\phi$  of a QG which have the identity matrix as the rotational component are equivalent to translations of a maximal-symmetry embedding of the equivalent net. These automorphisms, excluding the identity with a zero intrinsic translation, are called *translational automorphism*, and only these are of interest in the remainder of this chapter. QGs without a translational symmetry cannot be reduced (all embeddings of the net have necessarily a maximal translational symmetry).

Assume that  $\phi$  is a translational automorphism of  $\mathbf{Q}$ . For this  $\phi$ , the sizes of all edge orbits  $\hat{n}_i$  and node orbits  $\hat{e}_k$  are equal to the order  $\mathcal{O}$  of the symmetry operation. A reduced set of nodes  $\hat{\mathbf{Q}}_N$  is accordingly defined<sup>1</sup> as

$$\hat{\mathbf{Q}}_N = \{\hat{n}_i \mid \hat{n}_i \text{ is an orbit of some node in } \mathbf{Q}_N\}$$

The definition of a set of edges follows a similar scheme, but requires a calculation of appropriate edge labels. This calculation relies on the relative size of the new cell and therefore the translational symmetries of the smaller lattice: for all translational symmetries  $(\mathbf{I}, \mathbf{w})$  of order  $\mathcal{O}$ , the vector  $\mathcal{O} \cdot \mathbf{w}$  describes a translation compatible with all embeddings of  $\mathbf{G} = \langle \mathbf{Q}, \mathbb{Z}^D \rangle$ . On the other hand,  $\mathbf{w}$  describes a translation compatible with the sub-lattice of a suitable embedding of the net (that is a translation compatible with a unit cell of reduced size).

A key observation it is that for automorphism  $\phi$  of order  $\mathcal{O}$ , any node  $n(\mathbf{x}) \in \mathbf{G}_N$  and this vector  $\mathbf{w}$  the equation

$$\phi^{\mathcal{O}}(n(\mathbf{x})) = n(\mathbf{x} + \mathcal{O} \cdot \mathbf{w}) \quad (6.1)$$

holds. Furthermore, if a path  $p$  between  $n(\mathbf{x})$  and  $\phi(n(\mathbf{x}))$  exists in this net, then the path  $p$ , together with an appropriate choice of its isomorphic images, links  $n(\mathbf{x})$  and  $n(\mathbf{x} + \mathcal{O} \cdot \mathbf{w})$ . These paths form, if concatenated, a continuous path  $\hat{p}$ . An addition of the labels of the edges in the QG that correspond to path  $\hat{p}$  must result into a vector equal to  $\mathcal{O} \cdot \mathbf{w}$  (all edges in the path have to have the same orientation). Nets, in which no path between isomorphic nodes exist, are discussed in section 6.1.3.

Figure 6.3 shows examples for such paths. In this figure, shaded nodes are translationally equivalent (only one set of nodes is shown). All nodes in figure 6.3 represented by circles, shaded or not, are assumed to equivalent with respect to an automorphism of the net (though not necessarily translationally equivalent in a given embedding). The continuous lines designate

---

<sup>1</sup>The names of the orbits are reused for the nodes and edges in the newly defined QG.

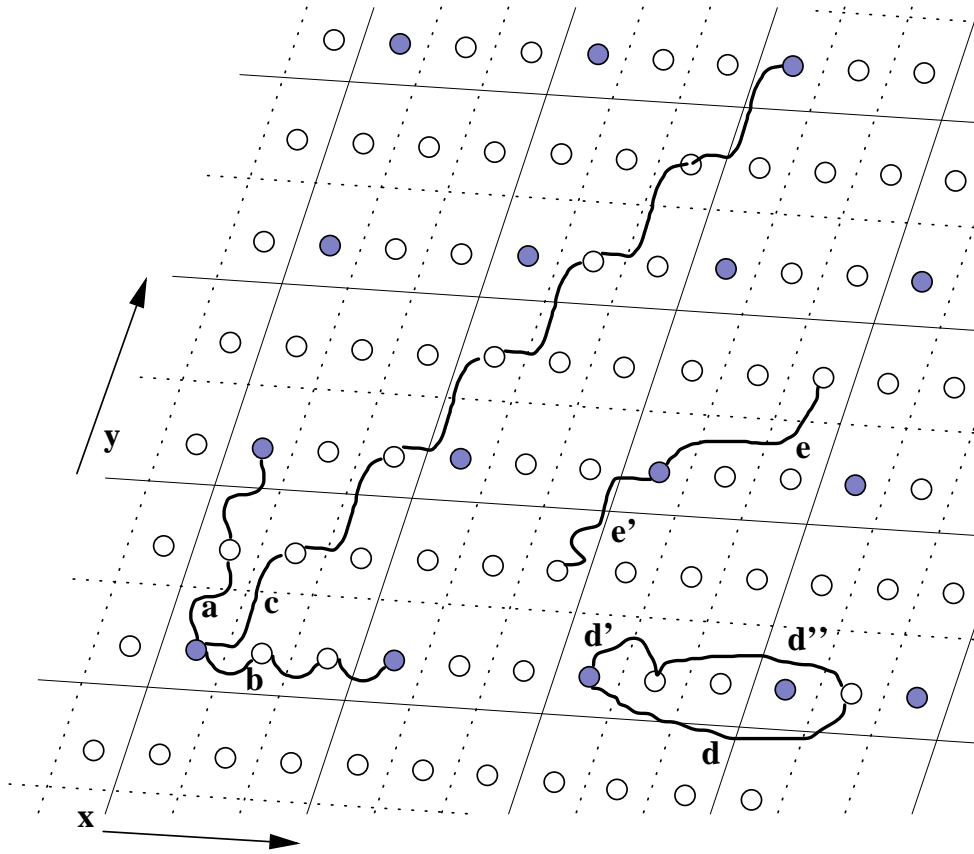


Figure 6.3: Examples for paths occurring for isomorphic paths between isomorphic nodes. For an explanation of labels, see text.

a possible choice of a (super-) cell, the dotted lines the primitive cell. The curved lines represent possible paths (including an arbitrary set of nodes); paths with the same shape are isomorphic.

Figure 6.3 can also be considered as the representative of an almost arbitrary embedding of a simply connected net. The only particularity of this embedding is that a 3x2 supercell exists as compared to an embedding with a maximal translational symmetry.

The simplest cases, where a path can be used to deduce information on translational symmetries for the sub-lattices, are represented by the paths labelled with **a** and **b**: three, respectively two, isomorphic “copies” of the paths span a distance equivalent to the length of the unit cell along the  $y$ - and  $x$ -axis. That two translationally equivalent instances of path **a** are needed to cover the distance between two shaded nodes implies that, compared to the original lattice, the lattices of all maximal-symmetry embeddings have half the spacing in the direction of the  $y$ -axis. From path **b** it can be concluded that the lattice is three times as wide. In the QG equivalent to the supercell, an accumulation of the edge labels in all possible QGs corresponding to paths **a** and **b** and their isomorphic copies results into the respective unit vectors. The vectors  $\frac{1}{2} \cdot (0, 1) = (0, \frac{1}{2})$  and  $\frac{1}{3} \cdot (1, 0) = (\frac{1}{3}, 0)$  must therefore describe a translation of an embedding with maximal translational symmetry. In these vectors, the non-zero elements indicate a reduction of the unit cell in the respective directions; zero-entries indicate that the cell is unchanged in this direction. Consequently, unit cells with relative sizes  $(\frac{1}{3}, 1)$  and  $(1, \frac{1}{2})$  result in lattices with higher translational symmetries. These vectors, which describe the reduction of the lattice, are called *reduction vectors* **t** (a detailed definition is proposed later). Similarly, from path **c**, it can be concluded that the size of a unit cell in a maximal symmetry embedding is a sixth of the size of the original cell. Accumulating the edge labels of the path onto which path **c** and its “copies” are mapped has to result into  $\mathbf{t} = \frac{1}{6}(2, 3) = (\frac{1}{3}, \frac{1}{2})$  as the accumulated path crosses the vertical cell boundaries twice, the horizontal boundaries three times.

For path **d**, the calculation yields  $\mathbf{t} = (\frac{4}{3}, 1)$ , which clearly does not define an appropriate size for the reduced unit cell. The reason is that path **d** is equivalent of a combination of two other paths: path **d''**, which is compatible with the original lattice, and path **d'**, which is proper to the reduced lattice. Similar observations are rather obvious in a (visual) inspection of a structure, and the path used to reduce the lattice can be chosen appropriately. However, this is not the case if - as intended in this work - an embedding of the net is to be avoided. The solution to this problem is rather trivial: the vector **t** can be split into an integer part, which is equivalent to a translation of the original lattice and a part that comprises elements with absolute values

smaller than one; the reduction vector  $\mathbf{t}$  becomes  $(\frac{1}{3}, 1)$ .

Path  $\mathbf{e}$  illustrates a similar problem: although  $\mathbf{t} = (\frac{2}{3}, \frac{1}{2})$  has no integer component, it does not define a reduction of the lattice. However, from the translational symmetry and the existence of path  $\mathbf{e}$ , it can be concluded that an alternative path  $\mathbf{e}'$  has to exist, which does define a valid reduction of the lattice.

In general, if  $\mathbf{t} = (\frac{s_1}{t_1}, \frac{s_2}{t_2}, \dots, \frac{s_D}{t_D})$  is a vector of fractions (it is assumed in the following that nominators and denominators have no common divisor other than one), then the vector  $(\frac{1}{t_1}, \frac{1}{t_2}, \dots, \frac{1}{t_D})$  can be represented by some path (without proof). Following these observations, a reduction vector  $\mathbf{t}$ , which is compatible with a chosen automorphism and suitable for a reduction of the QG, is defined as follows:

**Definition 6.1.1.** *Be  $\phi$  a QG automorphism with symmetry  $(\mathbf{I}, \mathbf{w})$ ,  $n \in \mathbf{Q}_N$ ,  $\mathbf{w} \neq \mathbf{0}$ , and  $p$  an arbitrary path between  $n$  and  $\phi(n)$  in the QG. Then, the reduction vector  $\mathbf{t}$  is defined as*

$$\mathbf{t} = \Downarrow \left( \frac{1}{\mathcal{O}} \sum_{i=0}^{\mathcal{O}-1} \sum_{e \in \phi^i(p)} \mathbf{v} \right) \quad (6.2)$$

with  $\mathcal{O}$  the size of the orbit of the nodes in the QG under  $\phi$  and  $\Downarrow (\cdot)$  the function that sets the nominator of fractions to one (note that  $\Downarrow (0) = 1$ ).

Figure 6.4 shows more examples of isomorphic paths - though in a lattice where the maximal degree of reduction is identical in two directions. Paths  $\mathbf{f}$  and  $\mathbf{g}$  both result in a reduction of the lattice by a third. The same must be true for path  $\mathbf{h}$  as the orbit of any node comprises only three sets of nodes that are not isomorphic with respect to the original lattice. However, unlike the other examples, the product over the elements in  $\mathbf{t}$  does not match this degree of reduction. This can be readily understood by an examination of all possible embeddings: an equilateral unit cell would have to have a length of  $\sqrt{\frac{1}{3}}$  times the length of the original unit cell in order to have the appropriate volume. Such a unit cell is for obvious reasons incompatible with the given lattice. Such cases can be recognised by an examination of the denominators in vector  $\mathbf{t}$ : a (sub-)set of denominators then has a greatest common divisor larger than one. This situation corresponds loosely to structures where alternative cells possess edges oblique to the original, larger unit cell.

In principle, a reduction vector  $\mathbf{t}$  can have both properties: in one direction, the direction follows the behaviour illustrated by paths  $\mathbf{a}$  to  $\mathbf{g}$ , in other

directions that of path  $\mathbf{h}$ . For example, the reduction vector  $(\frac{1}{3}, \frac{1}{6}, \frac{1}{5})$  describes a reduction in the  $x$ - $y$ -direction by 3, combined with reductions along the  $y$ - and  $z$ -axis by 2 and 5, respectively. Consequently, the volume of a unit cell in the reduced lattice is 30 time smaller than that of the original cell (as opposed to  $\prod t_i = \frac{1}{90}$ ). Even though a general formula could probably be formulated, a simpler approach is proposed here: combined reductions are expressed as sequences of the two simpler cases as presented in the following two sections.

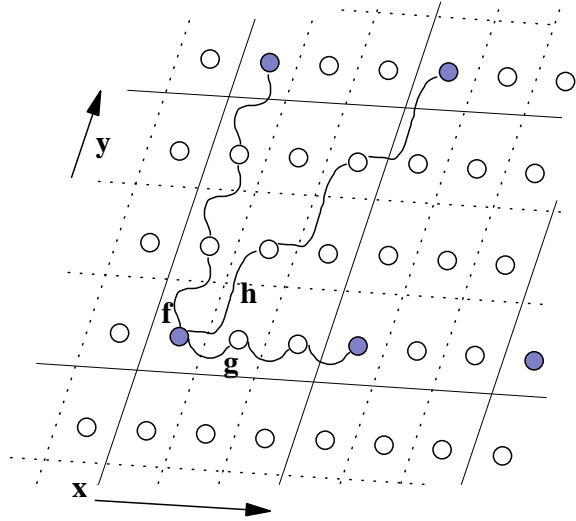


Figure 6.4: Second example for isomorphic paths:  $\mathbf{t} = (\frac{1}{3}, \frac{1}{3})$

### 6.1.1 Reduction for vectors of type $\mathbf{t} = (\frac{1}{k}, \frac{1}{\ell}, \frac{1}{m}, \dots)$

The reductions considered in this section possess reduction vectors in which all greatest common divisors of all pairs of denominators are equal to one. For these cases, equation 6.3 determines edge labels for the reduced QG  $\hat{\mathbf{Q}}$  ( $1 \leq k \leq D$ ).

$$\hat{v}_k = \sum_{\mathbf{v} \text{ with } (n \xrightarrow{\mathbf{v}} n') \in \hat{e}} v_k \cdot \prod_{i=1, i \neq k}^D t_i \quad (6.3)$$

The resulting labels  $\hat{\mathbf{v}}$  are integer if  $\mathbf{Q}$  has a spanning tree with zero labels<sup>2</sup> and the edges

$$\hat{\mathbf{Q}}_E = \{\hat{e}_k = \hat{n}_i \xrightarrow{\hat{\mathbf{v}}} \hat{n}_k | n \in \hat{n}_i, n' \in \hat{n}_k, \text{ and } n \xrightarrow{\mathbf{v}} n' \in \mathbf{Q}_E\} \quad (6.4)$$

permits to define  $\hat{\mathbf{Q}} = (\hat{\mathbf{Q}}_N, \hat{\mathbf{Q}}_E)$ , which is isomorphic to  $\mathbf{Q}$ .

That equation (6.3) defines edge labels for an isomorphic QG can be motivated with a simplified case: assume  $\mathbf{t}$  has only one element at position  $d$  that is equal to  $\frac{1}{\mathcal{O}}$  and the QG has a spanning tree with exclusively zero-labels (this can always be achieved, see section 5.2).

A comparison of  $\mathbf{Q}$  and an arbitrary embedding of the net  $\langle \mathbf{Q}, \mathbb{Z}^D \rangle$  shows that exactly one edge  $e$  per orbit in  $\mathbf{Q}$  has a non-zero element at position  $d$ . The product in equation (6.3) is equal to one and consequently  $\hat{v}_d$  is equal to the element in the edge  $e$ . Be  $p$  a path between  $n(\mathbf{0})$  and  $n(\mathbf{y})$  in  $\langle \mathbf{Q}, \mathbb{Z}^D \rangle$  with all  $y_i = 0$  if  $i \neq d$ . Then an isomorphic path exists in the reconstructed net  $\langle \hat{\mathbf{Q}}, \mathbb{Z}^D \rangle$  between the nodes  $\hat{n}(\mathbf{0})$  and  $\hat{n}(\mathcal{O} \cdot \mathbf{y})$ . The construction of  $\langle \mathbf{Q}, \mathbb{Z}^D \rangle$  and  $\langle \hat{\mathbf{Q}}, \mathbb{Z}^D \rangle$  allows to conclude that for all paths between  $n(\mathbf{x})$  and  $n(\mathbf{x} + \mathcal{O} \cdot \mathbf{y})$  possess isomorphic paths in  $\langle \hat{\mathbf{Q}}, \mathbb{Z}^D \rangle$ .

Following a similar argument, all vector elements excluding  $v_d$  in a chosen edge orbit must be equal (but not necessarily zero). This implies that the sum in equation (6.3) is equal to  $\mathcal{O}$ -times of the value of any of the elements. However, the product of the  $t_i$  in equation (6.3) is equal to  $\frac{1}{\mathcal{O}}$  and the resulting element is therefore equal to the corresponding vector elements of the edges in the orbit. Consequently, if a path between  $n(\mathbf{x})$  and  $n(\mathbf{y})$  with  $x_d = y_d$  exists in  $\langle \mathbf{Q}, \mathbb{Z}^D \rangle$ , then an isomorphic path exists in  $\langle \hat{\mathbf{Q}}, \mathbb{Z}^D \rangle$  between the nodes  $\hat{n}(\mathbf{x})$  and  $\hat{n}(\mathbf{y})$  with  $x_d = y_d$ . As the reduction further preserves the degree of the nodes, it is reasonable to assume that the reduction produces isomorphic QGs.

### 6.1.2 Reduction for vectors of type $\mathbf{t} = (\frac{1}{\mathcal{O}}, \frac{1}{\mathcal{O}}, \dots)$ .

The reduction of a QG with respect to a reduction vector  $\mathbf{t} \in \{\frac{1}{\mathcal{O}}, 1\}^D$  requires several steps. First, a set of labels is calculated by accumulating all labels in an orbit. Using these labels in a reduced QG defines a QG equivalent to a set of  $\mathcal{O}$  penetrating nets. Each of these nets is individually isomorphic to the original net. Then, the labels in the reduced QG are transformed such that it describes again a net with the original multiplicity. For simply connected, non-penetrating nets, this is achieved in four steps:

---

<sup>2</sup>If this is not the case,  $\mathbf{Q}$  or  $\hat{\mathbf{Q}}$  may have to be modified such that this is true; compare theorem 5.2.2.

1. Calculate temporary labels  $\tilde{\mathbf{v}}$  using

$$\tilde{\mathbf{v}} = \sum_{\mathbf{v} \text{ with } (n \xrightarrow{\mathbf{v}} n') \in \hat{e}} \mathbf{v}, \quad (6.5)$$

and create a  $\hat{\mathbf{Q}}_E$  using these labels as in equation (6.4).

2. Use theorem 5.2.1 to change these labels such that the reduced QG possesses a spanning tree with zero-vector labels  $\bar{\mathbf{v}}$ . This achieves that all non-zero edge labels are equal to cycle sums (all cycles can be chosen such that they comprise at most one edge with a non-zero label). Replacing the labels (as a set) by their product with an arbitrary orthogonal matrix consequently results in an isomorphic QG.
3. Choose a set of  $D$  labels among the vectors  $\bar{\mathbf{v}}$  such that the (quadratic) matrix  $\mathbf{M} = (\bar{\mathbf{v}}_1, \bar{\mathbf{v}}_2, \dots, \bar{\mathbf{v}}_D)$  has a determinant equal to  $\pm \mathcal{O}$ .
4. Set the vectors  $\hat{\mathbf{v}}_k$  in  $\hat{\mathbf{Q}}_E$  to

$$\hat{\mathbf{v}}_k = \mathbf{M}^{-1} \bar{\mathbf{v}}_k \quad (6.6)$$

The procedure of reducing penetrating nets to a simply connected net can be motivated as follows: as  $\mathbf{M}$  consists of cycle sums, its determinant defines the number of interpenetrating nets. Consequently, multiplying its inverse to all cycle sums ensures that the multiplicity  $\hat{m}$  of the QG is equal to one as  $\det(\mathbf{M} \cdot \mathbf{M}^{-1}) = 1$ . At the same time, the vectors  $\bar{\mathbf{v}}_1, \bar{\mathbf{v}}_2, \dots, \bar{\mathbf{v}}_D$  are aligned with the axes of the coordinate system. This ensures that the new labels are integer.

A few selected cases are discussed in the sections 6.2 to 6.7.

### 6.1.3 Reduction of disconnected QGs

For disconnected QGs, an automorphism may map nodes onto each other that are not linked by some path. The QGs of the graphite modifications discussed in section 5.8 are examples. In such cases, the sub-graphs form orbits and it is sufficient to choose from each orbit a QG and combine these in a new QG. In the case of the graphite QG shown in figure 5.11, a possible reduced QG is the sub-graph consisting of two nodes and the them connecting edges.

As for connected QGs, the degree of reduction is equal to the size of the node and edge orbits. However, a definition of a reduction vector is somewhat meaningless.

## 6.2 The reduction of the square net

The probably simplest QG that falls into the category discussed in section 6.1.2 is  $\mathbf{Q}^\square$ . This QG and a possible embedding are shown in figure 6.5. The dashed lines and the inscribed coordinate system indicate a possible choice for a unit cell that results into the QG on the left.

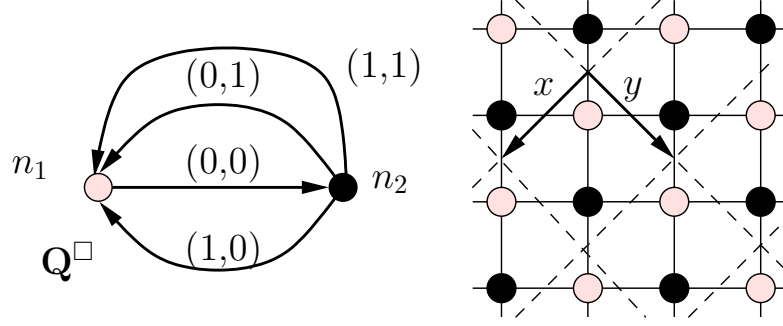


Figure 6.5: A QG for the square net with 2 nodes.

The only translational automorphism of  $\mathbf{Q}^\square$  maps  $n_1$  onto  $n_2$  and induces a reduction vector  $\mathbf{t} = (\frac{1}{2}, \frac{1}{2})$ . The reduced QG has a single node  $\hat{n}$  and two loops. Equation 6.5 determines the temporary labels as  $\tilde{\mathbf{v}}_1 = (1, 1)$  and  $\tilde{\mathbf{v}}_2 = (1, -1)$ . As the tree of the reduced QG comprises a single node, both edge labels are equivalent to cycle sums, which implies that  $\tilde{\mathbf{v}}_1 = \tilde{\mathbf{v}}_2$ . The matrix

$$\mathbf{M} = \begin{pmatrix} 1 & 1 \\ 1 & -1 \end{pmatrix}$$

results in a replacement of the edge vectors with

$$\mathbf{M}^{-1} \cdot \tilde{\mathbf{v}}_1 = \begin{pmatrix} 1 \\ 0 \end{pmatrix} \text{ and } \mathbf{M} \cdot \tilde{\mathbf{v}}_2 = \begin{pmatrix} 0 \\ 1 \end{pmatrix}$$

and the edges in the reduced QG are

$$\hat{\mathbf{Q}}_E^\square = \left\{ \hat{n} \xrightarrow{(1,0)} \hat{n}, \quad \hat{n} \xrightarrow{(0,1)} \hat{n} \right\}$$

## 6.3 The reduction of the triangle net

A distorted, 2-dimensional net and its QG  $\mathbf{Q}^\Delta$  are shown in figure 6.6. The arrows in the net's embedding indicate the translational symmetries used during its transformation into  $\mathbf{Q}^\Delta$ . Table 6.1 shows all three translational automorphisms of  $\mathbf{Q}^\Delta$  along with the corresponding  $\mathbf{w}^{(i)}$ ,  $\mathbf{t}$ , and the orbits



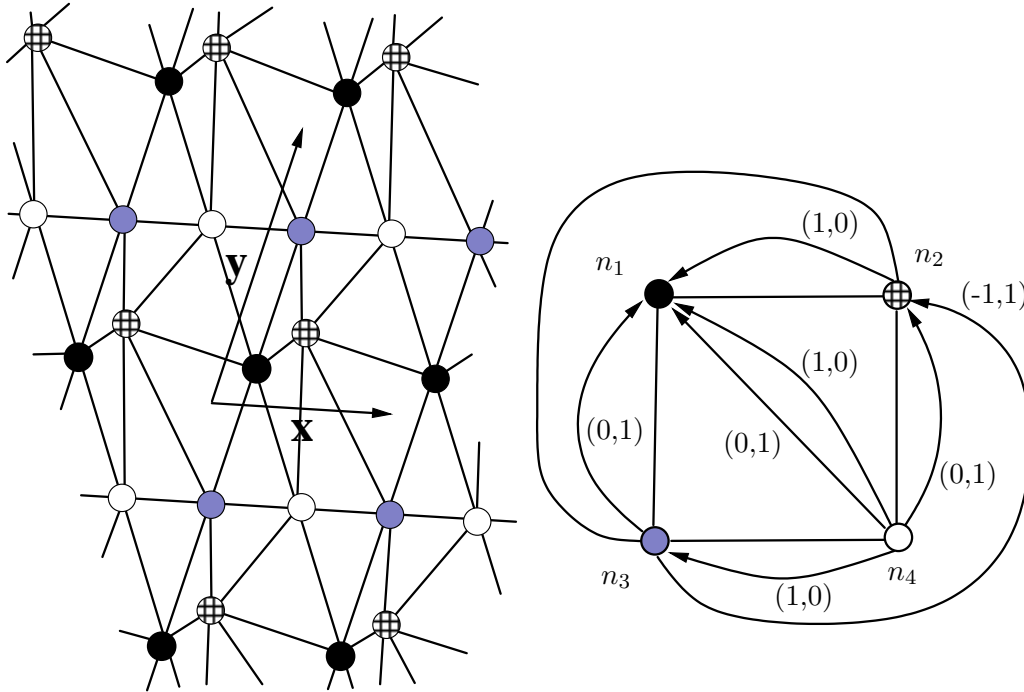


Figure 6.6: The distorted triangle net with its QG  $\mathbf{Q}^\Delta$ .

of nodes and edges. All reductions have as results QGs with two nodes and six edges.

For example, the QG  $\hat{\mathbf{Q}}^\Delta$  resulting from the reduction  $(\frac{1}{2}, 1)$  is depicted on the left side of figure 6.7. This graph can be further reduced with  $\mathbf{t} = (1, \frac{1}{2})$  to the irreducible graph  $\hat{\hat{\mathbf{Q}}}^\Delta$  at the right side of figure 6.7.

It is noteworthy that no direct reduction of  $\mathbf{Q}^\Delta$  to  $\hat{\hat{\mathbf{Q}}}^\Delta$  exists. In general, this absence of a direct reduction to a minimally sized QG seems to be tied to the presence of a reduction vector with denominators with a greatest common divisor larger than one.

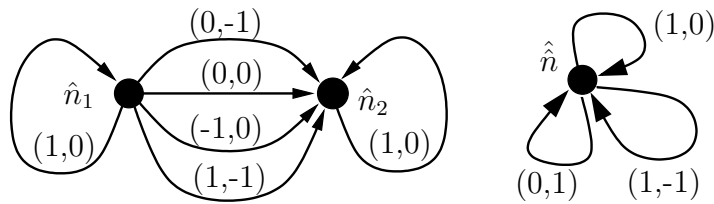


Figure 6.7: the QG  $\hat{\mathbf{Q}}^\Delta$  obtained from a reduction of  $\mathbf{Q}^\Delta$  with reduction  $(\frac{1}{2}, 1)$  and the irreducible QG  $\hat{\hat{\mathbf{Q}}}^\Delta$  obtained by reducing  $\hat{\mathbf{Q}}^\Delta$ .

$w^{(i)}$	$\mathbf{t}$	Node orbits	Edge orbits
$\begin{pmatrix} \frac{1}{2} \\ 0 \end{pmatrix}$	$\begin{pmatrix} \frac{1}{2} \\ 1 \end{pmatrix}$	$[\mathfrak{n}_1, \mathfrak{n}_2]$ $[\mathfrak{n}_3, \mathfrak{n}_4]$	$[\mathfrak{n}_2 \xrightarrow{(1,0)} \mathfrak{n}_1, \mathfrak{n}_1 \xrightarrow{(0,0)} \mathfrak{n}_2]$ $[\mathfrak{n}_3 \xrightarrow{(0,1)} \mathfrak{n}_1, \mathfrak{n}_4 \xrightarrow{(0,1)} \mathfrak{n}_2]$ $[\mathfrak{n}_3 \xrightarrow{(0,0)} \mathfrak{n}_1, \mathfrak{n}_4 \xrightarrow{(0,0)} \mathfrak{n}_2]$ $[\mathfrak{n}_4 \xrightarrow{(1,0)} \mathfrak{n}_1, \mathfrak{n}_3 \xrightarrow{(0,0)} \mathfrak{n}_2]$ $[\mathfrak{n}_1 \xrightarrow{(0,-1)} \mathfrak{n}_4, \mathfrak{n}_2 \xrightarrow{(1,-1)} \mathfrak{n}_3]$ $[\mathfrak{n}_4 \xrightarrow{(1,0)} \mathfrak{n}_3, \mathfrak{n}_3 \xrightarrow{(0,0)} \mathfrak{n}_4]$
$\begin{pmatrix} 0 \\ \frac{1}{2} \end{pmatrix}$	$\begin{pmatrix} 1 \\ \frac{1}{2} \end{pmatrix}$	$[\mathfrak{n}_1, \mathfrak{n}_3]$ $[\mathfrak{n}_2, \mathfrak{n}_4]$	$[\mathfrak{n}_2 \xrightarrow{(1,0)} \mathfrak{n}_1, \mathfrak{n}_4 \xrightarrow{(1,0)} \mathfrak{n}_3]$ $[\mathfrak{n}_2 \xrightarrow{(0,0)} \mathfrak{n}_1, \mathfrak{n}_4 \xrightarrow{(0,0)} \mathfrak{n}_3]$ $[\mathfrak{n}_3 \xrightarrow{(0,1)} \mathfrak{n}_1, \mathfrak{n}_1 \xrightarrow{(0,0)} \mathfrak{n}_3]$ $[\mathfrak{n}_4 \xrightarrow{(1,0)} \mathfrak{n}_1, \mathfrak{n}_2 \xrightarrow{(1,-1)} \mathfrak{n}_3]$ $[\mathfrak{n}_1 \xrightarrow{(0,-1)} \mathfrak{n}_4, \mathfrak{n}_3 \xrightarrow{(0,0)} \mathfrak{n}_2]$ $[\mathfrak{n}_2 \xrightarrow{(0,-1)} \mathfrak{n}_4, \mathfrak{n}_4 \xrightarrow{(0,0)} \mathfrak{n}_2]$
$\begin{pmatrix} \frac{1}{2} \\ \frac{1}{2} \end{pmatrix}$	$\begin{pmatrix} \frac{1}{2} \\ \frac{1}{2} \end{pmatrix}$	$[\mathfrak{n}_1, \mathfrak{n}_4]$ $[\mathfrak{n}_2, \mathfrak{n}_3]$	$[\mathfrak{n}_2 \xrightarrow{(1,0)} \mathfrak{n}_1, \mathfrak{n}_3 \xrightarrow{(0,0)} \mathfrak{n}_4]$ $[\mathfrak{n}_2 \xrightarrow{(0,0)} \mathfrak{n}_1, \mathfrak{n}_3 \xrightarrow{(-1,0)} \mathfrak{n}_4]$ $[\mathfrak{n}_3 \xrightarrow{(0,1)} \mathfrak{n}_1, \mathfrak{n}_2 \xrightarrow{(0,0)} \mathfrak{n}_4]$ $[\mathfrak{n}_3 \xrightarrow{(0,0)} \mathfrak{n}_1, \mathfrak{n}_2 \xrightarrow{(0,-1)} \mathfrak{n}_4]$ $[\mathfrak{n}_4 \xrightarrow{(1,0)} \mathfrak{n}_1, \mathfrak{n}_1 \xrightarrow{(0,-1)} \mathfrak{n}_4]$ $[\mathfrak{n}_2 \xrightarrow{(0,0)} \mathfrak{n}_3, \mathfrak{n}_3 \xrightarrow{(-1,1)} \mathfrak{n}_2]$

Table 6.1: The three non-trivial translational automorphisms of  $\mathbf{Q}^\Delta$ .

## 6.4 Halite

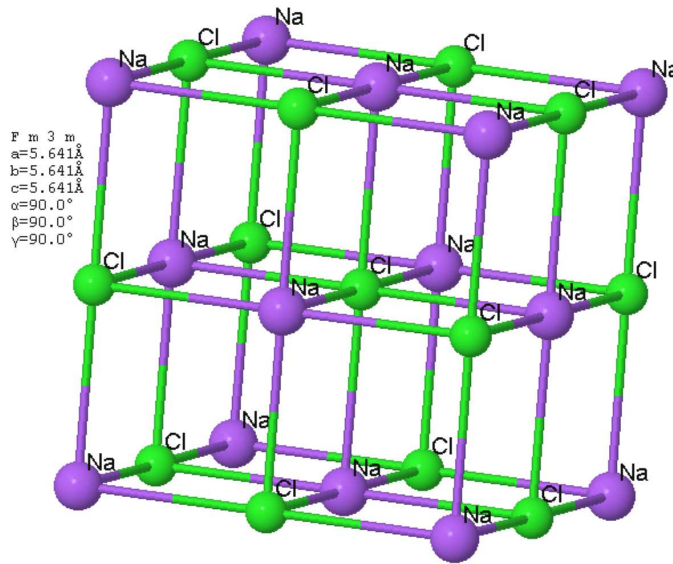


Figure 6.8: The face centred unit cell of the halite structure (NaCl): sodium atoms are at the corners and centres of the faces of the cell, chlorine atoms occupy the centre and the centre of the edges.

Halite or rock salt (NaCl) crystallises in space group  $F3\bar{m}3$  [Putnis, 1992]. In a conventional setting, sodium atoms are located at the fractional coordinates  $(0, 0, 0)$  and chlorine atoms at  $(0, \frac{1}{2}, 0)$  [Wenk and Bulakh, 2004]. Figure 6.8 shows the face centred cell (the axes coincide with the edges of the cell). If the structure of halite is converted into a QG based on a primitive cell, the resulting  $\mathbf{Q}^{\text{halite}}$  has 2 nodes and 6 edges:

$$\begin{aligned} e_1 &= \text{Cl} \xrightarrow{(1,0,1)} \text{Na}, & e_2 &= \text{Cl} \xrightarrow{(0,1,0)} \text{Na}, \\ e_3 &= \text{Cl} \xrightarrow{(0,1,1)} \text{Na}, & e_4 &= \text{Cl} \xrightarrow{(1,0,0)} \text{Na}, \\ e_5 &= \text{Cl} \xrightarrow{(1,1,0)} \text{Na}, & e_6 &= \text{Cl} \xrightarrow{(0,0,1)} \text{Na}. \end{aligned}$$

The only translational automorphism defines a reduction that places both nodes into the same orbit. Furthermore, the three edge orbits comprise the edges in each row in the list above. As the reduction vector is equal to  $(\frac{1}{2}, \frac{1}{2}, \frac{1}{2})$  and  $\mathcal{O} = 2$ , the  $\tilde{\mathbf{v}}$  are (the labels with an even index are subtracted to correct for their orientation in the edge orbit):

$$\begin{aligned} \tilde{\mathbf{v}}_1 &= \mathbf{v}_1 - \mathbf{v}_2 = (1, -1, 1) \\ \tilde{\mathbf{v}}_2 &= \mathbf{v}_3 - \mathbf{v}_4 = (-1, 1, 1) \\ \tilde{\mathbf{v}}_3 &= \mathbf{v}_5 - \mathbf{v}_6 = (1, 1, -1) \end{aligned}$$

As all edges in the reduced QG are loops, and the vectors  $\tilde{\mathbf{v}}_i$  are linearly independent, defining  $M = (\tilde{\mathbf{v}}_1, \tilde{\mathbf{v}}_2, \tilde{\mathbf{v}}_3)$  results in a QG with 3 edges:  $n \xrightarrow{(1,0,0)}$   $n$ ,  $n \xrightarrow{(0,1,0)}$   $n$ , and  $n \xrightarrow{(0,0,1)}$   $n$ . This QG is isomorphic to the QG of the cube net and is in accordance with the informal discussion at the introduction to this chapter.

Centred cells have a similar apparent reduction of the translational symmetry: if the QG of halite is created for a F-centred cell, the QG comprises 8 nodes and 24 edges. The set of reduction vectors includes all seven possible vectors  $\{\frac{1}{2}, 1\}^3$  with the exception of  $(1, 1, 1)$ . All reductions halve the size of the QG and the reduced QGs are twice the size of  $\mathbf{Q}^{\text{halite}}$ . Only the vectors  $(\frac{1}{2}, \frac{1}{2}, 1)$ ,  $(\frac{1}{2}, 1, \frac{1}{2})$ , and  $(1, \frac{1}{2}, \frac{1}{2})$  reduce the QG consistent with the atom types associated to the nodes.

## 6.5 Calcite and magnesite

The carbonates calcite ( $\text{CaCO}_3$ ) and magnesite ( $\text{MgCO}_3$ ) crystallise in space group  $R\bar{3}c$  [Graf, 1961]. The hexagonal unit cells contain six formula units. Their QGs therefore consist of six nodes corresponding to calcium or magnesium atoms, six to carbons and 18 to oxygen (see tables A.2 and A.8).

The structure is shown in figure 6.9. The QG of the two structures is shown

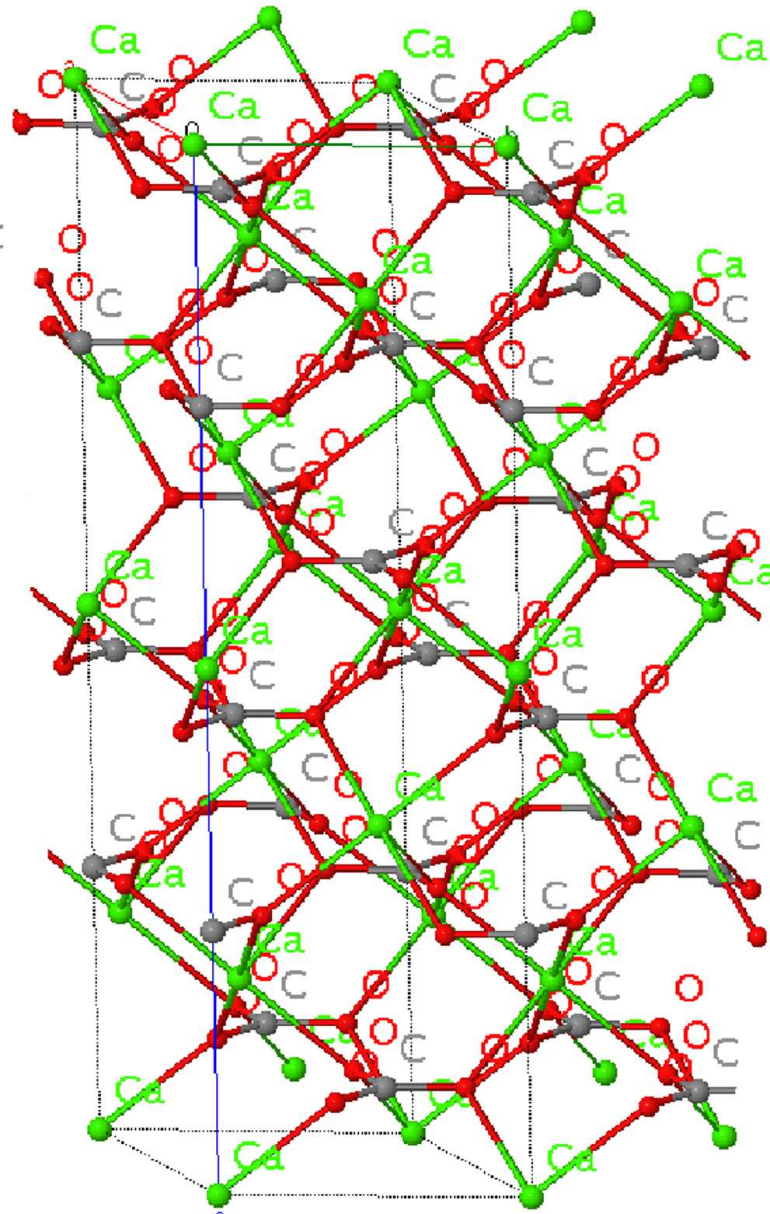


Figure 6.9: The structure of calcite. Bonds between the calciums and oxygens are included to reflect nearest neighbour relationships (structure see table A.2).

in table 6.2; the cations are represented by 'A'. The QG shown in table 6.2 possesses two translational automorphisms; both reduction vectors are equal

$C_1 \xrightarrow{(0,0,0)} O_1$	$C_1 \xrightarrow{(0,0,0)} O_2$	$C_1 \xrightarrow{(0,0,0)} O_3$
$C_2 \xrightarrow{(0,0,0)} O_{10}$	$C_2 \xrightarrow{(0,0,0)} O_5$	$C_2 \xrightarrow{(0,0,0)} O_6$
$C_3 \xrightarrow{(-1,-1,0)} O_{11}$	$C_3 \xrightarrow{(0,0,0)} O_{12}$	$C_3 \xrightarrow{(0,0,0)} O_{13}$
$C_4 \xrightarrow{(0,0,0)} O_{14}$	$C_4 \xrightarrow{(0,0,0)} O_{15}$	$C_4 \xrightarrow{(0,0,0)} O_{16}$
$C_5 \xrightarrow{(0,0,0)} O_7$	$C_5 \xrightarrow{(0,0,0)} O_8$	$C_5 \xrightarrow{(0,0,0)} O_9$
$C_6 \xrightarrow{(-1,0,0)} O_{18}$	$C_6 \xrightarrow{(0,-1,0)} O_{17}$	$C_6 \xrightarrow{(0,0,0)} O_4$
$A_1 \xrightarrow{(-1,-1,-1)} O_9$	$A_1 \xrightarrow{(-1,-1,0)} O_{10}$	$A_1 \xrightarrow{(-1,0,0)} O_6$
$A_1 \xrightarrow{(0,-1,-1)} O_8$	$A_1 \xrightarrow{(0,0,-1)} O_7$	$A_1 \xrightarrow{(0,0,0)} O_5$
$A_2 \xrightarrow{(0,-1,0)} O_8$	$A_2 \xrightarrow{(0,0,0)} O_{18}$	$A_2 \xrightarrow{(0,0,0)} O_4$
$A_2 \xrightarrow{(0,0,0)} O_9$	$A_2 \xrightarrow{(1,0,0)} O_{17}$	$A_2 \xrightarrow{(1,0,0)} O_7$
$A_3 \xrightarrow{(0,-1,0)} O_{14}$	$A_3 \xrightarrow{(0,0,0)} O_{11}$	$A_3 \xrightarrow{(0,0,0)} O_{13}$
$A_3 \xrightarrow{(0,0,0)} O_{15}$	$A_3 \xrightarrow{(1,0,0)} O_{12}$	$A_3 \xrightarrow{(1,0,0)} O_{16}$
$A_4 \xrightarrow{(-1,0,0)} O_{10}$	$A_4 \xrightarrow{(0,0,0)} O_{11}$	$A_4 \xrightarrow{(0,0,0)} O_{12}$
$A_4 \xrightarrow{(0,0,0)} O_5$	$A_4 \xrightarrow{(0,1,0)} O_{13}$	$A_4 \xrightarrow{(0,1,0)} O_6$
$A_5 \xrightarrow{(-1,0,0)} O_1$	$A_5 \xrightarrow{(0,0,0)} O_{17}$	$A_5 \xrightarrow{(0,0,0)} O_2$
$A_5 \xrightarrow{(0,0,0)} O_4$	$A_5 \xrightarrow{(0,1,0)} O_{18}$	$A_5 \xrightarrow{(0,1,0)} O_3$
$A_6 \xrightarrow{(-1,-1,0)} O_{14}$	$A_6 \xrightarrow{(-1,-1,0)} O_2$	$A_6 \xrightarrow{(-1,0,0)} O_1$
$A_6 \xrightarrow{(0,-1,0)} O_{16}$	$A_6 \xrightarrow{(0,0,0)} O_{15}$	$A_6 \xrightarrow{(0,0,0)} O_3$

Table 6.2: The magnesite and calcite QG obtained for a hexagonal setting.

to  $(\frac{1}{3}, \frac{1}{3}, \frac{1}{3})$ . The edge and node orbits are:

$$\begin{array}{llll} [C_1, C_3, C_5] & [C_2, C_4, C_6] & [A_1, A_3, A_5] & [A_2, A_4, A_6] \\ [O_4, O_{10}, O_{14}] & [O_1, O_9, O_{13}] & [O_2, O_8, O_{12}] & \\ [O_3, O_7, O_{11}] & [O_5, O_{16}, O_{18}] & [O_6, O_{15}, O_{17}] & \end{array}$$

Following the procedure described in section 6.1.2 results in the QG shown in table 6.3, which is isomorphic to the QG obtained for the primitive (rhombohedral) cell. The edge label with an element 2 is an artifact of the calculation. This can be corrected by subtracting vector  $(1, 0, 0)$  from the edges incident to node O2 (according to theorem 5.2.1).

$$\begin{array}{lll} C_1 \xrightarrow{(0,0,0)} O_1 & C_1 \xrightarrow{(0,1,0)} O_3 & C_1 \xrightarrow{(1,0,0)} O_2 \\ C_2 \xrightarrow{(0,0,0)} O_4 & C_2 \xrightarrow{(0,0,0)} O_5 & C_2 \xrightarrow{(0,0,1)} O_6 \\ A_1 \xrightarrow{(0,0,0)} O_1 & A_1 \xrightarrow{(0,0,0)} O_4 & A_1 \xrightarrow{(0,0,0)} O_6 \\ A_1 \xrightarrow{(1,-1,0)} O_5 & A_1 \xrightarrow{(1,0,0)} O_3 & A_1 \xrightarrow{(2,-1,1)} O_2 \\ A_2 \xrightarrow{(-1,0,-1)} O_1 & A_2 \xrightarrow{(-1,1,-1)} O_4 & A_2 \xrightarrow{(0,0,0)} O_2 \\ A_2 \xrightarrow{(0,0,0)} O_3 & A_2 \xrightarrow{(0,0,0)} O_5 & A_2 \xrightarrow{(0,0,0)} O_6 \end{array}$$

Table 6.3: The reduced QG for magnesite and calcite which corresponds to a rhombohedral setting.

The second translational automorphism defines the same node and edge orbits and therefore a reduction results into the same QG. The QG in table 6.3 possesses no reduction vector and consequently cannot be further reduced. This shows that both structures have a maximal translational symmetry and displacive phase transition can not lead to a structure with fewer atoms in a primitive cell. In other words, if  $\mathcal{G}$  is the space group of the structure that corresponds to the reduced QG and a displacive phase transition results in a structure which has the symmetry of space group  $\mathcal{H}$ , then

- $\mathcal{G}$  and  $\mathcal{H}$  are *translatonsgleiche*<sup>3</sup> (but not *klassengleiche*<sup>4</sup>) space groups, or
- $\mathcal{H}$  is not a *translatonsgleiche* supergroup of  $\mathcal{G}$ .

<sup>3</sup>A space group  $\mathcal{G}$  is a *translatonsgleiche* subgroup of  $\mathcal{H}$  if all translations in  $\mathcal{H}$  are elements in  $\mathcal{G}$  Hahn [1992].

<sup>4</sup>Space groups  $\mathcal{G}$  and  $\mathcal{H}$  are *klassengleiche* space groups if they belong to the same point group Hahn [1992].

## 6.6 Barytocalcite

Given that calcite ( $\text{CaCO}_3$ ) and barytocalcite ( $\text{BaCa}(\text{CO}_3)_2$ ) have a similar chemical make-up, one may suspect that the nets defined by these structures are isomorphic (structure see figure 6.10 and QG table A.1). This suspicion is supported by the matching coordination of the atoms in these structures. That calcite crystallises in  $R\bar{3}c$  and barytocalcite in  $P2_1$  may be attributed to a distortion of the later structure. However, a direct comparison of the

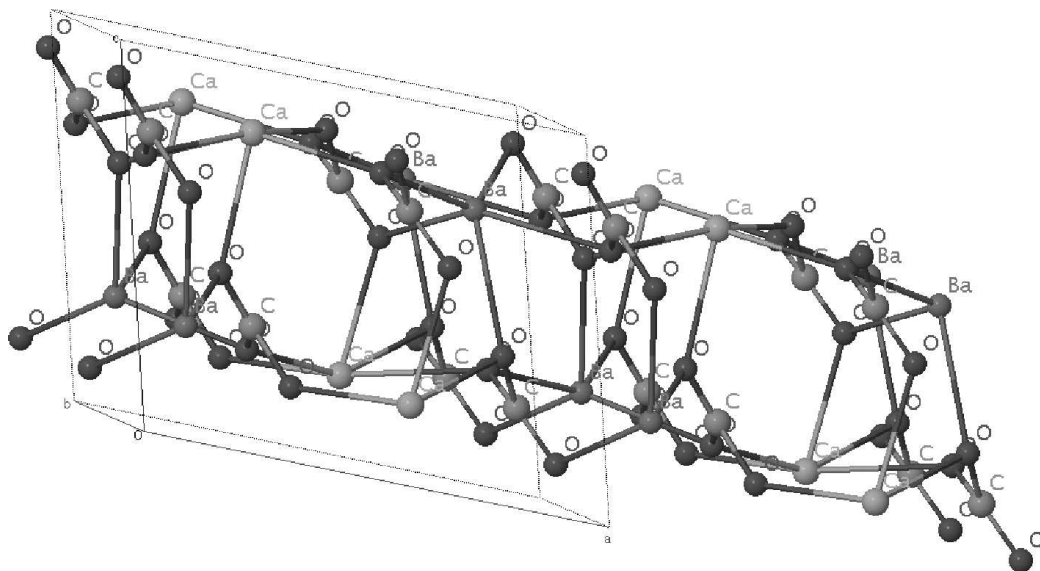


Figure 6.10: The barytocalcite structure ( $\text{BaCa}(\text{CO}_3)_2$ , see table A.1).

two nets is difficult as the QG of barytocalcite has twice the number of nodes.

The barytocalcite QG (table B.1) possesses three translational automorphisms: two with the reduction vector  $(\frac{1}{4}, \frac{1}{2}, \frac{1}{2})$  and one with the vector  $(\frac{1}{2}, 0, 0)$ . All corresponding translations of the structure mismatch cation types, which implies that a displacive phase transition to a structure with a smaller primitive cell is impossible. However, a complete Ba-Ca disorder would cause a phase transition to a structure with primitive cell containing only a quarter of the number of atoms. Only the second reduction vector can be used in the presented approach to reduce the QG. The resulting QG can again be reduced, resulting in a QG with the edges given in table 6.4 ('A' stands in for the earth alkali atoms). This QG comprises only half the number of nodes and edges of the maximally reduced calcite QG (see section 6.5). This conclusively shows that the two structures are not isomorphic. The comparative sizes of the barytocalcite QG and the twice reduced QG

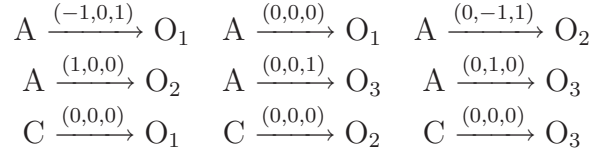


Table 6.4: The twice reduced barytocalcite QG.

imply that, if a disordered barytocalcite structure exists, this structure has a primitive cell holding half a formula unit.

## 6.7 Celsian and strontium feldspar

In this section it is shown phase transitions to non-*translationsgleiche* structures with a higher translational symmetry (*i.e.* with smaller primitive cells) resulting from order-disorder transitions can be predicted. This is achieved by an observation of the automorphisms used to reduce a QG.

Two structures are used to support this claim: celsian and a synthetic strontium feldspar. Celsian is a barium feldspar ( $\text{BaAl}_2\text{Si}_2\text{O}_8$ ) which occurs in space group  $I2/c$  (see figure 6.11, table A.3, [Newnham and Megaw, 1960]). The four tetrahedral sites in this partially ordered structure are occupied by Al and Si in site depended concentrations.

The synthetic strontium feldspar ( $\text{SrAl}_2\text{Si}_2\text{O}_8$ ) crystallises from melt in space group  $C2/m$  with Al and Si in a metastable disordered configuration. Thermal treatment evolves this structure to a partial Al-Si order and, as a result of this order, a phase transition to a structure in space group  $I2/c$  with a reduced translational symmetry. In other words, the phase transition to the ordered structure creates a *klassengleiche*, but not *translationsgleiche*, structure with a reduced symmetry. The partially ordered structure is shown in table A.15. This structure very similar to the celsian structure. During the transformation of the structures into QGs, atoms types and occupancy ratios were ignored (or, in other words, positions instead of atom types were considered).

First, QGs for non-primitive cells (corresponding to eight formula units) were created. Both QGs are essentially identical; only the atom types and occupancies associated with node differ (see table B.2). This QG possesses 3 reduction vectors:

1.  $\mathbf{t}_1 = (\frac{1}{2}, \frac{1}{2}, \frac{1}{2})$  is expected for a centred cell in space group  $I2/c$ .
2.  $\mathbf{t}_2 = (\frac{1}{2}, \frac{1}{2}, 1)$  reflects a translation that is not compatible with the symmetry of the crystal. In this reduction, sites that show different



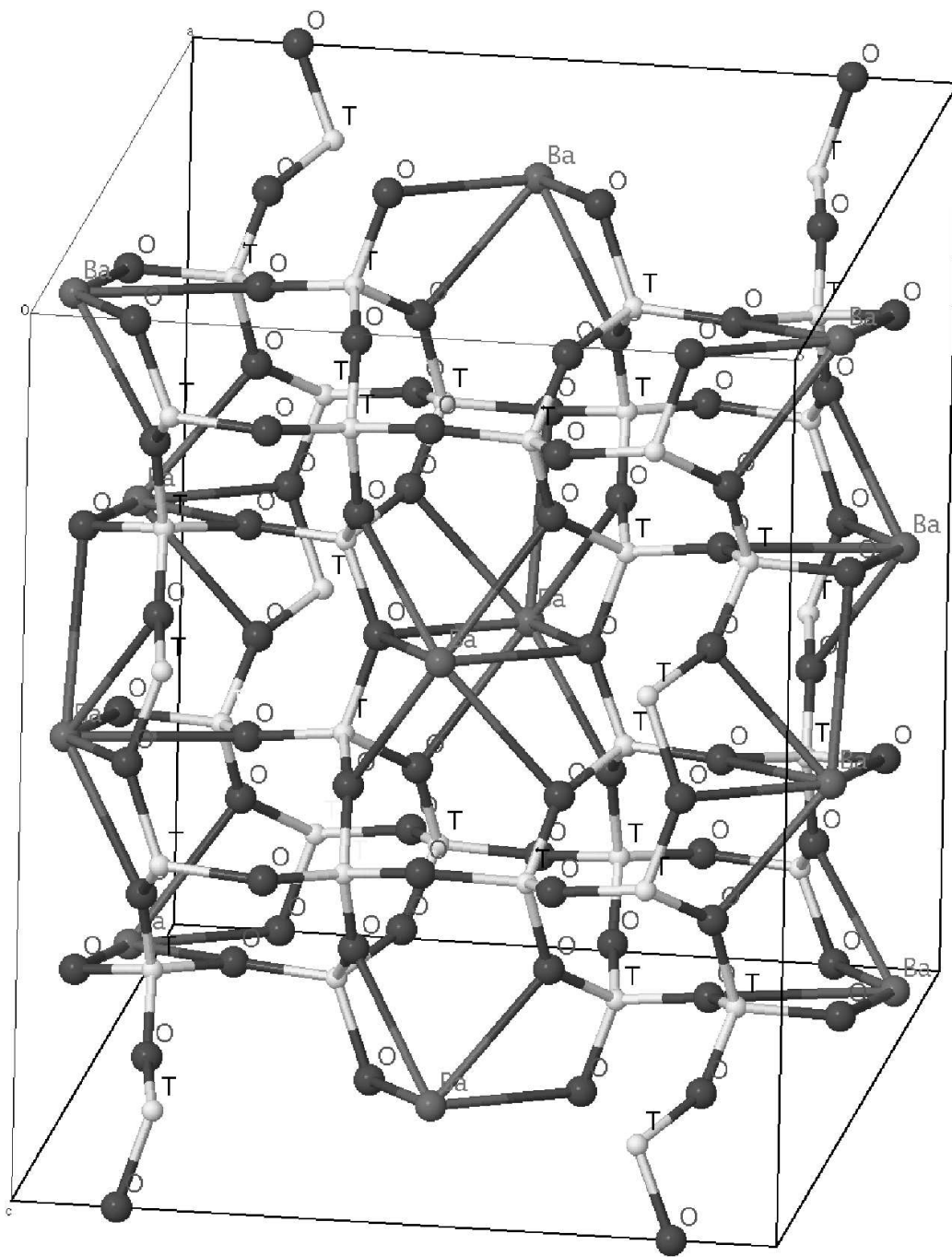


Figure 6.11: The celsian structure ( $\text{BaAl}_2\text{Si}_2\text{O}_8$ ). The Al-Si sites are labelled with 'T' (compare table A.3).

occupancies by Al and Si are mapped on each other: T1(0) on T1(z) and T2(0) on T2(z). A translation of the structure with  $(\frac{1}{2}, \frac{1}{2}, 0)$  brings these sites in close proximity.

3.  $\mathbf{t}_3 = (1, 1, \frac{1}{2})$  is equally incompatible with the crystal symmetry and, except that the translation is equal to  $(0, 0, \frac{1}{2})$ , everything stated for  $\mathbf{t}_2$  applies.

All reductions corresponding to these three vectors halve the size of the QG. All resulting QGs have a reduction vector which, if applied, halves the QG again (the maximally reduced QG is given in table B.3). All QGs - original and reduced - show the same stretched cycle sequence and it can therefore be assumed that the QGs, and the nets they represent, are isomorphic. Only vector  $\mathbf{t}_1$  is compatible with the symmetry of the structure and leads to a QG that is isomorphic to the QG obtained using a primitive cell. The other two reduction vectors correspond to mappings of tetrahedral sites with incompatible averages of Al and Si content.

The first two reduction vectors fall into the category discussed in section 6.1.2, the third is discussed in section 6.1.1.

The Sr-feldspar was prepared by annealing a crystal in which the Al and Si are disordered. One may therefore speculate that, after a ‘better’ annealing, the tetrahedral positions are always occupied by the atom type that dominantly occupies T positions (Benna and Bruno state, though, that this is unlikely achievable). Similarly, it may be suspected, that a complete Al and Si order in celsian causes a phase transition to a structure with a higher translational symmetry. In order to make a case, the QGs which correspond to primitive cells of the two structures were reduced. This reduction, however, implies for both feldspars a mapping of Si-dominated T1(0) sites onto Al-dominated T1(z) sites and similarly for the two T2 sites. This is compatible with the observation that if ordering causes a change of the translational symmetry, this transition leads to a structure with a larger primitive cell.

In conclusion, even a ‘better’ annealing or different geological history leading to a complete Al-Si order cannot result into a structure with a higher translational symmetry (that is a unit cell with a smaller volume). A phase transition to a structure with higher translational symmetry can only be caused by an Al-Si disorder. This is kinetically impossible once the feldspars are in an ordered state except maybe if the feldspars are exposed to temperatures close to their melting points.

It maybe worth noting that the conclusions concerning the phase transition were drawn without considering atom positions or a (visual) inspection of the structures. The statement that celsian (in space group  $I2/c$ ) cannot

undergo a phase transition to a structure with a higher translational symmetry without inducing a complete Al-Si disorder (*e.g.* applying heat) was made by the observation of the QG only (but was confirmed by comparison with the behaviour of the Sr-feldspar).

## 6.8 Remarks

The QGs were generated using TOPOLAN and a modified version of Jmol [Jmol]. A graphical user interface developed by the author was used to determine automorphisms and reductions. The later program is written in Java<sup>5</sup> and allows an examination of all QG automorphisms, node and edge orbits, and determines the symmetry operations except for the locational part of the Seitz symbol. The executable can be obtained from [Thimm, 2007].

---

<sup>5</sup>Java is a trademark by Sun Microsystems, Inc.



# Chapter 7

## Conclusion

The presented work explores the benefits of interpreting crystal structures as infinite graphs called nets, where atoms are mapped onto atoms and bonds onto edges. These nets are then described by so-called quotient graphs which have the advantage of being finite and can therefore be manipulated more easily. This approach allows to analyse crystal structures in ways difficult or impossible by approaches based on lattices and space groups.

A procedure for the enumeration of nets was revised with special attention on constraints arising from the aim to enumerate crystallographic structures. The proposed constraints on quotient graphs are shown to reduce the number of quotient graphs which do not correspond to a crystal structure greatly and therefore permit an enumeration of previously inaccessible structures.

The enumeration procedure was implemented and used to enumerate all nets that represent crystal structures with four four-coordinated atoms in a unit cell. Three of the nets resulted in plausible, to the author unknown carbon modifications.

The enumeration procedure uses certain constraints to eliminate redundant structures and those that cannot represent crystal structures. Two of these constraints arise from limits on specific densities and maximal unit cell volumes. The minimal specific density is determined from coordination sequences and the maximal volume of a unit cell from the topology of the nets.

This is complemented by an analysis of quotient graphs towards whether the equivalent nets are connected. Two sets of disconnected nets are distinguished: penetrating and non-penetrating. In non-penetrating nets, sub-nets are classified in islands, chains, or planes. In the case of penetrating nets (*e.g.* the net describing cuprite), the number of disconnected sub-nets is directly determined from a quotient graph and a limit on the number of sub-nets is given under the condition that edges (inter-atomic bonds) are shorter than

the lateral dimension of the unit cell.

It is shown that cycle sequences allow to efficiently distinguish between net topologies and therefore offer a way to classify crystals. The proposed fully stretched cycle sequences have an apparent 100% specificity in distinguishing topologies with nodes of degree two and above while being computationally much less onerous than conventional cycle sequences.

Nets, as used in publications prior to this work, are exclusively derived from crystals and therefore are encumbered by atom positions and cell parameters. In order to overcome this limitation, nets are redefined. Then, isomorphisms of nets are shown to have their equivalent in their finite representation (the quotient graphs). Based on this result, automorphisms of quotient graphs are put into a strong relationship with the symmetries of possible embeddings of the corresponding net (structures). It is shown that for a connected quotient graph the space group of an embedding or structure with a maximal symmetry is determined by the topology alone (with the exception of the setting). In detail, an automorphism of the quotient graph determines the vector corresponding to a possible screw or glide component of the corresponding symmetry operation (under the condition that two isomorphic nodes are connected by some path). Thus, without knowledge of the spatial arrangements of atoms in a structure, possible symmetry operations of all possible embeddings of a net are determined. As a result, for a specific structure, it is possible to determine if a displacive (bond-preserving) phase transition to a structure with higher symmetry is possible. Should this be the case, the space groups of these phases can be determined.

The theoretical deductions are complemented with worked examples for the 2D hexagon net, two FeS<sub>2</sub> modifications,  $\alpha$ - and  $\beta$ -quartz, and three graphite modifications.

The set of automorphisms of a quotient graph can include several automorphisms that correspond to translational symmetries that are not compatible with the lattice of the net-defining structure. In a sense, this corresponds to a situation where a supercell of the structure is used to determine a quotient graph. For these quotient graphs, a procedure is given that allows to see which positions in the original structure would be mapped on each other. Furthermore, this allows to reduce the size of the quotient graph in a manner comparable to reducing the size of a supercell or centred cell. This is demonstrated for two 2-dimensional examples and several structures. Among these structures are celsian and a strontium feldspar with partially ordered Al- and Si-positions. The analysis suggests that a complete ordering of the structures would not induce a phase transition to a structure with a higher translational symmetry (that is the unit cell is unchanged). A reduction of the barytoalcite net is used to show that its structure is not isomorphic to

the calcite structure. Overall, this work shows that the examination of QGs allows to predict or exclude possible displacive phase transitions to structures with reduced translational symmetry.

## 7.1 Future work

### Cycle sequences and net isomorphism

From numerous examples, it seems to be plausible that sufficiently long (plain, stretched or fully stretched) cycle sequences of a yet to be determined length completely define the topology of a net under the constraint that all nodes are of a minimal degree of two and the net is simply connected.

If this proposition is true, the (non-)isomorphism of QGs with non-isomorphic base graphs could be shown conclusively.

### Physical properties *versus* topology

Only little is yet known on which physical properties are reflected in a crystal's topology. One may, though, speculate that there are many more links than those presented in this and the work of other researchers: the topology determines to some extent the space group of a crystal, which in turn is closely linked to many physical properties.

### Investigate structures with displacive phase transitions

It would be interesting to systematically investigate, which crystal structures are in space groups with a lower symmetry than suggested by the topological analysis presented here. Such structures are likely to undergo displacive (thus requiring little energy) phase transitions to structures with a higher symmetry. As phase transitions often cause a considerable change in the macroscopic properties of a crystal, such structures may be of technological interest.





# Appendix A

## Crystal Structures

Cell parameters are given in Ångström (Å) and atom positions in fractional coordinates. Symmetrically equivalent positions are not shown.

space group: $P2_1$			
cell parameters:			
$a = 8.15, b = 5.22, c = 6.58,$			
$\alpha = \gamma = 90^\circ, \beta = 106.13^\circ$			
atom positions:			
Ba	0.14200	0.25000	0.28300
Ca	0.38300	0.73400	0.80000
C1	0.08300	0.20500	0.77000
C2	0.35800	0.74000	0.29900
O1	0.01200	0.15000	0.89300
O2	0.10500	0.44400	0.69700
O3	0.13300	0.02000	0.63900
O4	0.28700	0.68000	0.42200
O5	0.37900	0.97400	0.22600
O6	0.40700	0.55000	0.16800

Table A.1: The crystal structure of barytocalcite ( $\text{BaCa}(\text{CO}_3)_2$ ) from Downs and Hall-Wallace [2003].

space group: $R\bar{3}c$			
cell parameters: $a = b = 4.9900, c = 17.0615,$ $\alpha = \beta = 90^\circ, \gamma = 120^\circ$			
atom positions:			
Ca	0	0	0
C	0	0	0.25
O	0.2578	0	0.25

Table A.2: The structure of calcite ( $\text{CaCO}_3$ ) [Graf, 1961].

space group: $I2/c$				
cell parameters: $a = 8.627, b = 13.045,$ $c = 14.408, \alpha = \gamma = 90^\circ, \beta = 115.22^\circ$				
Atom	x	y	z	occ
Ba	0.2826	0.00	0.0653	
AlT1(0)	0.0091	0.1828	0.1096	.22
SiT1(0)	0.0091	0.1828	0.1096	0.78
AlT1(z)	0.0073	0.1832	0.6142	0.65
SiT1(z)	0.0073	0.1832	0.6142	0.35
AlT2(0)	0.7058	0.1205	0.1733	0.62
SiT2(0)	0.7058	0.1205	0.1733	0.38
AlT2(z)	0.7004	0.1165	0.6735	0.20
SiT2(z)	0.7004	0.1165	0.6735	0.80
OA(1)	0.9996	0.1382	0.0003	
OA(2)	0.6238	0.00010	0.1429	
OB(0)	0.8223	0.1388	0.1111	
OB(z)	0.8221	0.1368	0.6133	
OC(0)	0.0224	0.3072	0.1233	
OC(z)	0.0300	0.3130	0.6321	
OD(0)	0.1826	0.1298	0.1947	
OD(z)	0.1904	0.1232	0.7079	

Table A.3: The celsian structure ( $\text{BaAl}_2\text{Si}_2\text{O}_8$ , from Newnham and Megaw [1960]).

space group: $C2/c$			
cell parameters: $a = 7.1356$ , $b = 12.3692$ , $c = 7.1736$ , $\alpha = \gamma = 90^\circ$ , $\beta = 120.34^\circ$			
atom positions:			
O1	0	0	0
O2	.5	.1163	.75
O3	.2660	.1234	.9401
O4	.3114	.1038	.3282
O5	.0172	.2117	.4782
Si1	.14033	.10833	.07227
Si2	.50682	.15799	.54077

Table A.4: The crystal structure of coesite ( $\text{SiO}_2$ ) at ambient conditions [Levien and Prewitt, 1981].

space group: $P4_12_12$			
cell parameters: $a = b = 4.9717$ , $c = 6.9223$ , $\alpha = \beta = \gamma = 90^\circ$			
atom positions:			
Si	0.30028	0.30028	0.0000
O	0.2392	0.1044	0.1787

Table A.5: The structure of  $\alpha$ -cristobalite ( $\text{SiO}_2$ ) [Downs and Palmer, 1994].

space group: $Pn\bar{3}$			
cell parameters: $a = b = c = 4.2696$ , $\alpha = \beta = \gamma = 90^\circ$			
atom positions:			
Cu	0.25	0.25	0.25
O	0.00	0.00	0.00

Table A.6: The structure of synthetic cuprite ( $\text{Cu}_2\text{O}$ ) [Downs and Hall-Wallace, 2003].

space group: $Fd\bar{3}m$			
cell parameters: $a = b = c = 3.56679$ , $\alpha = \beta = \gamma = 90^\circ$			
atom positions:			
C	0.000	0.000	0.000

Table A.7: The structure of diamond.

space group: $R\bar{3}c$			
cell parameters: $a = b = 4.635$ , $c = 15.019$ , $\alpha = \beta = 90^\circ$ , $\gamma = 120^\circ$			
atom positions:			
Ca	0.0000	0.0000	0.0000
C	0.0000	0.0000	0.2500
O	0.2778	0.0000	0.2500

Table A.8: The crystal structure of magnesite ( $\text{MgCO}_3$ ) at ambient conditions (from Downs and Hall-Wallace [2003]).

space group: $Pn\bar{m}$			
cell parameters: $a = 4.436$ , $b = 5.414$ , $c = 3.381$ , $\alpha = \beta = \gamma = 90^\circ$			
atom positions:			
Fe	0.000	0.000	0.000
S	0.200	0.378	0.000

Table A.9: The marcasite ( $\text{FeS}_2$ ) structure from CCMS [2007]

space group: $Pbnm$			
cell parameters: $a = 5.380$ , $b = 5.440$ , $c = 7.639$ , $\alpha = \beta = \gamma = 90^\circ$			
atom positions:			
Ti	0.0000	0.5000	0.0000
Ca	0.0065	0.0356	0.2500
O	.5711	-0.0161	0.2500
O	0.2897	0.2888	0.0373

Table A.10: The perovskite structure ( $\text{CaTiO}_3$ ) [Beran et al., 1996]

space group: $Pa\bar{3}$			
cell parameters: $a = b = c = 5.4166$ , $\alpha = \beta = \gamma = 90^\circ$			
atom positions:			
Fe	0.0000	0.5000	0.0000
S	0.38510	0.38510	0.38510

Table A.11: The structure of cubic pyrite ( $\text{FeS}_2$ ) [Bayliss, 1977]

space group: $P3_221$			
cell parameters: $a = 4.916$ , $b = 4.916$ , $c = 5.4054$ , $\alpha = \beta = 90^\circ$ , $\gamma = 120^\circ$			
atom positions:			
Si	0.4697	0.0000	0.0000
O	0.4135	0.2669	0.1191

Table A.12: One of the enantiomorphic  $\alpha$ -quartz structures ( $\text{SiO}_2$ ) [Levien et al., 1980].

space group: $P6_222$			
cell parameters: $a = b = 4.9965$ , $c = 5.4570$ , $\alpha = \beta = \gamma = 90^\circ$			
atom positions:			
Si	0.500	0.0000	0.0000
O	0.4135	0.2076	1/6

Table A.13: One of the enantiomorphic  $\beta$ -quartz structures ( $\text{SiO}_2$ ) [Downs and Hall-Wallace, 2003].

space group: $P4_2/mnm$			
cell parameters: $a = b = 4.59373$ , $c = 2.95812$ , $\alpha = \beta = \gamma = 90^\circ$			
atom positions:			
Ti	0.00000	0.00000	0.00000
O	0.30530	0.30530	0.00000

Table A.14: The rutile structure ( $\text{TiO}_2$ ) [Downs and Hall-Wallace, 2003].

space group: $C2/m$				
cell parameters: $a = 8.379$ , $b = 12.963$ , $c = 14.245$ , $\alpha = \gamma = 90^\circ$ , $\beta = 115.46^\circ$				
Atom	x	y	z	occ
Sr	0.2691	-0.0021	0.0656	
AlT1(0)	0.0070	0.1747	0.1086	0.19
SiT1(0)	0.0070	0.1747	0.1086	0.81
AlT1(z)	0.0032	0.1776	0.6162	0.81
SiT1(z)	0.0032	0.1776	0.6162	0.19
AlT2(0)	0.6939	0.1203	0.1705	0.76
SiT2(0)	0.6939	0.1203	0.1705	0.24
AlT2(z)	0.6854	0.1133	0.6716	0.14
SiT2(z)	0.6854	0.1133	0.6716	0.86
OA(1)	0.0044	0.1294	0.0002	
OA(2)	0.5914	-0.0001	0.1428	
OB(0)	0.8280	0.1264	0.1066	
OB(z)	0.8089	0.1267	0.6111	
OC(0)	0.0134	0.2981	0.1184	
OC(z)	0.0182	0.3091	0.6304	
OD(0)	0.1876	0.1247	0.1961	
OD(z)	0.1975	0.1188	0.7037	

Table A.15: The strontium feldspar structure ( $\text{SrAl}_2\text{Si}_2\text{O}_8$ ) at ambient conditions (from [Benna and Bruno, 2001, Downs and Hall-Wallace, 2003]).

space group: $C2/c$			
cell parameters: $a = 5.26$ , $b = 9.10$ , $c = 18.81$ , $\alpha = \beta = 90^\circ$ , $\beta = 100.00^\circ$			
atom positions:			
Mg1	0	0	0
Mg2	0	0.333	0
Si1	-0.239	00	0.143
Si2	0.261	0.167	0.143
O1	0.203	0.5	0.058
O2	0.203	0.167	0.058
O3	0.025	0.083	0.176
O4	-0.475	0.083	0.176
O5	0.275	0.333	0.176
OH1	0.203	-0.167	0.058

Table A.16: The talc structure ( $\text{Mg}_3\text{Si}_4\text{O}_{12}\text{H}_2$ ) [Gruner, 1934, Downs and Hall-Wallace, 2003].





# Appendix B

## Quotient Graphs

This appendix lists QGs for some selected structures.

Table B.2 – continued on next page

$A_1 \xrightarrow{(-1,0,0)} OA(2)_7$	$A_1 \xrightarrow{(0,0,0)} OA(1)_1$	$A_1 \xrightarrow{(0,0,0)} OA(1)_7$
$A_1 \xrightarrow{(0,0,0)} OB(0)_7$	$A_1 \xrightarrow{(0,0,0)} OB(z)_2$	$A_1 \xrightarrow{(0,0,0)} OD(0)_7$
$A_1 \xrightarrow{(0,0,0)} OD(z)_5$	$A_2 \xrightarrow{(-1,1,0)} OA(1)_2$	$A_2 \xrightarrow{(0,1,-1)} OB(z)_5$
$A_2 \xrightarrow{(0,1,0)} OA(2)_3$	$A_2 \xrightarrow{(0,1,0)} OD(0)_1$	$A_2 \xrightarrow{(0,0,-1)} OA(1)_8$
$A_2 \xrightarrow{(0,0,-1)} OB(0)_8$	$A_2 \xrightarrow{(0,0,0)} OD(z)_4$	$A_3 \xrightarrow{(1,1,0)} OA(1)_6$
$A_3 \xrightarrow{(0,1,0)} OA(2)_6$	$A_3 \xrightarrow{(0,1,0)} OB(z)_1$	$A_3 \xrightarrow{(0,1,0)} OD(0)_6$
$A_3 \xrightarrow{(0,0,0)} OA(1)_4$	$A_3 \xrightarrow{(0,0,0)} OB(0)_3$	$A_3 \xrightarrow{(0,0,0)} OD(z)_8$
$A_4 \xrightarrow{(-1,0,0)} OA(1)_4$	$A_4 \xrightarrow{(0,1,0)} OA(1)_6$	$A_4 \xrightarrow{(0,1,0)} OB(0)_5$
$A_4 \xrightarrow{(0,1,0)} OD(z)_2$	$A_4 \xrightarrow{(0,0,0)} OA(2)_4$	$A_4 \xrightarrow{(0,0,0)} OB(z)_8$
$A_4 \xrightarrow{(0,0,0)} OD(0)_4$	$A_5 \xrightarrow{(1,0,0)} OA(1)_8$	$A_5 \xrightarrow{(0,1,1)} OA(1)_2$
$A_5 \xrightarrow{(0,1,1)} OB(0)_1$	$A_5 \xrightarrow{(0,1,0)} OD(z)_6$	$A_5 \xrightarrow{(0,0,1)} OB(z)_3$
$A_5 \xrightarrow{(0,0,0)} OA(2)_8$	$A_5 \xrightarrow{(0,0,0)} OD(0)_8$	$A_6 \xrightarrow{(1,0,0)} OA(2)_1$
$A_6 \xrightarrow{(0,0,-1)} OA(1)_5$	$A_6 \xrightarrow{(0,0,-1)} OB(0)_4$	$A_6 \xrightarrow{(0,0,-1)} OB(z)_6$
$A_6 \xrightarrow{(0,0,0)} OA(1)_3$	$A_6 \xrightarrow{(0,0,0)} OD(0)_2$	$A_6 \xrightarrow{(0,0,0)} OD(z)_1$
$A_7 \xrightarrow{(1,0,0)} OA(2)_2$	$A_7 \xrightarrow{(0,0,0)} OA(1)_1$	$A_7 \xrightarrow{(0,0,0)} OA(1)_7$
$A_7 \xrightarrow{(0,0,0)} OB(0)_6$	$A_7 \xrightarrow{(0,0,0)} OB(z)_4$	$A_7 \xrightarrow{(0,0,0)} OD(0)_3$
$A_7 \xrightarrow{(0,0,0)} OD(z)_3$	$A_8 \xrightarrow{(-1,0,0)} OA(2)_5$	$A_8 \xrightarrow{(0,0,1)} OA(1)_3$
$A_8 \xrightarrow{(0,0,1)} OB(0)_2$	$A_8 \xrightarrow{(0,0,1)} OB(z)_7$	$A_8 \xrightarrow{(0,0,0)} OA(1)_5$
$A_8 \xrightarrow{(0,0,0)} OD(0)_5$	$A_8 \xrightarrow{(0,0,0)} OD(z)_7$	$OA(1)_1 \xrightarrow{(0,0,0)} T1(0)_4$

Table B.2 – continued from previous page

$OA(1)_1 \xrightarrow{(0,0,0)} T1(z)_5$	$OA(1)_2 \xrightarrow{(1,0,0)} T1(0)_1$	$OA(1)_2 \xrightarrow{(0,0,-1)} T1(z)_6$
$OA(1)_3 \xrightarrow{(0,0,-1)} T1(z)_7$	$OA(1)_3 \xrightarrow{(0,0,0)} T1(0)_2$	$OA(1)_4 \xrightarrow{(1,0,0)} T1(0)_3$
$OA(1)_4 \xrightarrow{(0,0,0)} T1(z)_8$	$OA(1)_5 \xrightarrow{(0,0,1)} T1(z)_2$	$OA(1)_5 \xrightarrow{(0,0,0)} T1(0)_5$
$OA(1)_6 \xrightarrow{(-1,0,0)} T1(0)_6$	$OA(1)_6 \xrightarrow{(0,0,0)} T1(z)_1$	$OA(1)_7 \xrightarrow{(0,0,0)} T1(0)_7$
$OA(1)_7 \xrightarrow{(0,0,0)} T1(z)_3$	$OA(1)_8 \xrightarrow{(-1,0,0)} T1(0)_8$	$OA(1)_8 \xrightarrow{(0,0,1)} T1(z)_4$
$OA(2)_1 \xrightarrow{(0,0,0)} T(2)_3$	$OA(2)_1 \xrightarrow{(0,0,0)} T2(z)_8$	$OA(2)_2 \xrightarrow{(0,0,0)} T(2)_1$
$OA(2)_2 \xrightarrow{(0,0,0)} T2(z)_2$	$OA(2)_3 \xrightarrow{(0,-1,0)} T2(z)_3$	$OA(2)_3 \xrightarrow{(0,0,0)} T(2)_2$
$OA(2)_4 \xrightarrow{(0,1,0)} T2(z)_1$	$OA(2)_4 \xrightarrow{(0,0,0)} T(2)_4$	$OA(2)_5 \xrightarrow{(0,0,0)} T(2)_6$
$OA(2)_5 \xrightarrow{(0,0,0)} T2(z)_5$	$OA(2)_6 \xrightarrow{(0,-1,0)} T2(z)_4$	$OA(2)_6 \xrightarrow{(0,0,0)} T(2)_8$
$OA(2)_7 \xrightarrow{(0,0,0)} T(2)_7$	$OA(2)_7 \xrightarrow{(0,0,0)} T2(z)_6$	$OA(2)_8 \xrightarrow{(0,1,0)} T2(z)_7$
$OA(2)_8 \xrightarrow{(0,0,0)} T(2)_5$	$OB(0)_1 \xrightarrow{(1,0,0)} T1(0)_1$	$OB(0)_1 \xrightarrow{(0,0,0)} T(2)_2$
$OB(0)_2 \xrightarrow{(0,0,0)} T1(0)_2$	$OB(0)_2 \xrightarrow{(0,0,0)} T(2)_3$	$OB(0)_3 \xrightarrow{(1,0,0)} T1(0)_3$
$OB(0)_3 \xrightarrow{(0,0,0)} T(2)_4$	$OB(0)_4 \xrightarrow{(0,0,0)} T1(0)_5$	$OB(0)_4 \xrightarrow{(0,0,0)} T(2)_6$
$OB(0)_5 \xrightarrow{(-1,0,0)} T1(0)_6$	$OB(0)_5 \xrightarrow{(0,0,0)} T(2)_8$	$OB(0)_6 \xrightarrow{(0,0,0)} T1(0)_7$
$OB(0)_6 \xrightarrow{(0,0,0)} T(2)_7$	$OB(0)_7 \xrightarrow{(0,0,0)} T1(0)_4$	$OB(0)_7 \xrightarrow{(0,0,0)} T(2)_1$
$OB(0)_8 \xrightarrow{(-1,0,0)} T1(0)_8$	$OB(0)_8 \xrightarrow{(0,0,0)} T(2)_5$	$OB(z)_1 \xrightarrow{(1,0,0)} T1(z)_1$
$OB(z)_1 \xrightarrow{(0,0,0)} T2(z)_1$	$OB(z)_2 \xrightarrow{(0,0,0)} T1(z)_3$	$OB(z)_2 \xrightarrow{(0,0,0)} T2(z)_2$
$OB(z)_3 \xrightarrow{(1,0,0)} T1(z)_4$	$OB(z)_3 \xrightarrow{(0,0,0)} T2(z)_3$	$OB(z)_4 \xrightarrow{(0,0,0)} T1(z)_5$
$OB(z)_4 \xrightarrow{(0,0,0)} T2(z)_6$	$OB(z)_5 \xrightarrow{(-1,0,0)} T1(z)_6$	$OB(z)_5 \xrightarrow{(0,0,0)} T2(z)_7$
$OB(z)_6 \xrightarrow{(0,0,0)} T1(z)_7$	$OB(z)_6 \xrightarrow{(0,0,0)} T2(z)_5$	$OB(z)_7 \xrightarrow{(0,0,0)} T1(z)_2$
$OB(z)_7 \xrightarrow{(0,0,0)} T2(z)_8$	$OB(z)_8 \xrightarrow{(-1,0,0)} T1(z)_8$	$OB(z)_8 \xrightarrow{(0,0,0)} T2(z)_4$
$OC(0)_1 \xrightarrow{(0,0,0)} T1(0)_3$	$OC(0)_1 \xrightarrow{(0,0,0)} T(2)_1$	$OC(0)_2 \xrightarrow{(0,0,0)} T1(0)_1$
$OC(0)_2 \xrightarrow{(0,0,0)} T(2)_3$	$OC(0)_3 \xrightarrow{(0,0,0)} T1(0)_2$	$OC(0)_3 \xrightarrow{(0,0,0)} T(2)_2$
$OC(0)_4 \xrightarrow{(0,0,0)} T1(0)_5$	$OC(0)_4 \xrightarrow{(0,0,0)} T(2)_5$	$OC(0)_5 \xrightarrow{(0,0,0)} T1(0)_6$
$OC(0)_5 \xrightarrow{(0,0,0)} T(2)_7$	$OC(0)_6 \xrightarrow{(0,0,0)} T1(0)_4$	$OC(0)_6 \xrightarrow{(0,0,0)} T(2)_4$
$OC(0)_7 \xrightarrow{(0,0,0)} T1(0)_7$	$OC(0)_7 \xrightarrow{(0,0,0)} T(2)_8$	$OC(0)_8 \xrightarrow{(0,0,0)} T1(0)_8$
$OC(0)_8 \xrightarrow{(0,0,0)} T(2)_6$	$OC(z)_1 \xrightarrow{(0,0,0)} T1(z)_4$	$OC(z)_1 \xrightarrow{(0,0,0)} T2(z)_8$
$OC(z)_2 \xrightarrow{(0,0,0)} T1(z)_1$	$OC(z)_2 \xrightarrow{(0,0,0)} T2(z)_2$	$OC(z)_3 \xrightarrow{(0,0,0)} T1(z)_3$
$OC(z)_3 \xrightarrow{(0,0,0)} T2(z)_1$	$OC(z)_4 \xrightarrow{(0,0,0)} T1(z)_5$	$OC(z)_4 \xrightarrow{(0,0,0)} T2(z)_4$
$OC(z)_5 \xrightarrow{(0,0,0)} T1(z)_2$	$OC(z)_5 \xrightarrow{(0,0,0)} T2(z)_3$	$OC(z)_6 \xrightarrow{(0,0,0)} T1(z)_6$

Table B.2 – continued from previous page

$OC(z)_6 \xrightarrow{(0,0,0)} T2(z)_5$	$OC(z)_7 \xrightarrow{(0,0,0)} T1(z)_7$	$OC(z)_7 \xrightarrow{(0,0,0)} T2(z)_7$
$OC(z)_8 \xrightarrow{(0,0,0)} T1(z)_8$	$OC(z)_8 \xrightarrow{(0,0,0)} T2(z)_6$	$OD(0)_1 \xrightarrow{(0,0,0)} T1(0)_1$
$OD(0)_1 \xrightarrow{(0,0,0)} T(2)_8$	$OD(0)_2 \xrightarrow{(0,0,0)} T1(0)_2$	$OD(0)_2 \xrightarrow{(0,0,0)} T(2)_7$
$OD(0)_3 \xrightarrow{(0,0,0)} T1(0)_4$	$OD(0)_3 \xrightarrow{(0,0,0)} T(2)_6$	$OD(0)_4 \xrightarrow{(0,0,0)} T1(0)_3$
$OD(0)_4 \xrightarrow{(0,0,0)} T(2)_5$	$OD(0)_5 \xrightarrow{(0,0,0)} T1(0)_5$	$OD(0)_5 \xrightarrow{(0,0,0)} T(2)_1$
$OD(0)_6 \xrightarrow{(0,0,0)} T1(0)_6$	$OD(0)_6 \xrightarrow{(0,0,0)} T(2)_2$	$OD(0)_7 \xrightarrow{(0,0,0)} T1(0)_7$
$OD(0)_7 \xrightarrow{(0,0,0)} T(2)_3$	$OD(0)_8 \xrightarrow{(0,0,0)} T1(0)_8$	$OD(0)_8 \xrightarrow{(0,0,0)} T(2)_4$
$OD(z)_1 \xrightarrow{(0,0,0)} T1(z)_2$	$OD(z)_1 \xrightarrow{(0,0,0)} T2(z)_6$	$OD(z)_2 \xrightarrow{(0,0,0)} T1(z)_1$
$OD(z)_2 \xrightarrow{(0,0,0)} T2(z)_7$	$OD(z)_3 \xrightarrow{(0,0,0)} T1(z)_3$	$OD(z)_3 \xrightarrow{(0,0,0)} T2(z)_5$
$OD(z)_4 \xrightarrow{(0,0,0)} T1(z)_4$	$OD(z)_4 \xrightarrow{(0,0,0)} T2(z)_4$	$OD(z)_5 \xrightarrow{(0,0,0)} T1(z)_5$
$OD(z)_5 \xrightarrow{(0,0,0)} T2(z)_8$	$OD(z)_6 \xrightarrow{(0,0,0)} T1(z)_6$	$OD(z)_6 \xrightarrow{(0,0,0)} T2(z)_1$
$OD(z)_7 \xrightarrow{(0,0,0)} T1(z)_7$	$OD(z)_7 \xrightarrow{(0,0,0)} T2(z)_2$	$OD(z)_8 \xrightarrow{(0,0,0)} T1(z)_8$
	$OD(z)_8 \xrightarrow{(0,0,0)} T2(z)_3$	

Table B.2: The QG of celsian and a synthetic Sr-feldspar (structures tables A.3 and A.15). ‘A’ stands for the Ba- and Sr-atoms.

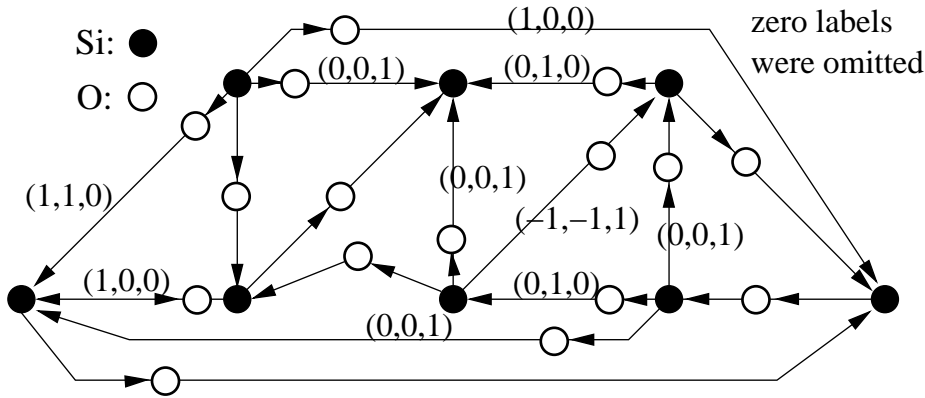


Figure B.1: The coesite QG (structure: table A.4). Zero-labels are omitted.

$\text{Ba}_1 \xrightarrow{(-1,-1,0)} \text{O1}_1$	$\text{Ba}_1 \xrightarrow{(0,0,-1)} \text{O1}_2$	$\text{Ba}_1 \xrightarrow{(-1,0,0)} \text{O2}_1$
$\text{Ba}_1 \xrightarrow{(0,0,0)} \text{O3}_1$	$\text{Ba}_1 \xrightarrow{(0,-1,0)} \text{O4}_1$	$\text{Ba}_1 \xrightarrow{(0,0,0)} \text{O5}_1$
$\text{Ba}_2 \xrightarrow{(0,0,1)} \text{O1}_1$	$\text{Ba}_2 \xrightarrow{(1,0,0)} \text{O1}_2$	$\text{Ba}_2 \xrightarrow{(1,1,0)} \text{O2}_2$
$\text{Ba}_2 \xrightarrow{(0,0,0)} \text{O3}_2$	$\text{Ba}_2 \xrightarrow{(0,0,0)} \text{O4}_2$	$\text{Ba}_2 \xrightarrow{(0,1,0)} \text{O5}_2$
$\text{C1}_1 \xrightarrow{(0,0,0)} \text{O1}_1$	$\text{C1}_1 \xrightarrow{(0,0,0)} \text{O2}_1$	$\text{C1}_1 \xrightarrow{(0,0,0)} \text{O3}_2$
$\text{C1}_2 \xrightarrow{(0,0,0)} \text{O1}_2$	$\text{C1}_2 \xrightarrow{(0,0,0)} \text{O2}_2$	$\text{C1}_2 \xrightarrow{(0,0,0)} \text{O3}_1$
$\text{C2}_1 \xrightarrow{(0,0,0)} \text{O4}_2$	$\text{C2}_1 \xrightarrow{(0,0,0)} \text{O5}_2$	$\text{C2}_1 \xrightarrow{(0,0,0)} \text{O6}_2$
$\text{C2}_2 \xrightarrow{(0,0,0)} \text{O4}_1$	$\text{C2}_2 \xrightarrow{(0,0,0)} \text{O5}_1$	$\text{C2}_2 \xrightarrow{(0,0,0)} \text{O6}_1$
$\text{Ca}_1 \xrightarrow{(0,0,0)} \text{O2}_1$	$\text{Ca}_1 \xrightarrow{(0,-1,0)} \text{O3}_2$	$\text{Ca}_1 \xrightarrow{(0,0,0)} \text{O4}_2$
$\text{Ca}_1 \xrightarrow{(0,0,0)} \text{O5}_1$	$\text{Ca}_1 \xrightarrow{(0,-1,0)} \text{O6}_1$	$\text{Ca}_1 \xrightarrow{(0,0,-1)} \text{O6}_2$
$\text{Ca}_2 \xrightarrow{(0,1,0)} \text{O2}_2$	$\text{Ca}_2 \xrightarrow{(0,0,0)} \text{O3}_1$	$\text{Ca}_2 \xrightarrow{(0,0,0)} \text{O4}_1$
$\text{Ca}_2 \xrightarrow{(0,1,0)} \text{O5}_2$	$\text{Ca}_2 \xrightarrow{(0,0,1)} \text{O6}_1$	$\text{Ca}_2 \xrightarrow{(0,0,0)} \text{O6}_2$

Table B.1: The QG of barytocalcite (structure table A.1).

$A_1 \xrightarrow{(0,0,0)} OA1_1$	$A_1 \xrightarrow{(0,0,0)} OA1_2$	$A_1 \xrightarrow{(1,0,0)} OA2_2$
$A_1 \xrightarrow{(0,0,0)} OB0_2$	$A_1 \xrightarrow{(0,0,0)} OB0_1$	$A_1 \xrightarrow{(0,1,0)} OD0_3$
$A_1 \xrightarrow{(0,0,1)} OD0_4$	$A_2 \xrightarrow{(0,0,0)} OA1_1$	$A_2 \xrightarrow{(0,0,0)} OA1_2$
$A_2 \xrightarrow{(-1,0,1)} OA2_1$	$A_2 \xrightarrow{(0,1,0)} OB0_3$	$A_2 \xrightarrow{(0,0,1)} OB0_4$
$A_2 \xrightarrow{(0,0,0)} OD0_1$	$A_2 \xrightarrow{(0,0,0)} OD0_2$	$OA1_1 \xrightarrow{(0,0,0)} SiT1_1$
$OA1_1 \xrightarrow{(0,1,0)} SiT1_2$	$OA1_2 \xrightarrow{(0,0,0)} SiT1_3$	$OA1_2 \xrightarrow{(0,0,1)} SiT1_4$
$OA2_1 \xrightarrow{(0,0,0)} SiT20_1$	$OA2_1 \xrightarrow{(0,0,0)} SiT20_2$	$OA2_2 \xrightarrow{(0,0,0)} SiT20_3$
$OA2_2 \xrightarrow{(0,0,0)} SiT20_4$	$OB0_1 \xrightarrow{(0,0,0)} SiT1_1$	$OB0_1 \xrightarrow{(0,0,0)} SiT20_1$
$OB0_2 \xrightarrow{(0,0,0)} SiT1_3$	$OB0_2 \xrightarrow{(0,0,0)} SiT20_2$	$OB0_3 \xrightarrow{(0,0,0)} SiT1_2$
$OB0_3 \xrightarrow{(0,-1,1)} SiT20_3$	$OB0_4 \xrightarrow{(0,0,0)} SiT1_4$	$OB0_4 \xrightarrow{(0,0,0)} SiT20_4$
$OC0_1 \xrightarrow{(0,1,-1)} SiT1_3$	$OC0_1 \xrightarrow{(0,0,0)} SiT20_1$	$OC0_2 \xrightarrow{(0,0,0)} SiT1_1$
$OC0_2 \xrightarrow{(-1,1,0)} SiT20_2$	$OC0_3 \xrightarrow{(0,0,0)} SiT1_2$	$OC0_3 \xrightarrow{(0,0,0)} SiT20_4$
$OC0_4 \xrightarrow{(0,0,0)} SiT1_4$	$OC0_4 \xrightarrow{(1,-1,0)} SiT20_3$	$OD0_1 \xrightarrow{(0,0,0)} SiT1_1$
$OD0_1 \xrightarrow{(0,0,0)} SiT20_3$	$OD0_2 \xrightarrow{(0,0,0)} SiT1_3$	$OD0_2 \xrightarrow{(0,0,0)} SiT20_4$
$OD0_3 \xrightarrow{(0,0,0)} SiT1_2$	$OD0_3 \xrightarrow{(0,-1,1)} SiT20_1$	$OD0_4 \xrightarrow{(0,0,0)} SiT1_4$
	$OD0_4 \xrightarrow{(0,0,0)} SiT20_2$	

Table B.3: The twice reduced QG of celsian and a synthetic Sr-feldspar. ‘A’ stands for the Ba- and Sr-atoms.

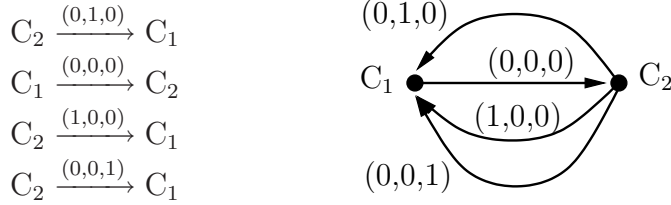


Table B.4: The diamond QG (structure: table A.7).



# Bibliography

- S. C. Abrahams. Structurally based predictions of ferroelectricity in seven inorganic materials with space group  $Pba2$  and two experimental confirmations. *Acta Crystallographica*, B45:228–232, 1989.
- Y. Akahama, M. Kobayashi, and H. Kawamura. Pressure induced structural phase transition in sulphur at 83 GPa. *Physical Review B*, 48(10):6882–6864, September 1, 1993.
- M. Bader, W. E. Klee, and G. Thimm. The 3-regular nets with 4 and 6 vertices per unit cell. *Zeitschrift für Kristallographie*, 212:553–558, 1997.
- Ch. Baerlocher and L. B. McCusker. Database of zeolite structures, 2007. URL <http://www.iza-structure.org/databases>.
- P. Bayliss. Crystal structure refinement of a weakly anisotropic pyrite. *American Mineralogist*, 62:1168–1172, 1977.
- P. Benna and E. Bruno. Single-crystal in situ high-temperature structural investigation on strontium feldspar. *American Mineralogist*, 86:690–699, 2001.
- A. Beran, A. Libowitzky, and Th. Armbruster. Spectroscopic infrared a single-crystal study and X-ray diffraction containing groups OH of untwinned San Benito perovskite. *The Canadian Mineralogist*, 34:803–809, 1996.
- A. Beukeman and W. E. Klee. Cycle classes as topological invariants of crystal structures. *Zeitschrift für Kristallographie*, 209:709–713, 1994.
- V. A. Blatov. Search for isotypism in crystal structures by means of the graph theory. *Acta Crystallographica, Section A: Foundations of Crystallography*, B56:178–188, 2000.
- W. L. Bragg. The analysis of crystals by the x-ray spectrometer. *Proceedings of the Royal Society of London*, A89:223–232, 1913.

- G. O. Brunner. The properties of coordination sequences and conclusions regarding the lowest possible density of zeolites. *Journal of Solid State Chemistry*, 29:41–45, 1979.
- CCMS. *Crystal Lattice Structures*. Center for Computational Materials Science of the United States Naval Research Laboratory, 2007. URL <http://cst-www.nrl.navy.mil/lattice>.
- S. J. Chung, T. Hahn, and W. E. Klee. Nomenclature and generation of three-periodic nets: The vector method. *Acta Crystallographica*, A40:42–45, 1984.
- J. H. Conway and N. J. A. Sloane. Low-dimensional lattices VII: Coordination sequences. *Proceedings Royal Society London, Series A*, 453:2369–2389, 1997.
- Ch. J. Cramer, W. B. Tolman, K. H. Theopold, and A. L. Rheingold. Variable character of O–O and M–O bonding in side-on ( $\eta^2$ ) 1:1 metal complexes of O<sub>2</sub>. *Proceedings of the National Academy of Science*, 100(7), April 1, 2003.
- O. Delgado-Friedrichs and M. O’Keeffe. Identification of and symmetry computation for crystal nets. *Acta Crystallographica Section A: Foundations of Crystallography*, 59(4):351–360, 2003.
- O. Delgado-Friedrichs, A. W. M. Dress, D. H. Huson, J. Klinowski, and A. L. Mackay. Systematic enumeration of crystalline networks. *Nature*, 400:644–647, 12 August 1999.
- O. Delgado-Friedrichs, M. O’Keeffe, and O. M. Yaghi. The CdSO<sub>4</sub>, rutile, cooperite and quartz dual nets: interpretation and catenation. *Solid State Sciences*, 5:73–78, 2003.
- I. Dodony, M. Posfai, and P. R. Buseck. Structural relationship between pyrite and marcasite. *American Mineralogist*, 81:119–125, 1996.
- R. T. Downs and D. C. Palmer. The pressure behavior of alpha cristobalite. *American Mineralogist*, 79(9-14), 1994.
- R. T. Downs and M. Hall-Wallace. The American mineralogist crystal structure database. *American Mineralogist*, 88:247–250, 2003. URL <http://rruff.geo.arizona.edu/AMS/amcsd.php>.



- G. Fadda and G. Zanzotto. The arithmetic symmetry of colored crystals: classification of 2-color 2-lattices. *Journal of Applied Crystallography*, 37: 1–7, 2004.
- M. D. Foster and M. M. J. Treacy. Atlas of prospective zeolite frameworks, accessed 2007. URL <http://www.hypotheticalzeolites.net/>.
- K. Goetzke. *Graphentheoretische und algebraische Verfahren für die Analyse von Kristallstrukturen, Bericht 9210*. PhD thesis, Institut für Informatik und Praktische Mathematik, Christian-Albrechts-Universität, Kiel, Mai 1992.
- K. Goetzke and H.-J. Klein. Properties and efficient algorithmic determination of different classes of rings in finite and infinite polyhedral networks. *Journal of Non-Crystalline Solids*, 127(2):215–220, 1991.
- R. Gould. *Graph Theory*. The Benjamin/Cummings Publishing Company, Inc, 1988.
- D. L. Graf. Crystallographic tables for the rhombohedral carbonates. *American Mineralogist*, 1961.
- J. L. Gross and T. W. Tucker. *Topological Graph Theory*. Dover, 2001. Reprint of the edition published by John Wiley & Sons, New York, 1987.
- R. W. Grosse-Kunstleve and P. D. Adams. Algorithms for deriving crystallographic space-group information. II. treatment of special positions. *Acta Crystallographica*, A58:60–65, 2002.
- R. W. Grosse-Kunstleve. Algorithms for deriving crystallographic space-group information. *Acta Crystallographica*, A55:383–396, 1999.
- R. W. Grosse-Kunstleve, G. O. Brunner, and N. J. A. Sloane. Algebraic description of coordination sequences and exact topological densities for zeolites. *Acta Crystallographica*, A52:879–889, 1996.
- J. W. Gruner. The crystal structures of talc and pyrophyllite. *Zeitschrift für Kristallographie*, 88:412–419, 1934.
- T. Hahn, editor. *International Tables for Crystallography*, volume A. Kluwer Academic Publishers, third edition, 1992.
- F. Harary. *Graph Theory*. Addison-Wesley Publishing Company, 3rd (1972) edition, 1969.

- P. J. Heany. Structure and chemistry of the low-pressure silica polymorphs. In P. J. Heany, C. T. Prewitt, and G. V. Gibbs, editors, *Silica. Physical Behavior, Geochemistry and Materials Applications. Review in Mineralogy*, volume 29, pages 1–40. Mineralogical Society of America, Washington, 1994.
- J. M. Igartua, M. I. Aroyo, and J. M. Pérez-Mato. Systematic search of materials with high-temperature structural phase transitions: application to space group  $P2_12_12_1$ . *Physical Review B*, 54(18):12744–12752, 1996.
- J. M. Igartua, M. I. Aroyo, E. Kroumova, and J. M. Pérez-Mato. Search for  $Pnma$  materials with high-temperature structural phase transitions. *Acta Crystallographica B*, 55:177–185, 1999.
- Jmol. Jmol: an open-source Java viewer for chemical structures in 3D, 2007. URL <http://www.jmol.org/>.
- W. E. Klee. Crystallographic nets and their quotient graphs. *Crystal Research and Technology*, 39(11):959–968, 2004.
- H.-J. Klein. Systematic generation of models for crystal structures. *Mathematical Modelling and Scientific Computing*, 6(325-330), 1996.
- E. Koch and W. Fischer. Sphere packings with three contacts per sphere and the problem of the least dense sphere packing. *Zeitschrift für Kristallographie*, 201:407–414, 1995.
- F. Laves. Die Bauzusammenhänge innerhalb der Kristallstrukturen, I. Teil. *Zeitschrift für Kristallographie*, 73:202–265, 1926a.
- F. Laves. Die Bauzusammenhänge innerhalb der Kristallstrukturen, II. Teil. *Zeitschrift für Kristallographie*, 73:273–324, 1926b.
- L. Levien, C. T. Prewitt, and D. J. Weidner. Structure and elastic properties of quartz at pressure. *American Mineralogist*, 65:920–930, 1980.
- L. Levien and C. T. Prewitt. High-pressure crystal structure and compressibility of coesite. *American Mineralogist*, 66:324–333, 1981.
- C. Marcos, A. Paniagua, D. B. Moreiras, S. Gracia-Granda, and M. R. Diaz. Villamaninite, a case of noncubic pyrite-type structure. *Acta Crystallographica*, B52:899–904, 1996.

- W. M. Meier, D. H. Olson, and Ch. Baerlocher. *Atlas for Zeolite Structure Types*. Structure Commission of the International Zeolite Association, 4 edition, 1996. URL <http://www.iza-structure.org/databases/>.
- R. E. Newnham and H. D. Megaw. The crystal structure of celsian (barium feldspar). *Acta Crystallographica*, 13(4):303–312, Apr 1960.
- M. O’Keeffe and N. E. Brese. Uninodal 4-connected 3D nets. I. Nets without 3- or 4-rings. *Acta Crystallographica Section A*, 48(5):663–669, Sep 1992.
- W. Pannhorst and J. Lohn. Zur Kristallstruktur von Strontianit,  $\text{SrCO}_3$ . *Zeitschrift für Kristallographie*, 131:455–459, 1970.
- E. V. Peresyphkina and V. A. Blatov. Molecular coordination numbers in crystal structures of organic compounds. *Acta Crystallographica, Section B: Structural Science*, B56:501–511, 2000.
- PhysLink.com. Physics & astronomy online, 2007. URL <http://www.physlink.com/>.
- A. Putnis. *Introduction to Mineral Sciences*. Cambridge University Press, 1992.
- S. Schumacher. *Periodische Graphen und Beiträge zu ihren Wachstumsfolgen*. PhD thesis, Fakultät für Physik, Universität Karlsruhe, Karlsruhe, Germany, 1994.
- H. T. Stokes and D. M. Hatch. *Isotropy subgroups of the 230 crystallographic space groups*. World Scientific, Singapore, 1988.
- R. T. Strong, Ch. J. Pickard, V. Milman, G. Thimm, and B. Winkler. Systematic prediction of  $sp^3$  hybridised carbon polymorphs. *Physical Review B*, 70, 2004.
- G. Thimm and W. E. Klee. Zeolite cycle sequences. *Zeolites*, 19:422–424, 1997.
- G. Thimm. Crystal structures and their enumeration via quotient graphs. *Zeitschrift für Kristallographie*, 219(9):528–536, 2004.
- G. Thimm. Home page, 2007. URL <http://www.adam.ntu.edu.sg/~mgeorg>.

- G. Thimm, W. E. Klee, and G. A. Britton. The topology of crystal structures. In K. Knorr and B. Winkler, editors, *Cecam Workshop on: Future developments in the study of structure-property relations by 'computational crystallography' and experiments*, volume 10 of *Berichte aus den Arbeitskreisen der DGK*, pages 171–176. Deutsche Gesellschaft für Kristallographie, ETH Zürich, 2000.
- M. M. J. Treacy, I. Rivin, E. Balkovsky, K.H. Randall, and M. D. Foster. Enumeration of periodic tetrahedral frameworks. II. Polynodal graphs. *Microporous and Mesoporous Materials*, 74(121-132), 2004.
- P. Villars and L.D. Calvert. *Pearson's handbook of crystallographic data for intermetallic phases*, volume 1-3. American Society for Metals, 1989.
- Y. Watanabe. The crystal structure of monoclinic  $\gamma$ -sulphur. *Acta Crystallographica Section B*, 30(6):1396–1401, Jun 1974.
- A. F. Wells. *Three-Dimensional Nets and Polyhedra*. Wiley, New York, 1977.
- A. F. Wells. *Further Studies of Three-dimensional Nets*. Polycrystal Book Service, Pittsburgh, 1979.
- H.-R. Wenk and A. Bulakh. *Minerals. Their Constitution and Origin*. Cambridge University Press, 2004.
- R. J. Wilson and J. J. Watkins. *Graphs: an introductory approach. A first course in discrete mathematics*. Wiley, 1990.
- B. Winkler, Ch. J. Pickard, V. Milman, W. E. Klee, and G. Thimm. Prediction of a nanoporous  $sp^2$ -carbon framework structure by combining graph theory with quantum mechanics. *Chemical Physics Letters*, 312:536–541, October 1999.
- B. Winkler, Ch. J. Pickard, V. Milman, and G. Thimm. Systematic prediction of crystal structures. *Chemical Physics Letters*, 337(1-3):36–42, March 2001.
- X. Yuan and A. N. Cormack. Efficient algorithm for primitive ring statistics in topological networks. *Computational Materials Science*, 24:243–360, 2002.

# Nomenclature

If not stated otherwise, this work follows the notations proposed by Hahn [1992].

$\hat{\rho}$	specific topological density.
$\phi$	isomorphism or automorphism of nets or quotient graphs.
$\Downarrow \left(\frac{n}{d}\right)$	function returning $\frac{1}{d}$ ( $n$ and $d$ integer with greatest common divisor equal to 1) .
$\circlearrowleft$	a cycle in a graph (a closed path without repetition of nodes or edges).
$ \circlearrowleft $	the size of a cycle (the number of nodes or edges).
$\oplus$	the sum over the edges' oriented labels.
$\mathcal{O}(n_i)$	the diameter of atoms associated with node $n_i$ .
$x \doteq y$	if $x \bmod 1 = y \bmod 1$ is true, that if is both sides of the equation are equal "modulus 1".
$a, b, c, \alpha, \beta, \gamma$	unit cell parameters.
$D$	dimension of an embedding ( $D \geq 1$ , usually $D = 3$ ).
$\hat{d}$	dimensionality (of a net).
$e_i = \left(n_i \xrightarrow{\mathbf{v}} n_j\right)$	an edge in a QG.
$\mathbf{G}, \mathbf{G}_N, \mathbf{G}_E$	a net (or a voltage graph $\langle \mathbf{Q}, \mathbb{Z}^D \rangle$ ) with nodes $\mathbf{G}_N$ and edges $\mathbf{G}_E$ .
$x \bmod 1$	represents the real value $0 \leq r < 1$ for which exists an integer $i$ such that $r + i = x$ .
$\hat{m}$	multiplicity (of a net).
$n_i$	node in a QG.
$n_i(\mathbf{x})$	node in a net. $\mathbf{x} \in \mathbb{Z}^D$ the coordinates of the node.
$n_i(\mathbf{x}) \leftrightarrow n_k(\mathbf{y})$	an edge in a net.
$\mathcal{O}$	the order of a symmetry operation.
$p = (e_i, e_j, \dots, e_k)$	a path in a quotient graphs represented as a sequence of edges.
$\mathbf{Q}, \mathbf{Q}_N, \mathbf{Q}_E$	a quotient graph with nodes $\mathbf{Q}_N$ and edges $\mathbf{Q}_E$ .
$\langle \mathbf{Q}, \mathbb{Z}^D \rangle$	a net defined as a voltage graph.
$\mathbb{R}$	the domain of real numbers.
$(s_1^{n_i}, s_2^{n_i}, \dots)$	a coordination sequence with elements $s_k^{n_i}$ the number of nodes connected by a path of length $k$ (but not shorter) to node $n_i(\mathbf{0})$ .
$(\bar{s}_1^{n_i}, \bar{s}_2^{n_i}, \dots)$	an average coordination sequence.
$\mathbf{t}$	a reduction vector.

$(\mathbf{W} \mathbf{w})$	the Seitz symbol for a symmetry operation with rotational matrix $\mathbf{W}$ and translation $\mathbf{w}$ .
$\mathbf{w}^{(i)}$	the intrinsic translation of a symmetry element (a possible glide or screw component).
$\mathbf{w}^{(\ell)}$	the translation proper to each symmetry element: $\mathbf{w} = \mathbf{w}^{(i)} + \mathbf{w}^{(\ell)}$ .
$x, y, z$	fractional atom positions.
$V$	volume.
$\mathbf{v}, \mathbf{v}_k$	an edge label / the label of edge $k$ .
$\mathbf{V}$	matrix formed from edge labels.
$\mathbb{Z}$	the domain of integer numbers.

# Index

- $\circlearrowleft$ , 20, 28
- $\oplus$ , 8
- $\doteq$ , 49
- $\hat{\rho}$ , 25
- $\delta$ , 25
- $\Downarrow (\cdot)$ , 70
- $\otimes$ , 25
- $\overline{\otimes}$ , 25
- $\phi$ , 41
  
- automorphism, 47
  - translational, 67
  
- BaAl<sub>2</sub>Si<sub>2</sub>O<sub>8</sub>, 82, 83, 92
- BaCa(CO<sub>3</sub>)<sub>2</sub>, 81, 91
- barytocalcite, 81, 91, 102
- base graph, 8, 10
  
- CaCO<sub>3</sub>, 77, 92
- calcite, 77, 81, 92
- CaTiO<sub>3</sub>, 26, 94
- cell
  - centred, 65
  - parameters, 28
  - super-, 65
  - volume, 27
- celsian, 82, 83, 92, 101, 103
- coesite, 21, 27, 93, 101
- connected
  - simply, 36
- coordination sequence, 11, 24
- copper, 65, 66
- cristobalite, 14, 27, 93
- crystallographic embedding, 7
  
- Cu, 65, 66
- CuDy, 65, 66
- Cu<sub>2</sub>O, 14, 93
- cuprite, 14, 27, 93
- cycle
  - fully stretched, 21
  - sequence, 20, 89
  - stretched, 21
- cycle sum, 8, 28
- cycles, 20
  
- $D$ , 18
- $\hat{d}$ , 13
- density
  - specific, 11, 24
  - specific topological, 25
  - topological, 11
- diameter
  - atom, 25
  - graph, 26
- diamond, 27, 28, 37, 93, 103
- disconnected net, 14
- distance, 21
  
- $e$ , 39
- edge, 39
  - anti-parallel, 34
  - parallel, 34
- $\hat{e}_k$ , 67
- enumeration, 31, 33
  
- FeS<sub>2</sub>, 54, 94
  
- $\mathbf{G}$ , 7, 40
- $\mathbf{G}_E$ , 7, 40

$\mathbf{G}_N$ , 7, 40  
 graphite, 13, 14, 16, 62  
 halite, 76  
 invariant, 10  
 isomorphism  
     net, 7, 40  
     quotient graph, 8, 40  
 lattice type, 10  
 lonsdaleite, 37  
 loop, 33  
 $\hat{m}$ , 16  
 magnesite, 77, 94  
 marcasite, 54, 56, 58, 94  
 $\text{Mg}_3\text{Si}_4\text{O}_{12}\text{H}_2$ , 13, 97  
 $\text{MgCO}_3$ , 77, 94  
 modulus 1, 49  
 morphology, 8  
 multiplicity, 18  
 NaCl, 77  
 net, 2, 5, 40  
     crystallographic, 32  
     dimensionality, 13, 35  
     disconnected, 13, 14  
     dual, 14  
     embedding, 47  
     isomorphic, 35  
     multiplicity, 16  
     pathological, 32  
     square, 74  
 $\hat{n}_i$ , 67  
 $n_i(\mathbf{x})$ , 40  
 $n_i(\mathbf{x}) \leftrightarrow n_j(\mathbf{x}')$ , 40  
 $n_i \xrightarrow{\mathbf{v}} n_j$ , 39  
 node, 39  
 non-penetrating, 35  
 $\mathcal{O}$ , 50  
 order, 50  
 $\mathbf{P}$ , 45  
 penetrating, 35  
 perovskite, 27, 94  
 phase transition, 53, 59, 61  
 point group, 10  
 pseudo-symmetries, 53  
 pyrite, 54, 55, 94  
 $\mathbf{Q}$ , 39  
 $\hat{\mathbf{Q}}$ , 71  
 $\mathbf{Q}_E$ , 39, 40  
 $\mathbf{Q}^{\text{marc}}$ , 56, 58  
 $\mathbf{Q}_N$ , 39  
 $\mathbf{Q}^\spadesuit$ , 47, 48  
 $\mathbf{Q}^\square$ , 74  
 $\mathbf{Q}^\triangle$ , 74  
 quartz, 60  
 $\alpha$ -quartz, 60, 61, 95  
 $\beta$ -quartz, 60, 61, 95  
 quotient graph, 2, 5, 39  
     disconnected, 73  
 $\langle \mathbf{Q}, \mathbb{Z}^D \rangle$ , 40  
 $\mathbf{R}$ , 45  
 reduction, 32, 65  
     vector, 69, 70  
 rings, 21  
 rutile, 56, 57, 95  
 $(\overline{s}_1, \overline{s}_2, \dots)$ , 11  
 $(s_1^{n_i}, s_2^{n_i}, \dots)$ , 11  
 Seitz symbol, 50  
 $\text{SiO}_2$ , 21, 60, 61, 93, 95  
 space group, 1  
     *klassengleiche*, 80  
     *translatonsgleiche*, 80  
 sphere packings, 31  
 $\text{SrAl}_2\text{Si}_2\text{O}_8$ , 82, 96, 101, 103  
 strontium feldspar, 82, 96, 101, 103  
 sub-lattice, 67  
 sub-nets, 14  
 symmetry, 47



**T**, 45  
talc, 13, 97  
tiling, 31  
TiO<sub>2</sub>, 56, 57, 95  
trail, 20  
translation  
    intrinsic, 50  
    location, 50

**V**, 44  
 $\bar{\mathbf{V}}$ , 44  
voltage graphs, 39

**W**, 43  
 $\mathbf{w}^{(i)}$ , 50  
 $\mathbf{w}^{(\ell)}$ , 50  
 $(\mathbf{W}|\mathbf{w})$ , 50

# Lebenslauf

Georg Thimm

- 2002 - heute Teilzeit Unterricht an der OpenUniversity.
- 2000 - heute Assistant Professor an der School of Mechanical and Aerospace Engineering, Nanyang Technological University, Singapore.
- 1999 - 2000 Research Fellow an der School of Mechanical and Aerospace Engineering, Nanyang Technological University, Singapore.
- 1997 - 99 Post-doc am Institut D'alle Molle d'Intelligence Perceptive, Martigny, Schweiz.
- 1997 Docteur és Sciences Techniques, EPFL, Lausanne, Schweiz. Vorbereitung der Doktorarbeit am IDIAP/Switzerland unter Prof. Dr. M Kunt und Dr. E. Fiesler.
- 1992 *Diplom Informatiker*, Technische Universität Karlsruhe, Deutschland (Diplomarbeit betreut von Prof. Dr. W. E. Klee und Prof. Dr. P. Deussen).
- 26. Oktober 1965 Geboren in Trossingen

## Related publications by the author

1. *Net Topologies, Space Groups, and Crystal Phases*, G. Thimm and B. Winkler. **Zeitschrift für Kristallographie**, 221(12), pp 749–758, 2006.
2. *Crystal Structures and Their Enumeration via Quotient Graphs*. G. Thimm. **Zeitschrift für Kristallographie**, 219(9), pp 528–536, 2004.
3. *Systematic Prediction of  $sp^3$  Hybridised Carbon Polymorphs*. Rachel T. Strong, Chris J. Pickard, Victor Milman, G. Thimm, Björn Winkler. **Physical Review B**, 70, 2004.
4. *Systematic prediction of crystal structures*. Björn Winkler, Chris J. Pickard, Victor Milman, and G. Thimm. **Chemical Physics Letters**, 337(1–3), pp. 36–42, 2001.
5. *Prediction of a Nanoporous  $sp^2$ -carbon Framework Structure by Combining Graph Theory with Quantum Mechanics*. Björn Winkler, Chris J. Pickard, Victor Milman, and G. Thimm. **Chemical Physics Letters**, 312, pp. 536–541, 1999.
6. *Zeolite Cycle Sequences*. G. Thimm and W. E. Klee. **Zeolites**, 19, pp. 422–424, 1997.
7. *The 3-regular Nets with 4 and 6 Vertices per Unit Cell*. M. Bader, G. Thimm, and W. E. Klee. **Zeitschrift für Kristallographie**, 212, pp. 553–558, 1997.
8. *Enumerating Buckminsterfulleran Isomers* (technical comment). G. Thimm and Wilfrid E. Klee. **Science**, 255, page 92, 1992.
9. *The Topology of Crystal Structures*. G. Thimm, W. E. Klee, and G. A. Britton, **Cecam Workshop on: Future developments in the study of structure-property relations by ‘computational crystallography’ and experiments**, (eds.) K. Knorr and B. Winkler. *Berichte aus den Arbeitskreisen der DGK*, 10, Deutsche Gesellschaft für Kristallographie, 2000.